In presenting the dissertation as a partial fulfillment of the requirements for an advanced degree from the Georgia Institute of Technology, I agree that the Library of the Institute shall make it available for inspection and circulation in accordance with its regulations governing materials of this type. I agree that permission to copy from, or to publish from, this dissertation may be granted by the professor under whose direction it was written, or, in his absence, by the Dean of the Graduate Division when such copying or publication is solely for scholarly purposes and does not involve potential financial gain. It is understood that any copying from, or publication of, this dissertation which involves potential financial gain will not be allowed without written permission.

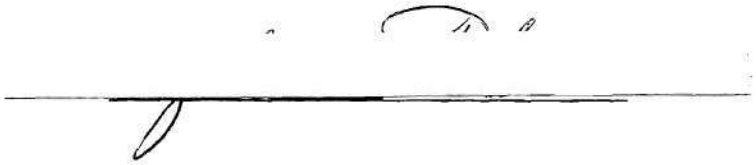

3/17/65
b

TRANSIENT FREE CONVECTION IN A CLOSED CONTAINER WITH HEATING AT THE BOTTOM AND AT THE SIDES

A THESIS

Presented to

The Faculty of the Graduate Division

by

John Wilbur Tatom

In Partial Fulfillment

of the Requirements for the Degree

Doctor of Philosophy in the

School of Mechanical Engineering

Georgia Institute of Technology

May, 1966

ACKNOWLEDGMENTS

To express proper thanks to all those who have helped in completing this work is not possible. However, there are individuals who have given so much of their time and patience that courtesy demands recognition of their contributions. First, to my wife Hilda whose support, forebearance, and understanding have given me the strength to complete this goal, I extend my sincerest appreciation and affection. To Dr. W. O. Carlson, whose thoughtful guidance has led to the culmination of this work, I offer my warmest thanks. In addition, the constructive comments, the willingness to be helpful and the time given by the members of my thesis committee, Dr. Thomas W. Jackson and Dr. Henderson Ward is gratefully acknowledged.

A special word of appreciation is due to Mr. Richard Brooks, Mr. C. R. Bannister and Mr. J. G. Doyal who greatly assisted in the fabrication of the experimental apparatus. Also appreciation is expressed to Mr. Reginald Pollard, who helped take the test data, and Mr. Francis Kiernan, without whose photographic skill little would have been accomplished. In addition, special thanks is extended to my able computer programmers Mr. Mike Spahr and Mr. Ken Defeo.

Finally, to the National Science Foundation and especially to the Lockheed-Georgia Company, whose financial support made this undertaking possible, I extend my deepest gratitude. I hope that I can be worthy of the investment so generously given.

TRANSIENT FREE CONVECTION

IN A CLOSED CONTAINER WITH HEATING

AT THE BOTTOM AND AT THE SIDES

Approved:

Chairman

Date approved by Chairman: 5/25/66

TABLE OF CONTENTS

LIST OF TABLES

LIST OF ILLUSTRATIONS

SUMMARY

Experimental studies of transient free convection phenomena have been conducted in a vertical, closed container where the fluid was uniformly heated both at the bottom and at the sides without change of phase and where a large percentage of the energy transfer occurred under turbulent conditions. Water was used as the test fluid in a 298-gallon tank approximately two feet wide, two feet in breadth, and ten feet deep. To heat the water, two parallel sides as well as the bottom of the tank were provided with electrical resistance elements. The other two parallel sides of the tank were made of glass to allow observation of the fluid motion. The heat flux at the bottom and along the sides could separately and continuously be varied from zero to a maximum of 0.193 Btu/secft^2 and 0.171 Btu/secft^2, respectively. A maximum modified Grashof number of 5×10^{14} was obtained, for which turbulent flow existed over approximately 80 per cent of the tank depth. In the tests, fluid temperature measurements at various axial positions were made starting at time zero with the water in an isothermal quiescent state. Using a photographic technique employing neutral-density particles, time exposure photographs of the fluid motion at various locations within the tank were also made. In addition, Schlieren photographs of the fluid behavior were taken. From the photographic data, information concerning both the fluid velocity and the fluid flow patterns were obtained.

In the test program, axial temperature and velocity measurements were made at various aspect ratios (L/H), modified Grashoff numbers

(Gr^*), and bottom-to-side heat flux ratios (q_b/q_s). Measured temperature profiles correlate satisfactorily with available semi-empirical predictions with combined bottom and side heating. With side heating only, predicted profiles vary substantially from experimental measurements for $Gr^* > 5 \times 10^{13}$. Results indicate that a significant fraction of the sidewall heating is transfered directly through the boundary layer to the bulk liquid. The mechanism of this heat transfer appears to be governed by the ratios (q_b/q_s), (L/H), and Gr^*. However, even without bottom heating, at large values of Gr^*, a substantial amount of heat diffuses through the turbulent boundary layer. An analysis of this diffusion mechanism which correlates satisfactorily with the test data has been made.

NOMENCLATURE

Latin Symbols	Definition	Units
a	coefficient of x in linearization of $x^{8/7}$	$ft^{1/7}$
A	dimensional constant in boundary layer diffusion analyses	ft^2/sec
A_1	constant in solution for turbulent boundary layer characteristic velocity, U_1	$ft^{8/5}/sec^{14/5}$
b	constant in linearization of $x^{8/7}$	$ft^{8/7}$
B	dimensional constant in boundary layer diffusion analyses	ft
B_1	constant in solution for characteristic velocity U_1	dimensionless
c	heat capacity	Btu/lbm°F
C_1	constant appearing in separation of variables solution to boundary layer diffusion equation	———
C_2	constant appearing in separation of variables solution to boundary layer diffusion equation	———
C_3	coefficient in equation for characteristic velocity U_1	$ft^{4/7}/sec$
C_m	coefficients in assumed power series form for $K_o(x)$ in boundary layer diffusion analysis	dimensionless
C_n	coefficients in final solution for θ_2 in boundary layer diffusion analysis	dimensionless
D_p	particle diameter	ft
E_{rms}	root mean square deviation between computed least squares curve and true temperature profile	F
$f(s)$	Laplace transform of $F(\tau)$	———
$F(x)$	pure function of x in separation of variable solution to the boundary layer diffusion equation	———

Latin Symbols	Definition	Units
Gr	$g\beta\theta l^3/\nu^2$ Grashof number	dimensionless
Gr^*	$g\beta q_s l^4/k\nu^2$ modified Grashof number	dimensionless
g_o	standard acceleration of gravity (32.2)	ft/sec^2
$g(x)$	generating function for $\bar{U}\delta$ in boundary layer diffusion analyses	dimensionless
H	tank width	ft
J	dimensional constant in approximation for $\bar{U}\delta$	ft^2
J_1	constant arising in boundary layer momentum integral	dimensionless
J_2	constant arising in boundary layer energy integral	dimensionless
J_3	constant arising in definition of average boundary layer velocity	dimensionless
k	thermal conductivity	Btu/ft sec°F
K	constant in approximation for $\bar{U}\delta$	$ft^{6/7}/sec$
K'	constant in approximation for $\bar{U}\delta$	ft/sec
K_o	per cent of sidewall heating which passes through the boundary layer into the bulk liquid	dimensionless
$\bar{K}_o$	time average value of K_o	dimensionless
K_1	thermal layer mixing velocity modulus	dimensionless
K_2	constant coefficient in the product $\bar{U}\delta$	$ft^{6/7}/sec$
ℓ	thermal layer depth	ft
L	liquid depth	ft
ℓ_∞	asymptotic thermal layer depth	ft
m	exponent in assumed power series form for $K_o(x)$ in boundary layer diffusion analysis	dimensionless

Latin Symbols	Definition	Units
M	one plus the assumed least squares polynomial order	dimensionless
n	exponent governing shape of the thermal layer temperature profile	dimensionless
N	one minus the number of data points using a least squares fit	dimensionless
p	boundary layer velocity profile shape parameter	dimensionless
Pr	$\mu c/k$, Prandtl number	dimensionless
q_b	bottom heat flux	Btu/ft^2 sec
q_d	apparent heat flux due to diffusion across boundary layer to the bulk liquid	Btu/ft^2 sec
q_s	sidewall heat flux	Btu/ft^2 sec
Q_B	total bottom heating rate	Btu/sec
Q_S	total sidewall heating rate	Btu/sec
r	number of particles per cubic inch	in^{-3}
R_c	radius of vortex in particle response analysis	ft
R_o	initial particle radius from center of vortex	ft
R_p	apparent particle radial position	ft
R_p	true particle radial position	ft
R_{PA}	initial apparent particle radial position	ft
R_{PB}	final apparent particle radial position	ft
s	suppressed time parameter in Laplace transform	sec^{-1}
St	= Nu Re/Pr, Stanton number	dimensionless
T	temperature	^oF
$\bar{T}$	overall average fluid temperature	^oF
T_{exp}	experimental temperature	^oF

Latin Symbols	Definition	Units
T_p	predicted temperature	°F
T_s	surface temperature	°F
T_{min}	minimum fluid temperature at time τ	°F
T_{ms}	surface temperature at end of test	°F
T_{tl}	thermal layer temperature	°F
$\bar{T}_{tl}$	average thermal layer temperature	°F
T_v	bulk liquid temperature	°F
T_{vo}	initial liquid temperature	°F
U	velocity component in x direction	ft/sec
$\bar{U}$	average x velocity	ft/sec
U_l	characteristic velocity in boundary layer	ft/sec
U_{mix}	mixing velocity due to bottom heating	ft/sec
U_o	fluid velocity in x direction in particle response analysis	ft/sec
U_p	particle velocity in x direction	ft/sec
U_∞	bulk liquid velocity outside free convection boundary layer	ft/sec
V	velocity component in y direction	ft/sec
V_{bl}	y velocity of fluid entering boundary layer	ft/sec
V_o	fluid velocity in y direction in particle response analysis	ft/sec
V_p	particle velocity in y direction	ft/sec
w	parameter introduced in separation of variables approach to solving boundary layer diffusion equation	°F
W	tank breadth	ft

Latin Symbols	Definition	Units
x	position coordinate measured from the tank bottom	ft
x_t	location of the bottom of the thermal layer	ft
x_{tr}	location of transition point	ft
y	position coordinate normal to heated vertical sidewalls	ft

Greek Symbols		
α_g	angular displacement due to glass refraction effects	dimensionless
α_w	angular displacement due to water refraction effects	dimensionless
β	$-\frac{1}{\rho}\frac{\partial \rho}{\partial T})p$, constant pressure thermal expansion coefficient	$^oF^{-1}$
β_r	apparent particle angular displacement from optical axis	dimensionless
γ	exponent in assumed form for characteristic velocity, U_1	dimensionless
Γ	circulation of potential vortex	ft^2/sec
δ	boundary layer thickness	ft
$\delta_r(R_p)$	radial displacement of true particle position from apparent position	ft
ε	position coordinate measured from the bottom of the thermal layer	ft
$\bar{\varepsilon}_{rms}$	root mean square deviation between least squares fit of order n and measured temperatures	^oF
ζ	$U-U_p$	ft/sec
η	exponent in final power series solution for θ_2 in boundary layer diffusion analysis	dimensionless

Greek Symbols	Definition	Units
Θ	temperature difference between fluid inside and outside idealized boundary layer	^{o}F
Θ_1	$T - T_{min}$	^{o}F
Θ_{1m}	$T_s - T_{min}$	^{o}F
Θ_2	$T - T_{vo}$	^{o}F
$\bar{\Theta}_2$	overall average liquid temperature rise	^{o}F
$\bar{\bar{\Theta}}_2(s,x)$	transformed Θ_2 in solution of boundary layer diffusion equation	^{o}F
Θ_{2m}	$T_{ms} - T_{vo}$	^{o}F
Θ_p	Particle angular position in focal plane	dimensionless
Θ_w	fluid to wall temperature difference across boundary layer	^{o}F
λ	separation constant in boundary layer diffusion analyses	dimensionless
μ	dynamic viscosity	$lb_m/ft\ sec$
μ_r	refraction coefficient	dimensionless
μ_{rg}	refraction coefficient of glass	dimensionless
μ_{rw}	refraction coefficient of water	dimensionless
ν	fluid kinematic viscosity	ft^2/sec
ρ	fluid density	lbm/ft^3
ρ_p	particle density	lbm/ft^3
σ_{Tx}	time space root mean square deviation between predicted and test results	^{o}F
τ	time	sec
τ_w	wall shear	$\frac{lb}{ft^2}$

Greek Symbols	Definition	Units
T	pure function of time in separation of variables solution to boundary layer diffusion equation	———
ϕ	$V - V_p$	ft/sec
$\psi(x)$	parameter introduced in separation of variables approach to solving boundary layer diffusion equation	^{o}F
ω	frequency of oscillating fluid y velocity component in particle response analysis	dimensionless

CHAPTER I

LITERATURE SURVEY

Until recently free convection in liquids within closed containers has received little attention. While the investigations of Lighthill (1) and Martin (2) have certainly had a large influence on recent contributions in this area, almost no work concerned with completely enclosed fluids can be found in the literature prior to 1957. Part of the current interest in this problem was kindled by the developing area of missile technology, since rocket propellant tanks contain large volumes of liquids which are particularly sensitive to free convection effects. The cooling of turbine blades and the removal of heat from liquid fueled nuclear reactors are current areas which have also supported interest in this problem.

The influence of Lighthill is seen in almost all of the available analyses in that integral techniques have been used copiously. With only one exception all of the analyses assume a boundary layer flow along the sidewalls; no allowances are made for end effects in the fluid at either the enclosure bottom or top. Both laminar and turbulent analyses have been made; however, greatest success has been obtained with laminar analyses in checking the experimental results. Testing has been conducted in water, a mixture of trichloroethane and ethyl alcohol, freon, methyl alcohol, a water-glycerol solution, liquid nitrogen and liquid hydrogen.

Perhaps the earliest of the really meaningful analyses pertinent to the problem were performed by Hammitt (3), (4), (5). His work was generally concerned with free convection effects within a cylindrical vessel containing a heat generating liquid with heat rejection through the container sidewalls only. He used the Lighthill technique modified to account for the heat sources. The agreement between the calculated and measured values of Nusselt number is only fair although the predicted results agree qualitatively with the trends of the test data. This may be due to the fact that, following Lighthill, he assumed laminar flow in his test tank. The test results, however, showed that even at extremely low heat source strengths, turbulent flow existed in certain regions of the tank. Thus the effects of turbulence, not included in the analysis, are perhaps responsible for the departure between the predicted and the measured Nusselt number. The presence of turbulence may also explain the discrepancy between Martin's test data and the predictions by Lighthill.

Neff (6), in a paper concerned with missile tank propellant thermal stratification, reported on an experimental study using liquid nitrogen. He simulated conditions in a missile tank using a quarter scale model test vessel. To obtain the required similarity conditions, the test tank was mounted on a 20-foot centrifuge. The liquid nitrogen was located at the sides only at very high heat fluxes. Since all of the temperature profiles have a characteristic S-shape, the data were correlated with the probability bell curve. The work is valuable in that it provides the first quantitative data concerning stratification.

The problem was also studied by Huntly (7) and later by the

Lockheed-Georgia Company (8). More recently, a combined experimental and analytical program was conducted by Lockheed using an improved, but still approximate, analytical model. The results of this program were reported by Tatom (9) et al. In the experimental study liquid hydrogen was used as the test fluid in a 500-gallon dewar vessel with an L/D of approximately 2. Heating occurred at both the sides and at the tank bottom. The effects on stratification of the liquid aspect ratio were investigated. In the analysis, turbulent free convection along the tank sidewalls was assumed and an integral technique was used to determine the temperature profile in the liquid. Two empirical constants to account for the effects of bottom heating were introduced. The first, K_1, governed the maximum depth to which stratification penetrated. The second, K_o, was the fraction of the total sidewall area over which heat passed directly into the bulk liquid. Correlation of the analysis with the test data produced values of K_o between 0.6 and 0.7.

Recently Tellep et al. (10), (11), (12), conducted an experimental and analytical study of the same problem. In their test program the effects of Gr^* on stratification were investigated. Several test fluids were used in three different small-scale tanks heated at the sides only. All the tanks had an aspect ratio of 2.32. The flow conditions were mixed between laminar and turbulent. Their analysis is similar to that of references 8 and 9. The predictions of the stratification depth were consistently low with a turbulent boundary layer model but somewhat improved with a laminar model.

Bailey et al. (13), (14), have also conducted an experimental and analytical study of free convection in closed containers. In their

tests liquid hydrogen was heated at large wall heat fluxes. The test results resembled those of Neff with the characteristic S-shaped temperature profile. Their analysis, using a very simplified model, was only in fair agreement with the test results. Ruder (15) has also developed an analysis similar to that of Neff and Bailey. Barnett (16) et al. have reported on a large-scale experimental investigation using liquid hydrogen in an S-IV stage rocket propellant tank. They also present an analysis of the test results which has similarities to that of reference 9.

Vliet, et al.,(17) and Robbins and Rogers (18) have recently presented elaborate numerical analyses of the stratification problem using electronic computers. In many ways these two works are similar to that of Hammitt except that turbulent rather than laminar flow is assumed. Neither analysis includes the effect of bottom heating. Both analyses are shown to correlate well with test results. However, when all the assumptions are considered, it is doubtful whether the elaborateness of these analyses is warranted, since the more simplified analyses check the data about as well.

One of the most informative experimental investigations of free convection in closed containers was performed by Anderson and Kolar (19). In their work the motion of fluid contained in a small tank was studied under the following heating conditions:

1. Non-uniform source heating in which most of the heat was generated near the tank bottom.

2. Simple sidewall heating.

3. Non-uniform source heating in conjunction with wall heating.

The experiment was designed to provide axial temperature data and to permit a visual inspection of fluid behavior induced by wall and non-uniform source heating. The influence on the velocity field due to these modes of heating was viewed by means of a Schlieren system. Where non-uniform source heating was present, the results indicated that there was mixing such that a constant temperature in the axial direction was produced. Wall heating always produced a stable temperature gradient near the liquid surface. The two modes of heating, acting in conjunction, tended to form two regions where the characteristic effects of each were dominant.

Study of the data shows that for a given rate of bottom heating the maximum depth of the stratified region increases as the rate of side heating increases. The temperature profiles show a marked resemblance to those of reference 9. Unfortunately no attempt was made to insulate the test vessel and no heat balance was made. Both the bottom geometry and the fluid aspect ratio were constant in all the tests.

In a recent study, Barakat and Clark (20), (21) have obtained a laminar flow solution to the problem with side heating only using a finite difference method to solve the time dependent two-dimensional Navier Stokes equations. Their results show some interesting fluid behavior and should be useful in obtaining an understanding of the motion near the tank bottom and the liquid-vapor interface. To check the analysis, a test program using water in both a cylindrical and a two-dimensional test tank was also conducted. It was found that the theoretical and measured temperatures were in good agreement.

Another paper by Schwind and Vliet (22) provides a valuable

discussion of the mechanism of stratification particularly with regard to the upper regions of the test container. Among other interesting observations, they point out that with no bottom heating the S-shaped profile seems to occur for larger values of Gr^*, while a simpler profile is present for smaller Gr^*. Vliet and Brogan (23) and Neff (24) have recently investigated the effects of baffles and other defices on stratification reduction. Both studies indicate that baffles are not very effective in promoting bulk liquid mixing.

As a result of the preceding work, an analytical model has emerged which has been used with variations in almost all of the laminar and turbulent analyses to date. This model is shown in Figure 1. The model involves the main assumption of simple boundary-layer flow along the wall through which heat passes at a constant rate. The boundary layer forms at $x = 0$, grows in thickness δ as it develops along the wall, intersects the bottom of the thermal layer of depth ℓ, and finally mixes with the thermal layer itself. Depending on the absence or presence of bottom heating, the bulk liquid is assumed to remain at its initial temperature or increase in temperature with time. In the model the effects of horizontal temperature gradients and starting transients are ignored, and the boundary layer properties are assumed to be those resulting from steady natural convection over a vertical flat plate in an infinite uniform temperature fluid. Analysis of the model usually involves integral techniques to predict the axial temperature profile. The thermal layer depth is obtained from computation of the flow rate along the sidewalls from steady-state natural convection theory.

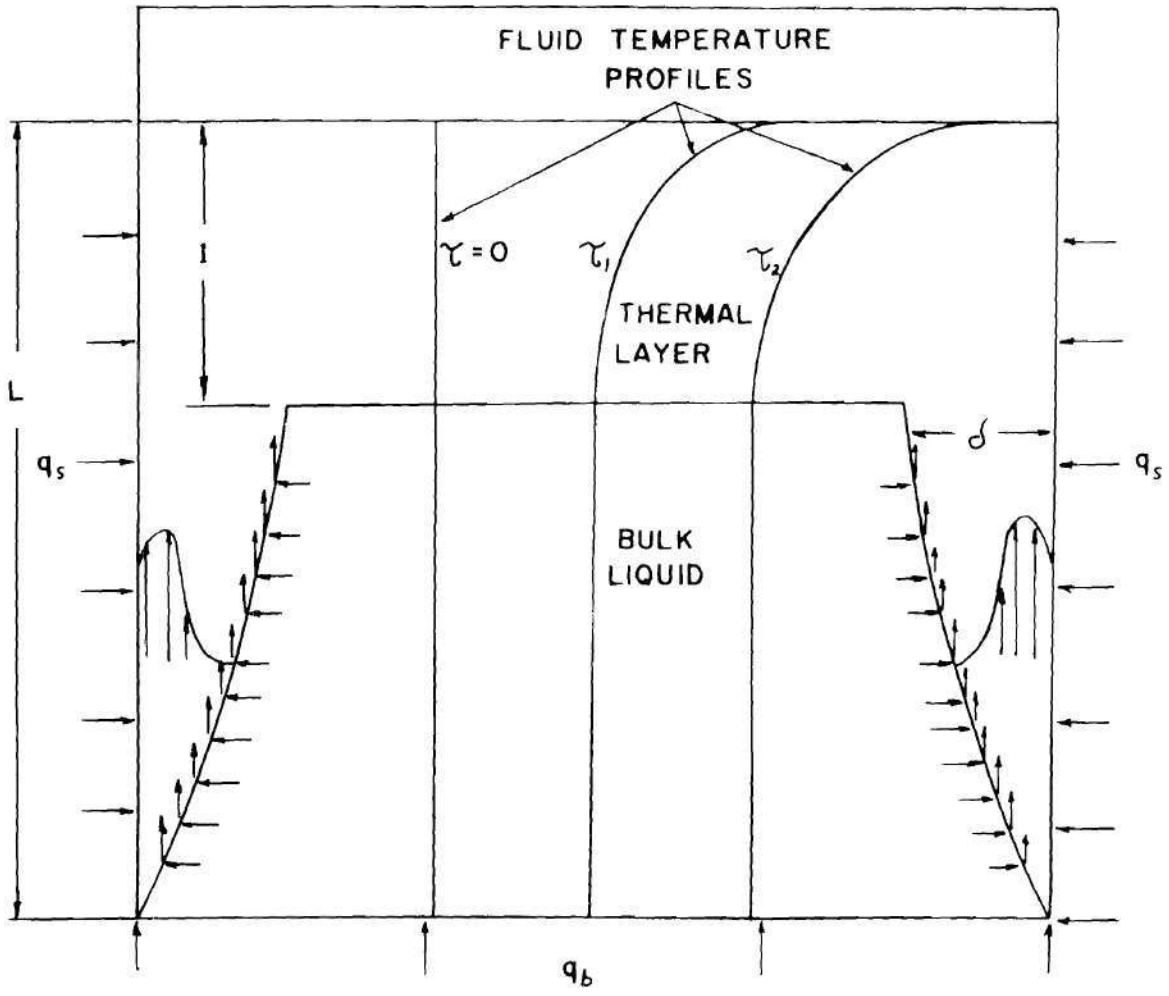

Figure 1. Analytical Model of Stratification.

In most analyses the model implicitly requires the assumption that the edge of the boundary layer represents a surface across which fluid in the bulk liquid region may enter but not leave; i.e., none of the sidewall heat passes through the boundary layer to the bulk liquid. Satisfying this assumption in reference 9 required translation of the edge of the boundary layer from the tank bottom to allow the heat flux to pass directly to the bulk liquid over a fraction K_o of the sidewall area. In making this assumption, however, one of the basic conclusions of the primary investigation of natural convection by Griffiths and Davis (35) has been ignored. This conclusion was that for turbulent free convection flows the boundary layer does not carry the heat away; instead, the heat is transmitted by turbulent mixing directly to the fluid outside the boundary layer. To quote from reference 35:

> A study of the air stream data shows that above a certain height the strata of air nearest the plate do not increase appreciably either in temperature or in velocity. Consequently they are not themselves carrying away the heat from the upper heaters, but are merely transmitting this heat to the outer layers, which by their increase in temperature and velocity carry it away. In this case the method of heat transmission through the close lying strata can hardly be pure conduction through streamline layers, for the heat transfer is greater than gaseous conduction could ordinarily effect. Thus probably the motion of the air is turbulent, resembling rolling, any particle in effect alternately proceeding to the hot plate and then to outer cooler air in its progress upwards, thus carrying away the heat and at a rate greater than could be the case if this turbulence were absent.

To explain how this basic conclusion was ignored by so many investigators can only be speculated upon. The relative unavailability of the paper may be partially responsible; however, a clear statement of the results of the study appears in Max Jakob's *Heat Transfer*, Vol. 1 (41). The need for a "working model" may have also lead to this occurrence together with

the appeal of Eckert and Jackson's report, "Analysis of Turbulent Free-Convection Boundary Layer on Flat Plate" (34), which presents an elegant, although heuristic, analytical treatment of turbulent free convection flow, that checks the data nicely. Eckert and Jackson make the following comment about the work of Griffiths and Davis:

> Whereas the velocity and temperature profile shapes . . . are typical of turbulent free convection flow, the order of magnitude of these profiles appears to be in error. It can be shown that there is disagreement within the measured values themselves. The heat given off by the plate to the airstream must be carried away within the boundary layer. The measured temperature and velocity profiles as well as the measured maximum velocity and the boundary-layer thickness vary little along the plate in the turbulent range, which means that only a small part of the heat given off by the wall is found in the boundary-layer.

From the above it is not difficult to see how the present circumstances arose, since this latter paper has probably served as the basis for almost all the stratification analyses involving turbulent flow. In addition, the limited capability of the analyses of stratification in predicting the test results has further complicated the situation, because due to the success of these analyses there was little reason to question the original assumptions involved.

CHAPTER II

PRESENT INVESTIGATION

The present experimental investigation was designed to provide a more general approach to the problem of fluid stratification in the turbulent regime than has previously been possible. In this investigation the effects on the vertical temperature profile of varying modified Grashof number, Gr^*; aspect ratio, L/H; and the ratio of bottom to side heat flux, q_b/q_s, were studied. Testing was conducted in water which offers numerous advantages both in availability and test flexibility over cryogenic and other non-cryogenic fluids. In order to gain a better understanding of the problem, both temperature and velocity data were obtained.

Approach to the Problem

In planning the test program there were several factors which had a decisive influence on the size of the test tank, the test fluid to be used, and the method for measuring fluid velocity. When these factors are considered, much of the possible arbitrariness of the experiment is removed. The influencing factors are:

1. Free convection velocities are generally very small; thus some means for accurate velocity measurement must be available.

2. The system is always in a transient state; thus the fluid velocity is a function of both position and time. This implies the need for a large number of simultaneous velocity measurements or the need to

conduct a large number of identical tests.

3. The two available fluids most convenient and economical for testing are air and water. If transition from laminar to turbulent flow is assumed to occur for a Grashof number (Gr) equal 10^9, the length to transition (x_{tr}) can be obtained using the equation for θ_w, the fluid-to-wall temperature difference for laminar flow with a constant wall flux (25). Thus for water at 100°F, the position from the tank bottom at which transition occurs can be computed from

$$x_{tr} = \frac{4.4}{(q_s)^{1/4}}$$

where: x_{tr} = transition length, ft.

q_s = wall heat flux, Btu/ft^2 hr.

While for air at 100°F and 1 atmosphere

$$x_{tr} = \frac{4.9}{(q_s)^{1/4}}$$

At higher fluid temperatures x_{tr} increases for air but decreases for water. Another consideration is that the fluid-to-wall temperature difference is 30 to 50 times larger in air than that in water for a given heat flux. Therefore, it appears that if turbulent flow over, say, 80 per cent of the tank walls is to be desired, θ_w would be considerably less for water than for air, although both would require a relatively large tank.

4. With simple bottom heating, free convection flow over hori-

zontal surfaces is laminar for Rayleigh numbers between 1,700 and 45,000. Above Rayleigh numbers of 45,000, the flow becomes turbulent. Thus the flow remains laminar at the bottom only for very viscous fluids in relatively small tanks. It appears therefore that a turbulent flow will exist at the tank bottom for all practical fluids with reasonable bottom heating rates.

When these four factors are considered it becomes apparent that to guarantee turbulent flow over a majority of the sidewalls, a large-scale tank is necessary. In addition, because of the large values of θ_w associated with turbulent free convection in air, water is a preferable test fluid. Due to the transient nature of the problem and the need for a large number of simultaneous velocity measurements, a photographic technique combined with neutral density particles suspended in the test medium is indicated. The usefulness of a Schlieren system to visualize the flow within the test tank is also suggested.

Conventional methods for obtaining velocity data such as pitot tubes or hot wire anemometers are not practical because of the low dynamic heads involved, the orientation difficulties, and, especially, because of the large amount of data required to define a given test condition. Water is a convenient choice as a medium since the size of the neutral buoyancy particles can be considerably greater than those for use in air. This occurs because of the much higher density of water. This is an important circumstance because the optical and photographic problems involved in the measurement of microscopic particle motion in air in a large test tank are of a magnitude sufficient to rule out the photographic approach if air were chosen as the test medium.

Another problem is the selection of a thermal boundary condition at the wall. Two convenient choices available are a constant temperature and a constant heat flux wall. Because the transient nature of the problem requires rapid response of the wall to the design conditions, a thick wall with a large heat capacity must be avoided. This rules out the constant temperature condition since it normally involves thick, highly conductive walls. Another disadvantage of a constant temperature wall is that the maximum temperature of the test fluid is limited by that of the wall. If a large θ_w is used, the power requirements become excessive because of the large film coefficients associated with water. A constant heat flux wall is not limited to any extent by either of the mentioned conditions. Thus, although there are some disadvantages, a constant flux boundary condition was chosen.

CHAPTER III

EXPERIMENTAL PROGRAM

Test Apparatus

There are several systems which together comprise the test apparatus. Figure 2 presents a view of the total test system which is composed of:

1. The test tank.
2. The temperature measurement system.
3. The velocity measurement system.
4. The power supply, pump and filtration system.

A discussion of each of these major systems follows.

Main Test Tank

The main test tank, constructed largely of aluminum and plate glass, is 117 inches deep, 24 inches wide, 24.5 inches in breadth, and contains 298 gallons at a maximum. It is supported on a steel pedestal approximately 2 feet tall. By means of a bearing system, the tank can be lowered to a horizontal position for easy access.

The tank depth was chosen to allow turbulent flow along 80 per cent of the sidewalls. The maximum value of Gr^{*} obtained (assuming water at 70°F) was approximately 5×10^{14}. To prevent end effects and for easy access, the tank breadth and width were taken as approximately ten times the maximum predicted turbulent boundary layer thickness.

Two sides and the bottom of the tank are designed to heat the test

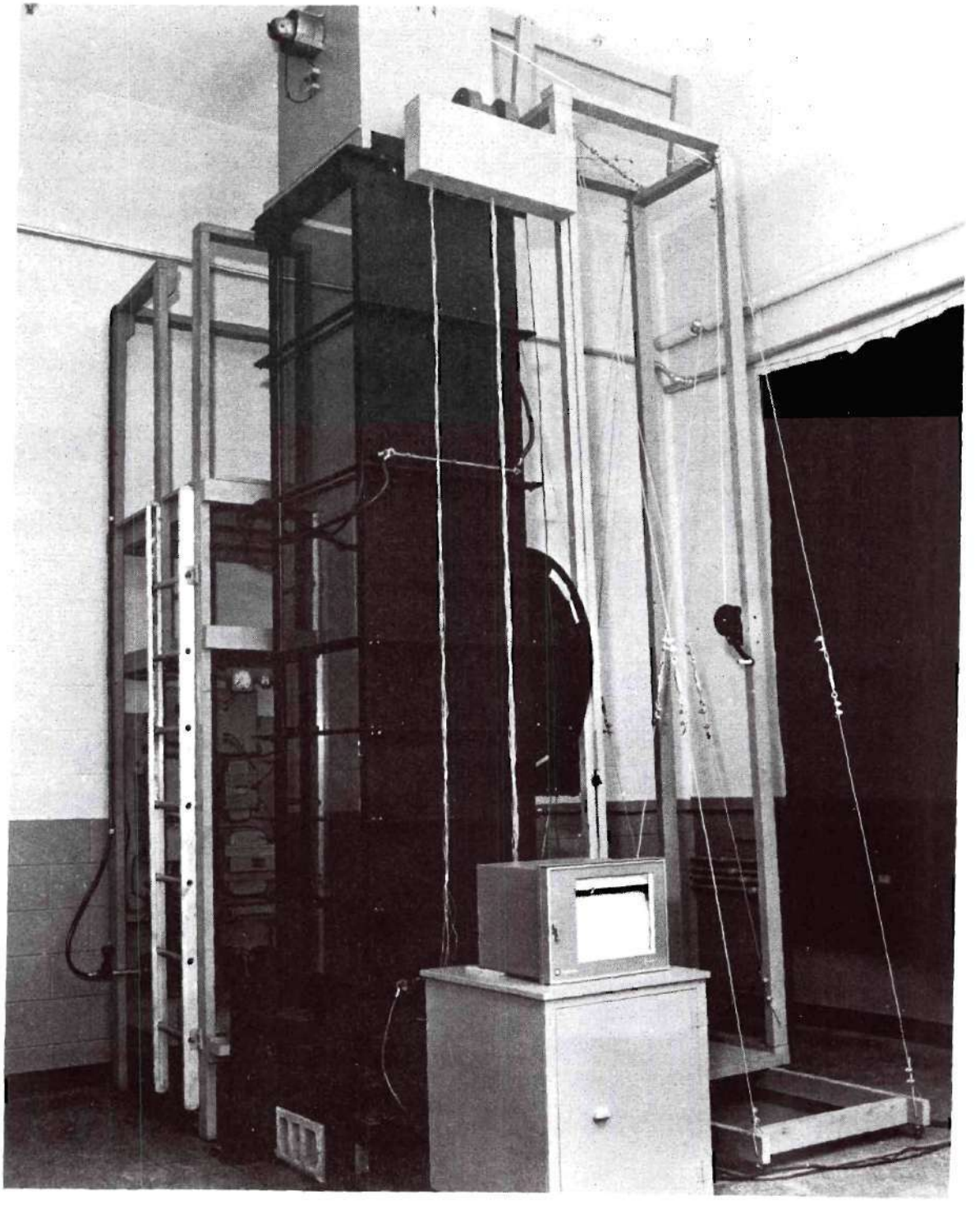

Figure 2. Experimental Test Apparatus.

fluid and two sides are transparent to permit observation of the fluid motion. The side heating surfaces are made of 0.025-inch Inconel sheet backed by a 2-inch layer of Pittsburg-Corning Foamglass insulation and a 0.25 - inch aluminum support plate. The bottom heater utilizes 0.018-inch Inconel. At various locations from the tank bottom provision is made to connect the Inconel sheet to the electrical power system. The total maximum series resistance of both the sidewall heaters is 0.0162 ohms, and the resistance of the bottom heater is 0.0023 ohms.

Inconel was chosen as the resistive element because of its high resistivity and because available Inconel sheet was particularly uniform in thickness, chemical composition and heat treat. Stainless steel strip was considered but rejected because available tolerances in per cent of the required thickness were too large. Measurement of the Inconel sheet thickness using a precision micrometer indicates that there are no variations greater than 0.001 inches. Thus the maximum variations from a uniform heat flux should be no more than 4 per cent. Foamglass insulation was used because of its low conductivity, extremely low water absorptivity, due to its closed cell construction, and relatively high compressive strength. As the main tank construction material, aluminum was chosen for its lightness and rust resistance. However, even using aluminum, the tank weighs approximately 1,100 pounds. Thus a cable hoist is necessary to erect and lower it.

The tank is constructed mainly of angle sections and plate. Horizontal ribs are used to stiffen the heater support plate and the lower region of the inner glass plate. In addition, several struts in pure tension are used to tie two sides of the tank together. The aluminum

sections are sized so that the maximum deflection of the full tank from its original shape is less than 0.1 inches.

The transparent sides of the tank are made of two Libby-Owens Ford plate glass panels separated by a 1/2-inch air gap. The inside glass plate is 3/4 inches thick, and the outside is 1/4 inches thick. The design factor of safety for the 3/4-inch plate glass is approximately 6. The air gap between the glass plates was provided to reduce the heat loss through the glass. Using the results of reference 26, the gap width of 1/2 inch was chosen to minimize the heat flux. The total heat loss from the tank, assuming a 10°F average temperature above ambient, is approximately 0.06 KW.

Sealing the tank was one of the most difficult operations required in the construction of the entire test apparatus. There were three main problem areas:

1. Sealing up the heater-insulation-support plate system.
2. Emplacing the 3/4-inch inner glass plates.
3. Sealing the internal corner joints between the glass and the heater.

The first operation was relatively straightforward although tedious and messy. Several gallons of low viscosity polysulfide rubber aircraft fuel tank sealant were used to bond the three components together. This provided an effective internal resistance to leaks and prevented the need for any metal fasteners which could have shorted the heater plate to the tank structural members.

Before the glass plates could be emplaced in the tank, the surfaces along which the glass is supported had to be made plane. In a tank

as large as this, tolerances within 1/8 inches were impossible. Using a combination of polyester resin and metallic shims, a plane surface was finally achieved and the 250-pound glass plates were installed along with the side and the bottom heating panels.

In sealing the 2 x 3/16 x 117-inch corner gap between the glass and the heater panels, a strip of compressed oakum about 1 inch thick was first inserted. Then both high and low viscosity rubber sealant was used in several layers to fill the remaining inch. This combination provided an effective resistance to leaks but did not stop them entirely. Finally, several layers of plastic sealant, epoxy paint, flat black paint and Glyptol were used to bring the leak rate to less than 0.1 per cent per hour at maximum liquid depth. This leak rate, which became essentially zero at 6 feet of water, was considered acceptable.

Temperature Measurement System

This system is comprised of two main components:

1. The vertical temperature probe, including two horizontal temperature rakes and the surface temperature thermocouple.

2. A potentiometer system to measure the thermocouple outputs.

In addition to the surface temperature thermocouple, the probe contains 59 calibrated thermocouples located at various depths. A discussion of the thermocouple calibration is presented in Appendix E. Figure 3 and Table 1 show the probe and the nominal location of each thermocouple. The spacing between thermocouples is chosen to be approximately inversely proportional to the axial temperature gradient in the test tank. The probe is constructed of plexiglass tubing with a 2-inch inside diameter and is 119 inches long. Twenty-gage copper constantan wire with a double

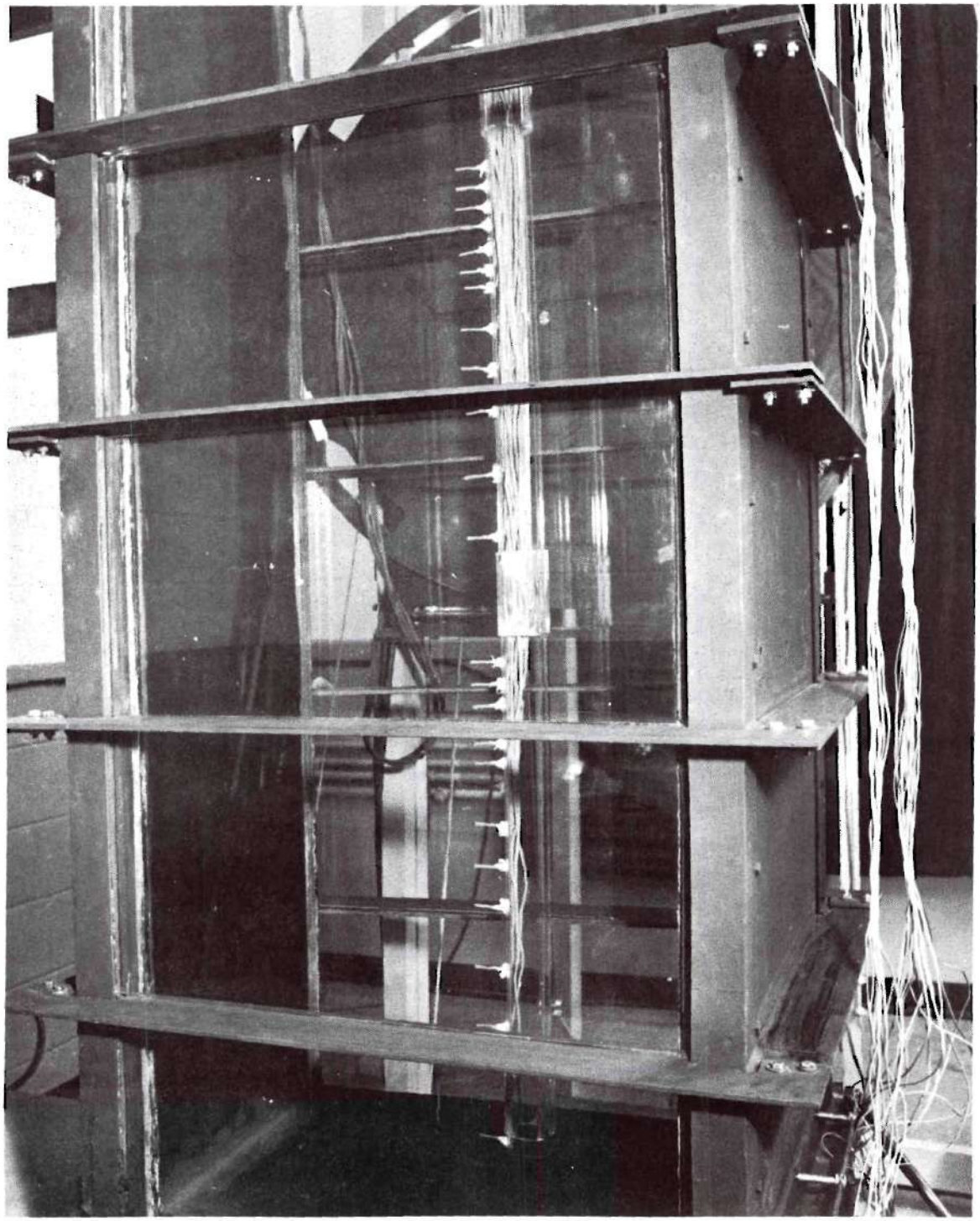

Figure 3. Vertical Temperature Probe.

Table 1. Test Sensor Locations

Sensor Number	Location (Inches from Bottom)	Sensor Number	Location (Inches from Bottom)
1	1	31	66
2	6	32	67
3	9	33	68
4	12	34	69
5	14	35	70
6	16	36	71
7	18	37	72
8	19	38	78
9	20	39	81
10	21	40	84
11	22	41	86
12	23	42	88
13	24	43	90
14	30	44	91
15	33	45	92
16	36	46	93
17	38	47	94
18	40	48	95
19	42	49	96
20	43	50	102
21	44	51	105
22	45	52	108
23	46	53	110
24	47	54	112
25	48	55	113
26	54	56	114
27	57	57	115
28	60	58	116
29	62	59	117
30	64	s	

coating of waterproof polyvinyl plastic is used for the thermocouples. The thermocouple wire passes through the center of the tube and out through holes drilled in the plexiglass. The thermocouple junctions are located about 2 inches from the probe. The wire is sufficiently stiff to prevent sagging; thus the thermocouple locations remain rela-

tively fixed during the tests.

The thermocouple leads run from the probe through a wooden rectangular duct, which also supports the probe, to a junction box near the top of the tank. A small blower is used to cool the interior of the junction box in order to minimize any temperature gradients that may exist across the junction connections, especially when the tank is full. At the junction box 16 of the 60 liquid temperature sensors are connected to leads running to the potentiometer system. Eight other channels are connected to the two horizontal temperature variation rakes.

Because of the relatively large gage of the thermocouple wire, significant conduction effects may be present. This is true primarily near the top of the tank where lead lengths to the junction box are shortest. To minimize these effects in this region the insulation within approximately 1.5 inches of each thermocouple junction was stripped off. Calculations show that this reduces the maximum error due to conduction to less than 0.04°F for thermocouples within one foot of the tank top. This error is felt to be negligible. Below one foot the error due to conduction effects is essentially zero.

The temperature-time data during most of the testing were obtained manually using a stop watch and a Leeds and Northrup millivolt potentiometer , Model 8686. A portion of the test data, however, was obtained using a Honeywell 24-channel strip chart recorder, model Electronik 16. In practically no case was the error in absolute temperature measurement for any sensor greater than ± 0.25°F. Because of the number (16) of thermocouple readings taken during each traverse, it can be shown that the resulting smoothed experimental temperature profiles themselves are

somewhat more accurate than the figure mentioned above for the individual sensors.

To obtain a measure of the profile accuracy, least square fits using up to 10th order polynomials were made to several typical test temperature profiles. The assumption of a polynomial fit to the test data is somewhat arbitrary; however, it does provide a convenient quantitative means for determining the smoothness of the data by calculation of $\bar{\varepsilon}_{rms}$, the root mean square deviation. The maximum root mean square deviation found between chosen test profiles and the corresponding polynomials was .05°F.

If, in addition to a polynomial fit, it is further assumed that the temperature errors are all random, a technique described by Hildebrand (36) allows an estimate (E_{rms}) of the root mean square deviation between the true temperature profile and the measured temperature profile to be obtained using the expression:

$$E_{rms} = \sqrt{\frac{N + 1}{N - M}}\ \bar{\varepsilon}_{rms}$$

where: $N + 1$ = Number of data points.

M = One plus the order of polynomial assumed.

$\bar{\varepsilon}_{rms}$ = Root mean square deviation between least squares fit of order n and measured temperatures.

Thus, it appears that a value of ± 0.1°F is perhaps more representative of the overall temperature error than the ± .25°F maximum error for any single sensor.

Velocity Data Instrumentation System

To obtain quantitative fluid velocity data in the tank, a photographic technique similar to that reported by Brooks (27) was used. This technique involves the photography of 0.002-inch hollow glass spheres suspended in the water. These particles, called Eccospheres, are manufactured by Emerson & Cuming Inc. An intense 4-kilowatt line source of light located in the box at the top of the tank was used to provide a thin curtain of light parallel to and midway between the glass sides. Thus the fluid motion was observed in the vertical plane of symmetry.

At the lower depths within the tank, the intensity of the light emitted from the light box is noticeably diminished. This occurs because of the divergence of the light beam and attenuation due to light absorption by the water and the particles. In addition, a significant amount of light is lost because of reflection at the surface. This situation generally requires the use of a fast film and/or a camera with a small f number lens. Even though the width of the lighted region may be several inches at the tank bottom, the fact that the particles are so small and the camera is open near its maximum aperture, in order to get as much light as possible, results in a minimum depth of field, due to the lens characteristic. Thus even though a relatively large number of particles reflect light into the camera lens, only those particles within less than 1/4 inches of the focal plane are observed. However, there is less fuzziness and greater contrast in the pictures taken near the top of the tank than in those taken in the lower regions. This is because there is more light near the top and fewer out-of-focus lighted particles.

For many of the photographs, the camera and shutter system were fastened to a large vertical frame (Figure 2) normally placed adjacent to the glass side of the tank. Using this frame, the vertical position of the camera can be changed rapidly and easily. In addition, the frame supports a boom which is used to raise and lower the light box. The whole apparatus is on rollers and can be readily moved when this is necessary.

Several different types of film and two different cameras were used in the photographic investigation. Velocity data were obtained from time exposure streak photographs and by multiple exposure photographs of the particle motion. Because the location of the particles was considerably further from the light source than in reference 27 due to the size of the present test tank, there was a significant reduction in the amount of light available. For this reason results using a 35 mm Nikon reflex camera with an f 1.5 lens were found superior to those obtained from the f 4.7, 125 mm, 4 x 5 Crown graphic presstype camera used in investigation of reference 27. In addition, the streak photographs were found to provide a less confusing and less cluttered image of the particle motion than those obtained using the intermittent exposure technique of reference 27. Thus the 35 mm Nikon camera with a calibrated 1.07 second shutter speed was used with Tri-X film in all of the pictures of the particle motion shown here.

In addition to the suspended particles, a 6-inch Schlieren system manufactured by the Aerolab Supply Company was used to study the fluid flow within the test tank. Since mirrors used in the Schlieren are essentially fixed, an additional system of 4 adjustable second-surface

mirrors mounted on the test tank was devised. This allows the fluid motion in any region within the tank to be studied, although there is some loss of light and image sharpness due to the multiple reflections.

Power Supply, Pump and Filtration System

Because of the low resistance of the heaters, low voltage currents up to 600 amperes are necessary to provide the desired heating rates. This requires the use of a system of large transformers with appropriate control devices to vary the power over the desired range. To provide independent operation of the bottom and side heaters, two separate systems are necessary. The side heating system utilizes a 7.5 KVA transformer controlled by a 5 KVA saturable reactor. The bottom heating system utilizes a 7.5 KVA transformer controlled by a 2 KVA saturable reactor. Both transformers and saturable reactors were manufactured by the General Electric Company. The saturable reactors are controlled in turn by a small, variable transformer-silicon rectifier bridge system which produces a variable voltage direct current. Using the system described, it is possible to obtain maximum heating power levels of approximately 5 KW for the side heater and 1 KW for the bottom heater.

To empty the test vessel a 3/4-horsepower pump connected to a length of garden hose, which enters the tank from above, is used. A simple drain at the tank bottom must be avoided to preserve the test conditions of a uniform wall heat flux. Because of the technique chosen for observing the fluid motion, it is necessary to maintain the test water as free of dirt and dust particles as possible. To accomplish this a filtration system is used to remove extraneous particles down to 5 microns in diameter. This practically insures that the only visible

particles are the Eccospheres. The filtration unit includes a 1/3-horsepower motor, a small centrifugal pump and a Cuno Micro Klean filter unit.

Test Procedure

To obtain both fluid temperature data and fluid velocity data, it was necessary to conduct duplicate tests since simultaneous operation of the photographic equipment and the potentiometer was not practical. In the temperature testing, the liquid depth in the test tank was first established and the liquid agitated to obtain a desired thermal equilibrium state. This procedure was relatively simple at liquid depths of 2 feet, but at depths of 6 feet and 9.75 feet it was surprisingly difficult to obtain a constant temperature throughout the tank. For this reason, some of the tests at depths of 6 and 9.75 feet were begun with small axial temperature gradients present. In no case, however, did the variations from the initial mean temperature exceed 0.15°F.

At least once each day before testing began, the temperature data system was calibrated. This was accomplished by locating the moveable surface probe at different points in the tank and comparing its output with the output of various thermocouples. It was found that the system calibration changed from day to day by small amounts, generally less than 0.25°F. This change in the system calibration is largely responsible for the possible error of ± 0.25°F in absolute temperature present for each sensor. During any single test, however, the calibration of the system changed only slightly; and therefore the errors present in terms of temperature changes are considerably less than the absolute error.

The variations in the system calibration are believed to have resulted from changing thermal gradients present in the lead wire connections both at the junction box located near the top of the tank and in the connections to the potentiometer selector switch. Every effort was made to minimize these gradients but they could never be eliminated entirely.

Once the desired initial conditions were obtained and the test liquid was in a quiescent state, simultaneously the chosen heating conditions were established by introducing low-voltage current into the heaters and the stop watch was started. The former operation could usually be accomplished within approximately 10 seconds. Then at various intervals during the test, traverses of the axial temperature profile were made. In some tests both axial and horizontal temperature measurements were obtained. The test ended when the thermal behavior approached a quasi-steady state in which all temperatures became approximate linear functions of time. The time versus thermocouple output data taken during the tests were in most cases manually recorded on the input forms for the data reduction computer program. This allowed rapid computer processing of the test data and provided a continual status report on the results of the testing. A discussion of this program, together with a listing is presented in Appendix C.

In the photographic studies of motion in the test tank, somewhat more elaborate preparations for the testing were required than in the temperature studies. These preparations are discussed in some detail by Brooks (27). Briefly, they consisted of emptying and thoroughly cleaning the inside of the test tank from the previous operation, filling the tank

with filtered tap water, and then continually filtering the water over a period of 24 to 72 hours. This procedure, when properly followed, guaranteed almost perfectly clear, deaerated water for use in the testing. Approximately one half hour before the beginning of tests using the suspended particles, the Eccospheres were injected into the water near the bottom of the tank. Since the glass particles are less dense than the water, and because some flow disturbance was usually created by the injection, the particles gradually rose up and appeared to fill the tank approximately homogeneously. The quantity of particles injected varied somewhat between the tests; however, best results were obtained when r, the number of particles per cubic inch, was in the range

$$100 < r < 500$$

Testing began when the particles were for practical purposes at rest. Throughout the testing, a record was made of the time and duration of the various exposures. During each exposure the camera f number was manually decreased, thus making the forward portion of each streak brighter than the rear and giving a sense of direction to the traces. In tests utilizing Schlieren photography, the above procedure was also followed, except no particles were used.

Test Results

Fluid Thermal Behavior

In the experimental study of fluid thermal behavior a total of 30 tests were conducted in which Gr^* was varied from 1.3×10^{11} to

5×10^{14}, L/H varied between 1 and 4.88, and q_b/q_s varied between 0 and 9.4. A summary of this program appears in Table 2. To insure accuracy of the test results, more than 20 per cent of the tests were rerun. The results showed that the tests were reproducible to a satisfactory precision and thus provide confidence in the overall program. For example, test 2100 was rerun and the maximum root mean square deviation between the two tests was 0.1°F.

Typical measured centerline temperature profiles obtained from the testing are shown in Figures 4, 5, 6, and 7 at different times. A tabulation of all the data from the 30 tests is presented in Appendix F. In Figures 4, 5, and 6, the dimensionless temperature ratio θ_l/θ_{lmax} is presented as a function of the dimensionless height X/L. Figure 4 illustrates the thermal behavior of the fluid with side heating only in the lower range of Gr^* investigated. It is seen that the thermal stratification begins immediately after sidewall heating commences and gradually penetrates to the bottom of the test tank. It is interesting to note that while the initial curvature of the profile is convex toward the surface, it becomes decreasingly so and finally approaches an almost linear form. Results from other tests in the same range of Gr^* indicate that for even longer test times the shape becomes slightly convex downwards. Of interest is the fact that the temperature at the tank bottom did not change for practical purposes even for extended test times, as in test 1000.

Figure 5 presents the thermal behavior of the fluid with side heating only in the upper range of Gr^* investigated. From the onset of heating, there is marked difference in the shape of the temperature

Table 2. Summary of Test Conditions

Test No.	L/H	q_b/q_s	Gr^*_{max}	Test Time (sec)	$\bar{\theta}_2$ (°F)	$\bar{\theta}_{2max}$ (°F)	q_b Btu/sec-ft^2	q_s Btu/sec-ft^2
0100	1	1.29	1.55×10^{12}	2100	8.37	10.1	.1933	.150
0200	1	.92	2.97×10^{12}	2450	8.87	11.74	.141	.153
0300	1	0	1.75×10^{12}	2400	6.23	14.78	0	.171
0400	1	3.67	6.86×10^{11}	2400	5.89	6.78	.197	.0536
0500	1	1.57	5.81×10^{11}	2400	3.91	5.58	.0888	.0565
0600	1	.802	5.68×10^{11}	3600	4.77	7.87	.0473	.059
0700	1	0	5.48×10^{11}	3600	3.66	8.62	0	.0632
0800	1	8.14	1.54×10^{11}	3600	5.21	5.53	.144	.0177
0900	1	.875	1.32×10^{11}	4800	1.57	2.66	.0124	.0141
1000	1	0	1.61×10^{11}	5400	1.77	3.44	0	.0204
1100	3	1.775	9.14×10^{13}	2016	5.22	8.39	.22	.124
1200	3	.941	1.09×10^{14}	2304	5.09	8.55	.1115	.1183
1300	3	0	1.078×10^{14}	2304	4.81	10.168	0	.1295
1400	3	3.92	5.7×10^{13}	3600	5.027	6.053	.204	.052
1500	3	1.91	5.67×10^{13}	3200	3.59	5.22	.101	.053
1600	3	1.09	5.28×10^{13}	3200	2.82	5.083	.0502	.046
1700	3	0	5.14×10^{13}	3200	2.68	4.408	0	.052
1800	3	9.4	1.07×10^{13}	5250	3.18	3.66	.1385	.0147
1900	3	0.97	1.35×10^{13}	6000	1.66	2.57	.0144	.0148
2000	4.88	0	1.41×10^{14}	7200	2.072	3.08	0	.0179
2100	4.88	1.35	5.01×10^{14}	1800	4.01	7.72	.164	.121
2200	4.88	.95	5.28×10^{14}	1800	3.63	6.52	.108	.114
2300	4.88	0	5.22×10^{14}	1800	3.13	6.19	0	.108
2400	4.88	4.13	2.11×10^{14}	2700	2.67	3.73	.178	.043
2500	4.88	1.876	1.97×10^{14}	2700	2.13	3.39	.077	.041
2600	4.88	.96	2.24×10^{14}	3600	3.11	5.17	.047	.049
2700	4.88	0	2.1×10^{13}	3600	2.61	4.59	0	.045
2800	4.88	1.8	7.33×10^{13}	5400	1.62	2.40	.0289	.016
2900	4.88	.912	8.13×10^{13}	5400	1.68	2.62	.0164	.018
3000	4.88	0	8.7×10^{13}	5400	1.63	2.69	0	.019

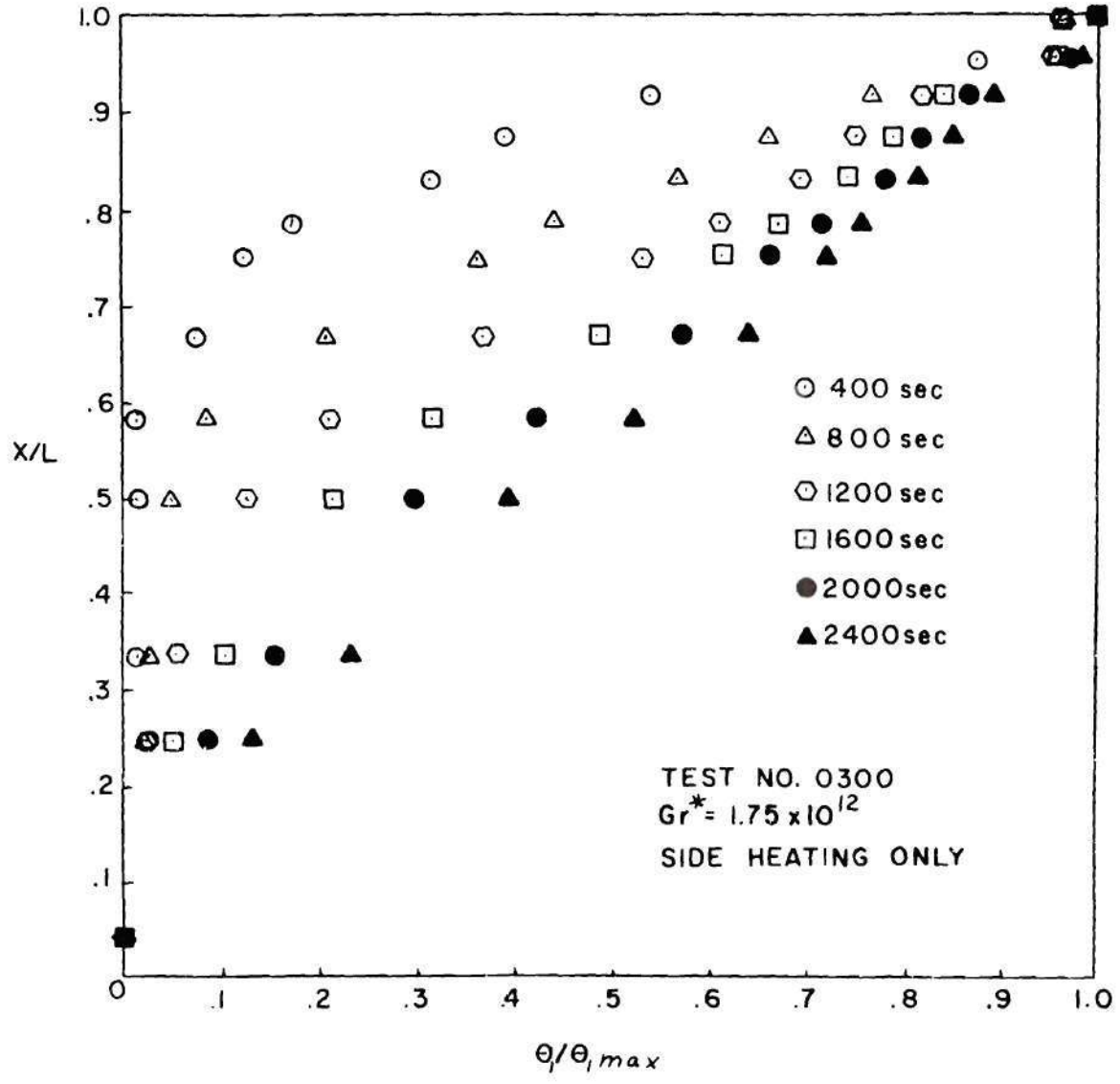

Figure 4. Temperature Profiles with Side Heating Only.

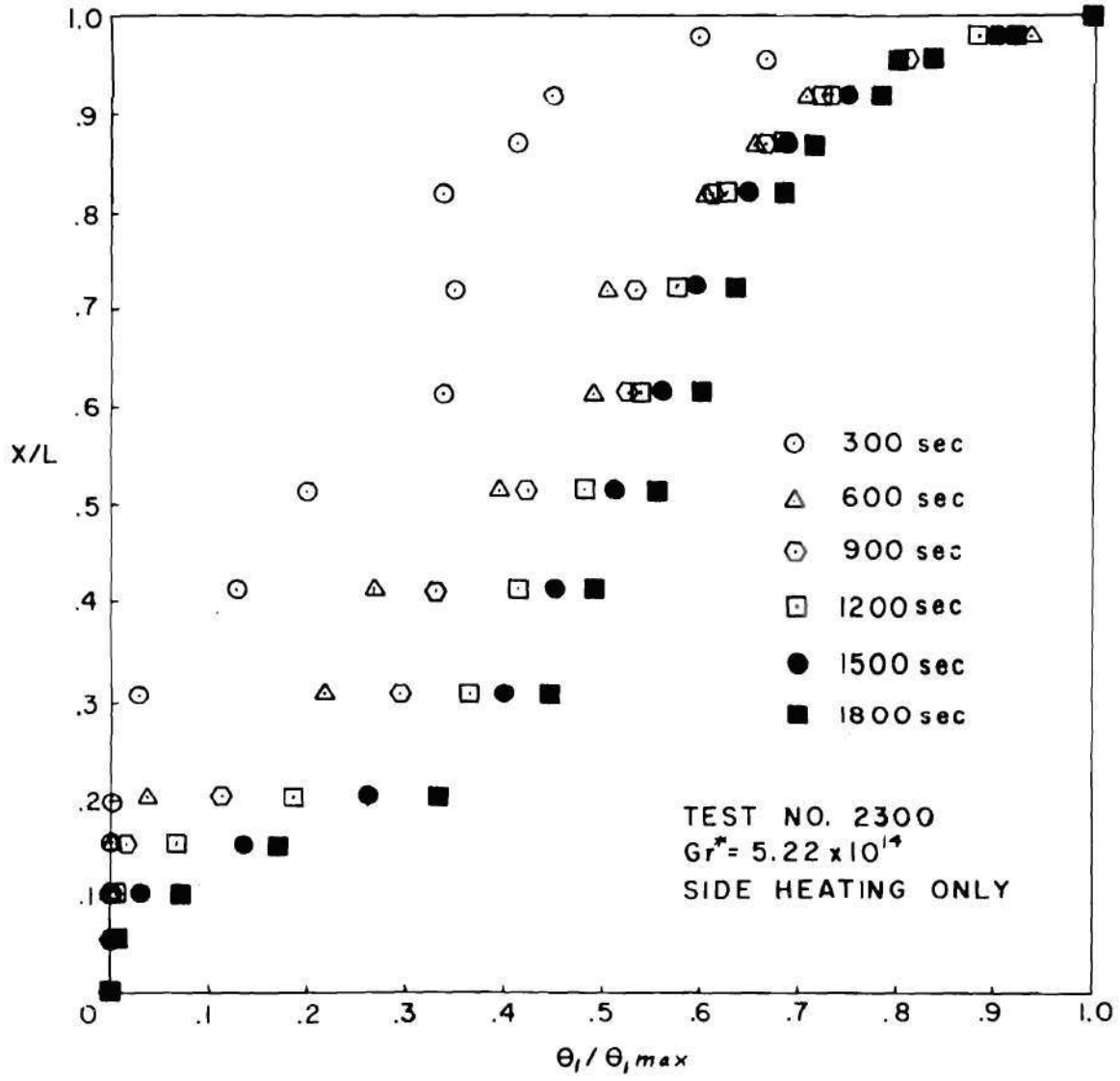

Figure 5. Temperature Profiles with Side Heating Only.

profile from that observed in Figure 4. While the shape of the temperature profile in Figure 4 is relatively simple with no inflection points, it is seen that for Figure 5 there are always two inflection points. Again the bottom temperature remained fixed during the entire test. A point of interest is the zero slope of the temperature profile near the tank bottom. Thus it appears that even for very long test times:

$$\theta_1(0,\tau) = \left.\frac{\partial\theta_1}{\partial x}\right|_{x=0} = \left.\frac{\partial\theta_1}{\partial\tau}\right|_{x=0} = 0$$

The double inflection characteristic at large values of Gr^* is distinctly different from the results reported by Harper, et al. (12), where even at $Gr^* = 10^{14}$ the temperature profiles were simply curved as in Figure 4. This variation may be the result of the difference in the physical scale of the tests and the fact that a definite distance is required for transition from laminar to turbulent flow. There is, however, a strong similarity to the S-shaped temperature profiles reported by Neff, Bailey, and Vliet in generally larger test vessels.

Figure 6 illustrates a typical thermal response to combined bottom and side heating. From the figure it is seen that characteristic of the results with combined heating is the similarity of the temperature profiles once the stratification approaches its asymptotic depth. The temperature near the tank bottom was subject to strong and rapid fluctuations due to the induced circulation patterns. Thus the temperatures shown are instantaneous and not mean values at the time indicated. Usually there is a decrease in temperature moving away from the bottom and

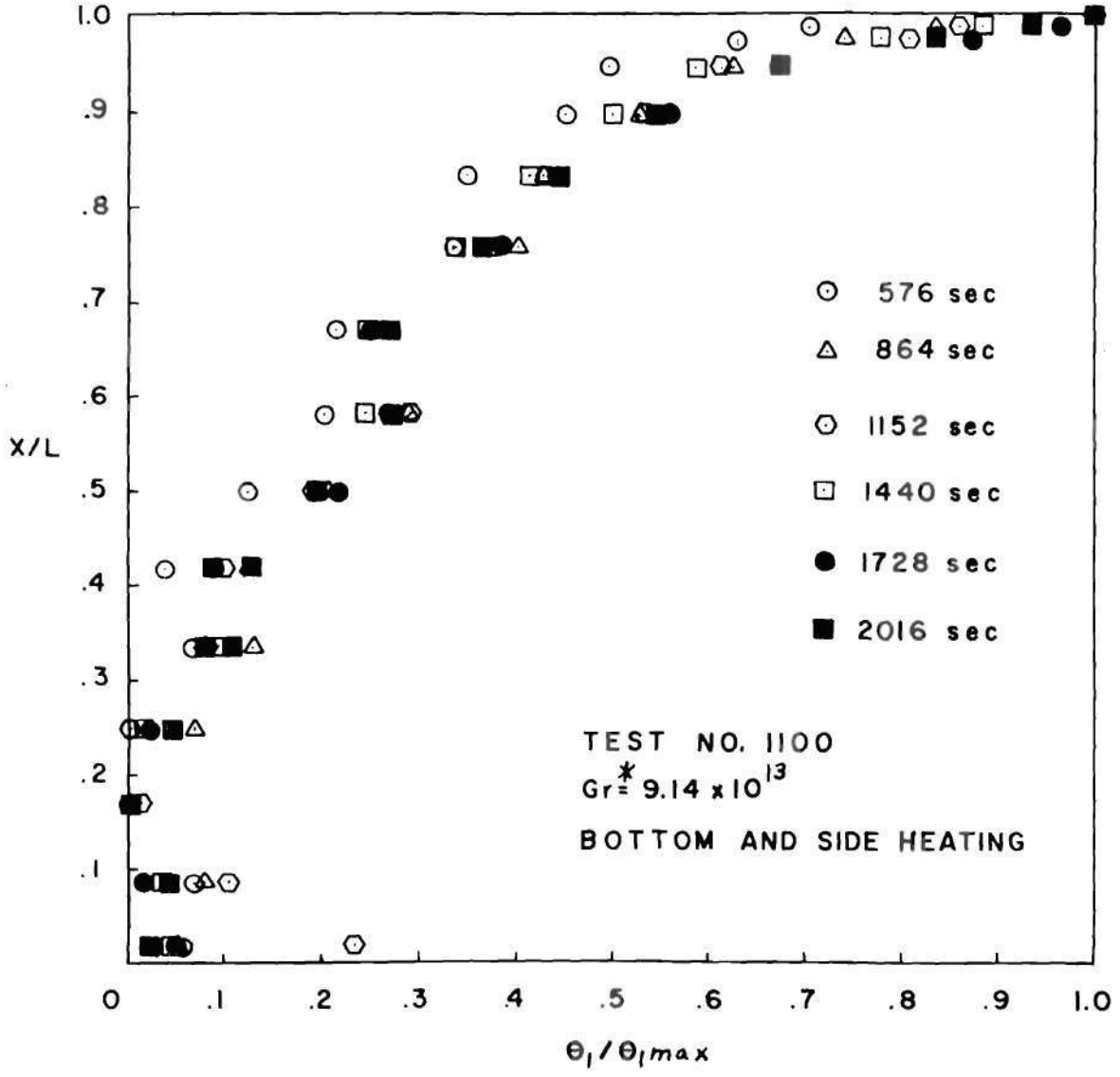

Figure 6. Temperature Profiles with Combined Bottom and Side Heating.

the temperature reaches a minimum for values of X/L between 0.1 and 0.3 and then rises toward the surface temperature. Close inspection of the temperature profile reveals the presence of two inflection points as in Figure 5. This type behavior was also observed more distinctly in the results of testing with bottom heating at L/H = 4.88; however, it was not present in the results with bottom heating at L/H = 1.

In Figure 7, the effects of increasing the ratio q_b/q_s are illustrated. Here the dimensionless temperature θ_2/θ_{2max} is plotted versus X/L. The use of the ratio θ_2/θ_{2max} rather than θ_1/θ_{1max} is made in this case because the former gives a better representation of the shape of the temperature profile than the latter. This is because the ratio θ_1/θ_{1max} tends to magnify variations in the temperature profile at a given time, while the ratio θ_2/θ_{2max} puts the temperature variations in a more proper perspective. From the figure, the near uniformity in the temperature profile, even for early test times, is apparent. For larger values of q_b/q_s the temperature profile becomes even more nearly constant as in test 1800.

As a part of each test series temperature traverses were made at various elevations in the bulk fluid to check for the possible existence of horizontal temperature gradients. It was found that they were negligible, a fact which confirms the findings of Tatom, et al. (9), Harper, et al. (12), and Barakat and Clark (21).

Fluid Motion

In the investigation of fluid motion within the test tank, the thermal conditions corresponding to tests 1100 and 1300 were studied.

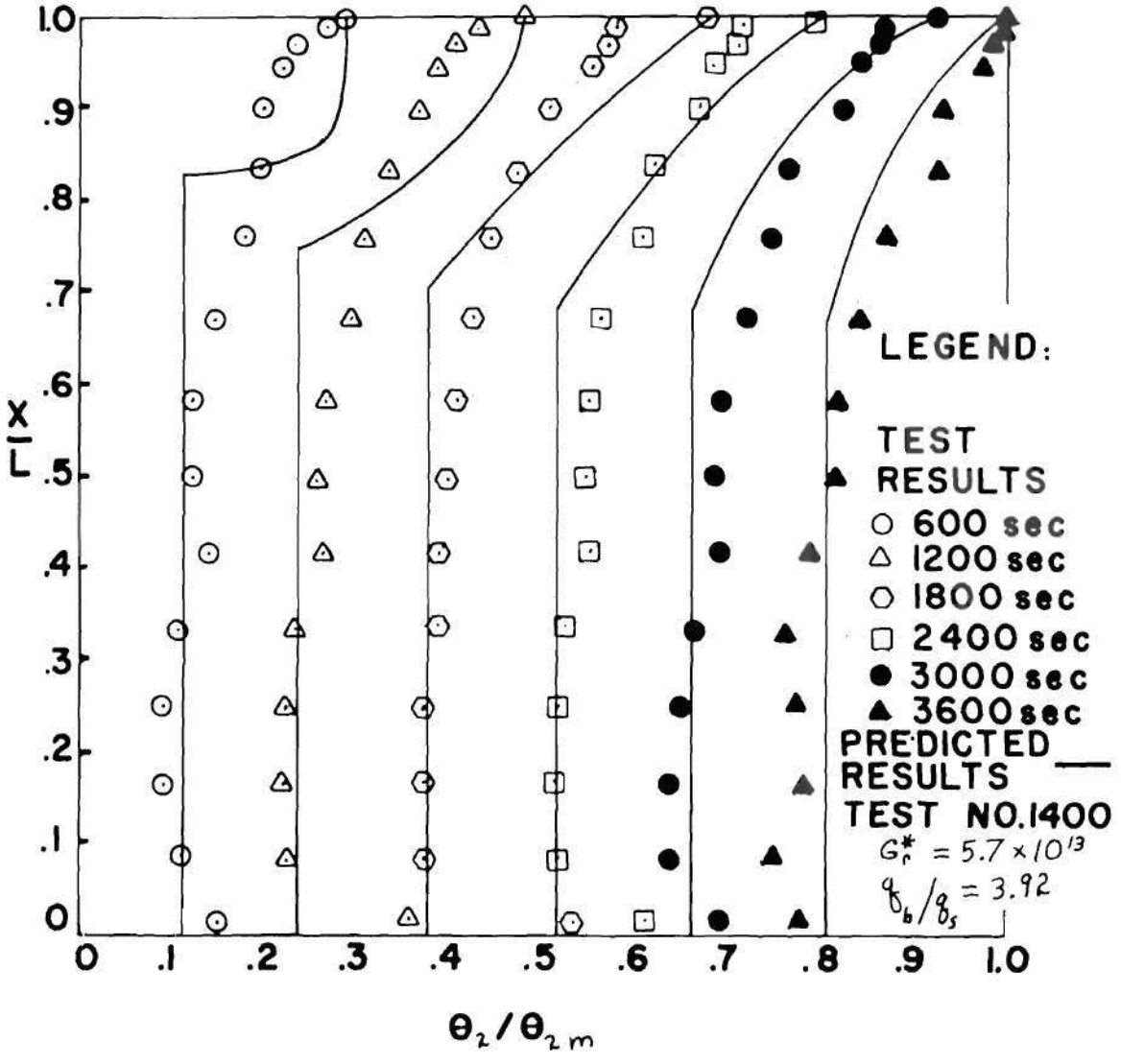

Figure 7. Temperature Profiles with Combined Bottom and Side Heating.

Fluid motion and velocity data were obtained using a Schlieren system and by photographic observation of the motion of particles suspended in the water. Numerous photographs of the fluid behavior were taken using both techniques at various times and locations within the test tank. These photographs provide both qualitative and quantitative information on the fluid motion.

Figures 8 and 9 present typical particle streak and Schlieren photographs of the flow near and within the natural convection boundary layer along the vertical sidewalls with side heating only. Examination of Figure 8 shows the presence of at least two vortices at the outer region of the turbulent boundary layer which indicates that fluid is simultaneously leaving and entering the bulk liquid. The type motion shown in both pictures occurs in all predominantly turbulent regions and for all time after the boundary layer has been established. In addition this type flow is present in both the stratified and the unstratified regions of the tank. From these pictures and others taken at earlier times, together with motion pictures taken using the Schlieren system, it appears that the presence of vortices at the outer edge of the boundary layer is a characteristic of turbulent free convection flows, a conclusion which verifies the speculation of Griffiths and Davis (35).

Fluctuations at the outer edge of the turbulent free convection boundary layer have also been observed by numerous investigators. For example, the results of Eckert and Soehngen (30)(31) using interferometry photographs of the free convection boundary layer demonstrate this clearly. To quote from the second paper: "In the outer portion of the boundary layer, the scale of the fluctuations is remarkably large."

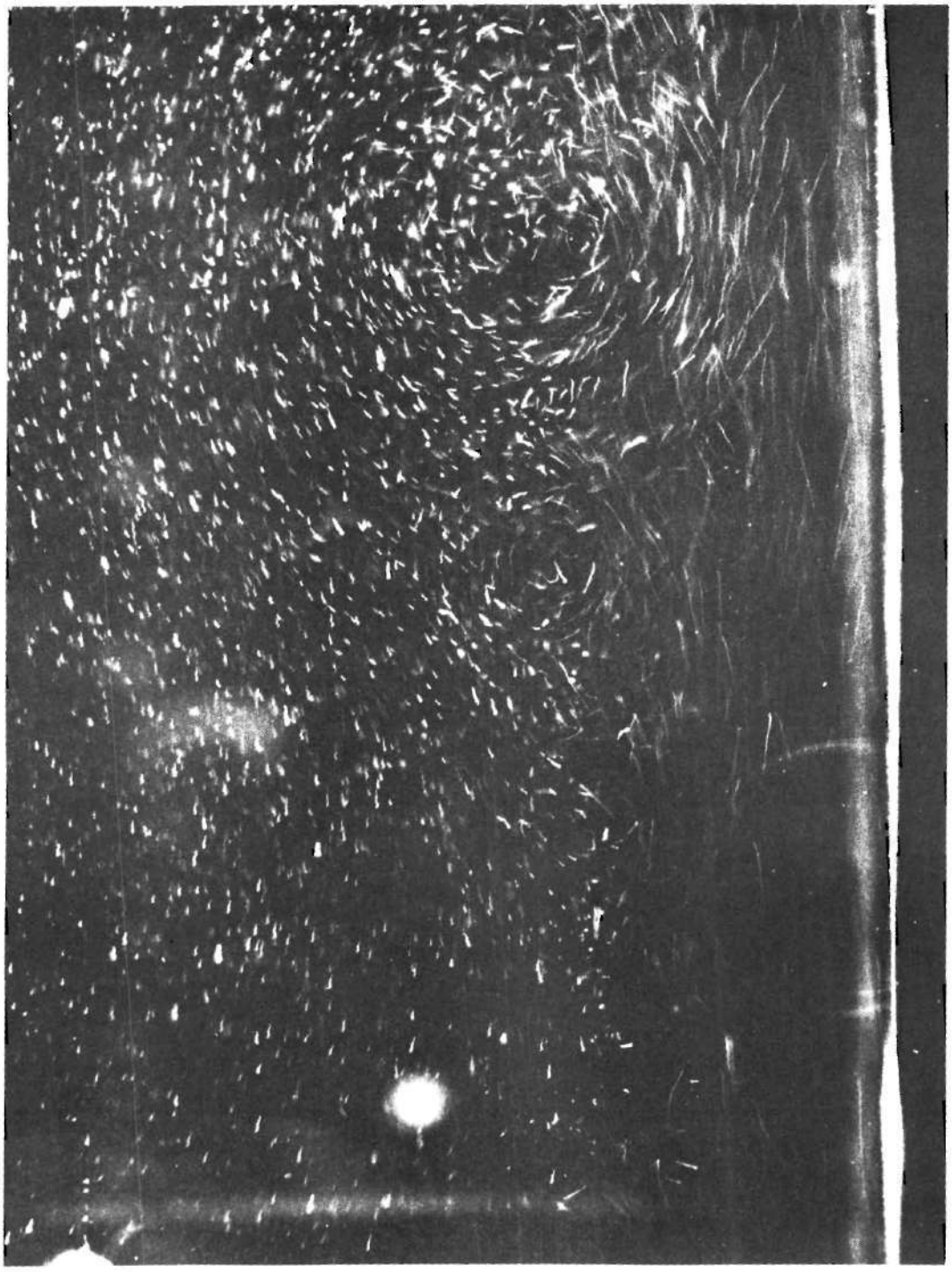

Figure 8. Particle Streak Photograph In and Near Boundary Layer. $Gr^* = 2 \times 10^{13}$, $\tau = 90$ sec.

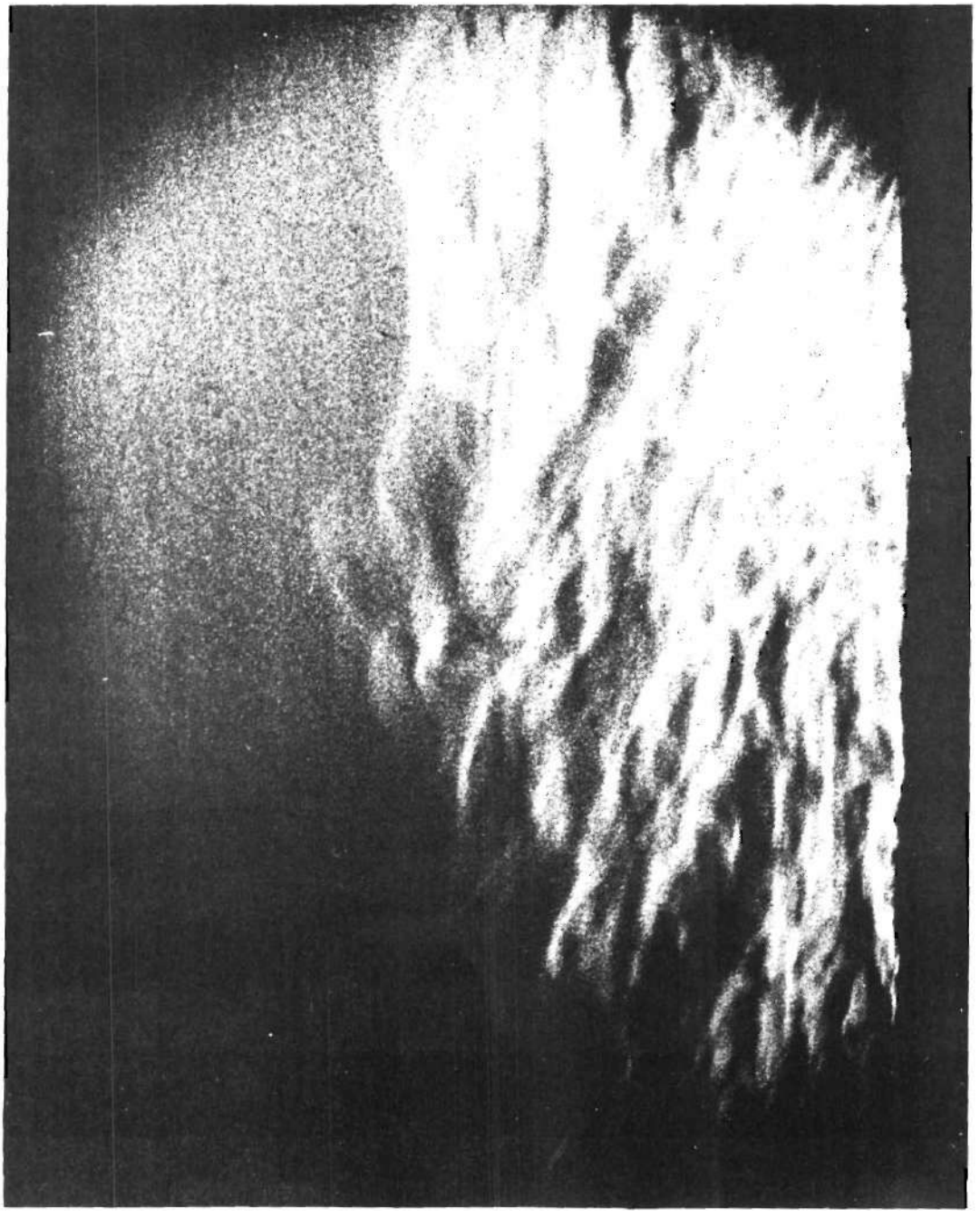

Figure 9. Schlieren Photograph of Boundary Layer.
$Gr^* = 2 \times 10^{13}$, $\tau = 66$ sec.

In another paper by Eckert, et al. (32), an unsuccessful attempt was made using a hot wire anenometer to accurately measure the velocity profile in a tube with combined turbulent forced and free convection. The large velocity fluctuations present in the boundary layer were given as one of the reasons for the lack of accuracy in the measurements. In a still more recent paper by Mordchelles-Regnier and Kaplan (33), the steady transitional and turbulent natural convection boundary layer flow in a vertical air gap with heating and cooling at opposite sides was investigated. Interferometer photographs taken of the turbulent boundary layer bear a strong resemblance to those of (31) and to the Schlieren photographs presented here.

In Figure 8 the presence and extent of the region of high shear between the boundary layer and the downward moving bulk liquid is of considerable interest since it effectively restricts the bulk liquid motion and, therefore, increases its velocity. An analysis of the motion shown in Figure 8 has been made using a method described in Appendix G. A sketch of the results is presented in Figure 10. The figure shows qualitatively the flow field observed and typical velocity magnitudes. In addition, the figure divides the flow field into three regions: the boundary layer, the vortex layer, and the bulk flow; and presents approximate values for the thickness of the first two. Using the method mentioned above, an investigation of the product $\bar{U}\delta$, which governs the growth of the thermal layer, was also made from the results of the picture. It was found that while separate values of $\bar{U}$ and δ differ significantly from those predicted, the product was within 5 per cent of that computed using the analysis of Appendix A. Thus it appears that

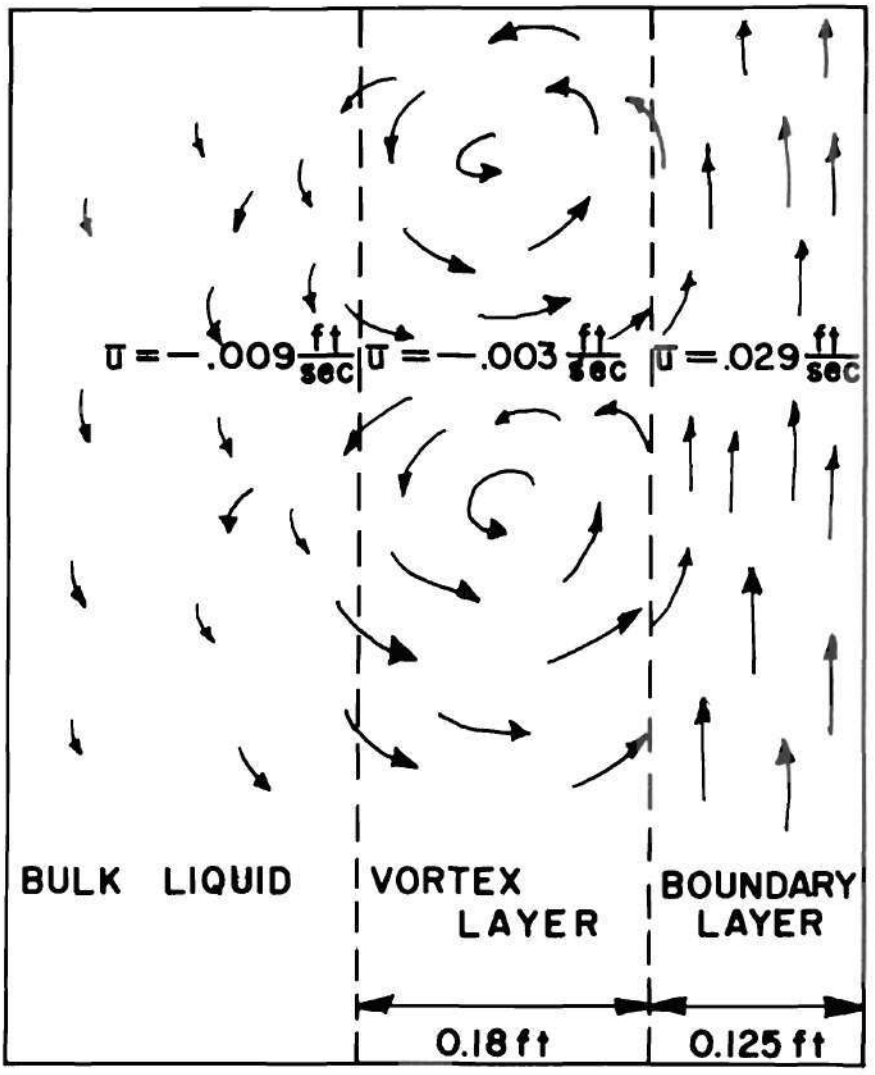

Figure 10. Analysis of Flow In and Near Boundary Layer.

even though there is a loss of warm fluid from the boundary layer, the approximation of simple turbulent boundary layer flow near the sides provides a good method for calculating the free convection flow into the thermal layer.

Figures 11 and 12 present typical Schlieren and particle photographs taken at the bottom corner with combined bottom and side heating. Both pictures illustrate the complexity of the flow near the bottom under these heating conditions. Upon initiation of heating, the Schlieren pictures indicate a flow development similar to that observed by Jacobs (28); however, the "mushroom" lobes seem to grow much faster near the corner with the heated vertical surface. After only a short time a relatively uniform thermal front is formed which moves upward into the cooler liquid. After considerable time passes, the character of the motion seems to change and becomes extremely random or of a very coarse turbulence. Occasionally the flow becomes more orderly as illustrated in Figure 12. Here it appears that a very large circulation pattern has formed.

Figure 13 presents a Schlieren photograph of motion close to the liquid surface near the sidewalls with side heating only. The behavior shown bears a strong resemblance to the Schlieren photographs presented in (19). Figure 14 presents an overall view of the particle motion in the top portion of the test tank. For this picture the camera was located 33 inches from the outer glass panel, or approximately 45 inches from the focal plane. The picture clearly shows the symmetry of the fluid motion which appears almost laminar in the inner regions. This laminar flow, however, ultimately gives way to a coarse turbulence.

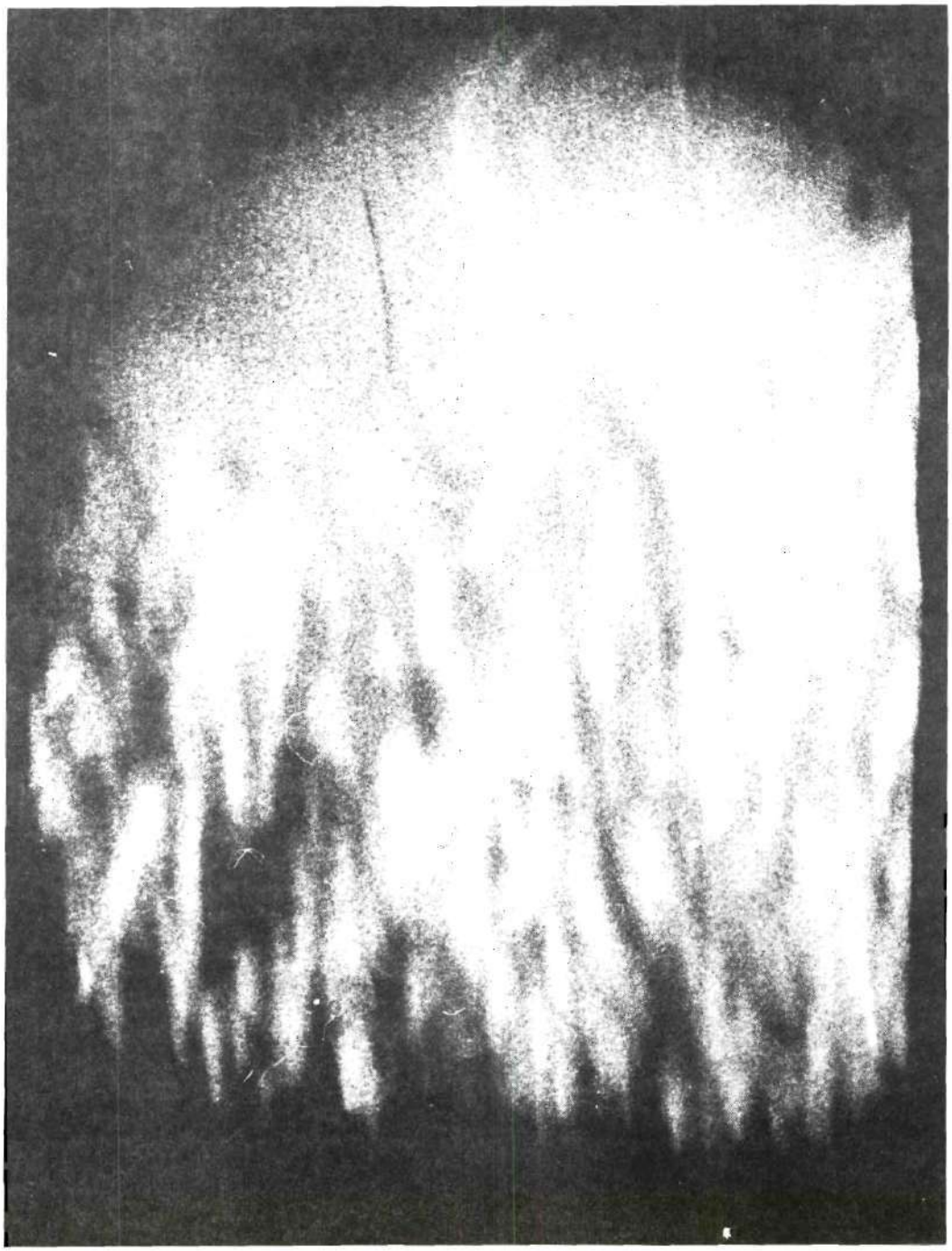

Figure 11. Schlieren Photograph Near Bottom with Combined Heating. $q_b/q_s = 1.7$, $\tau = 39$ sec.

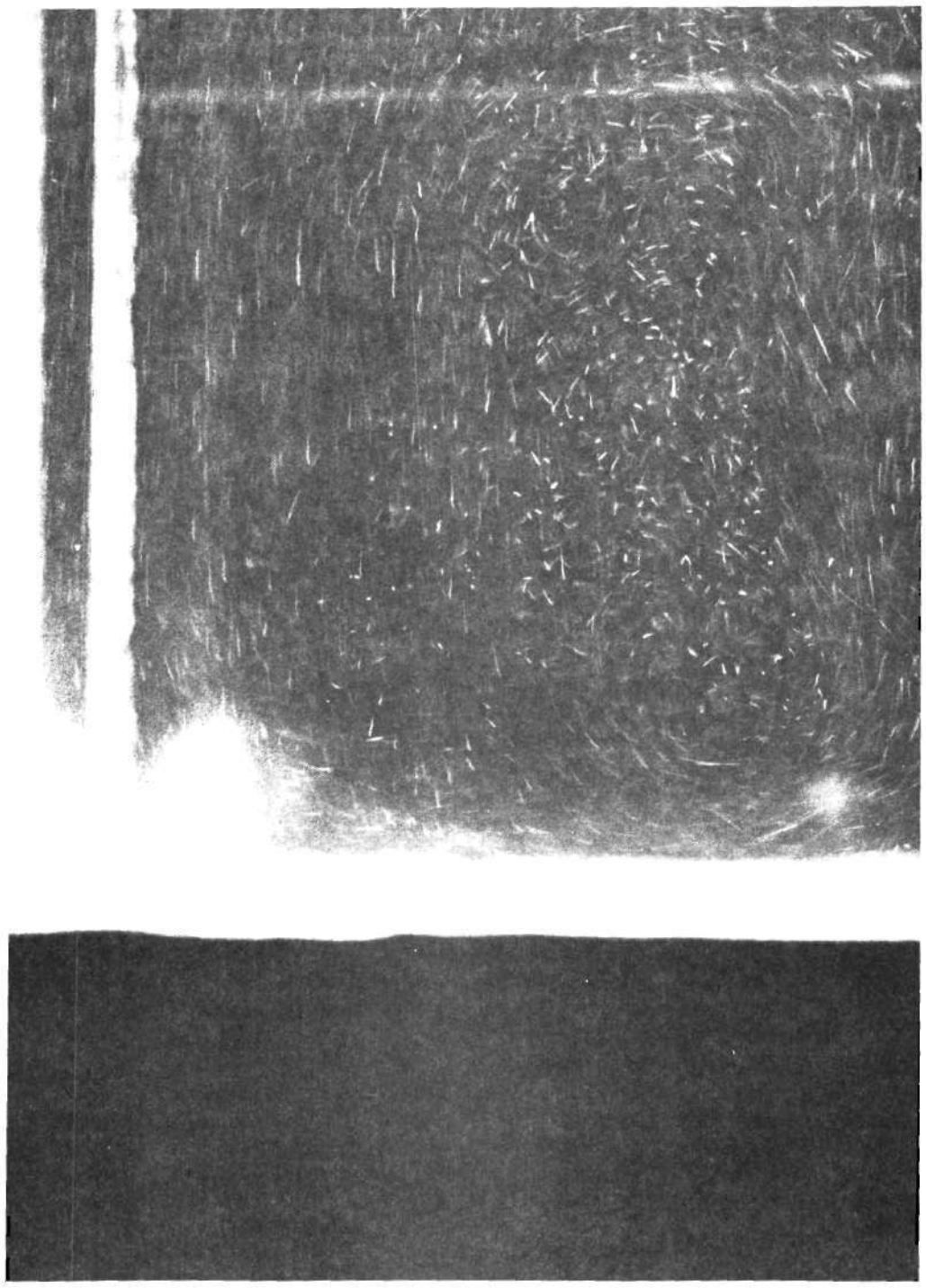

Figure 12. Particle Streak Photograph Near Bottom with Combined Heating.
$q_b/q_s = 1.7$, $\tau = 156$ sec.

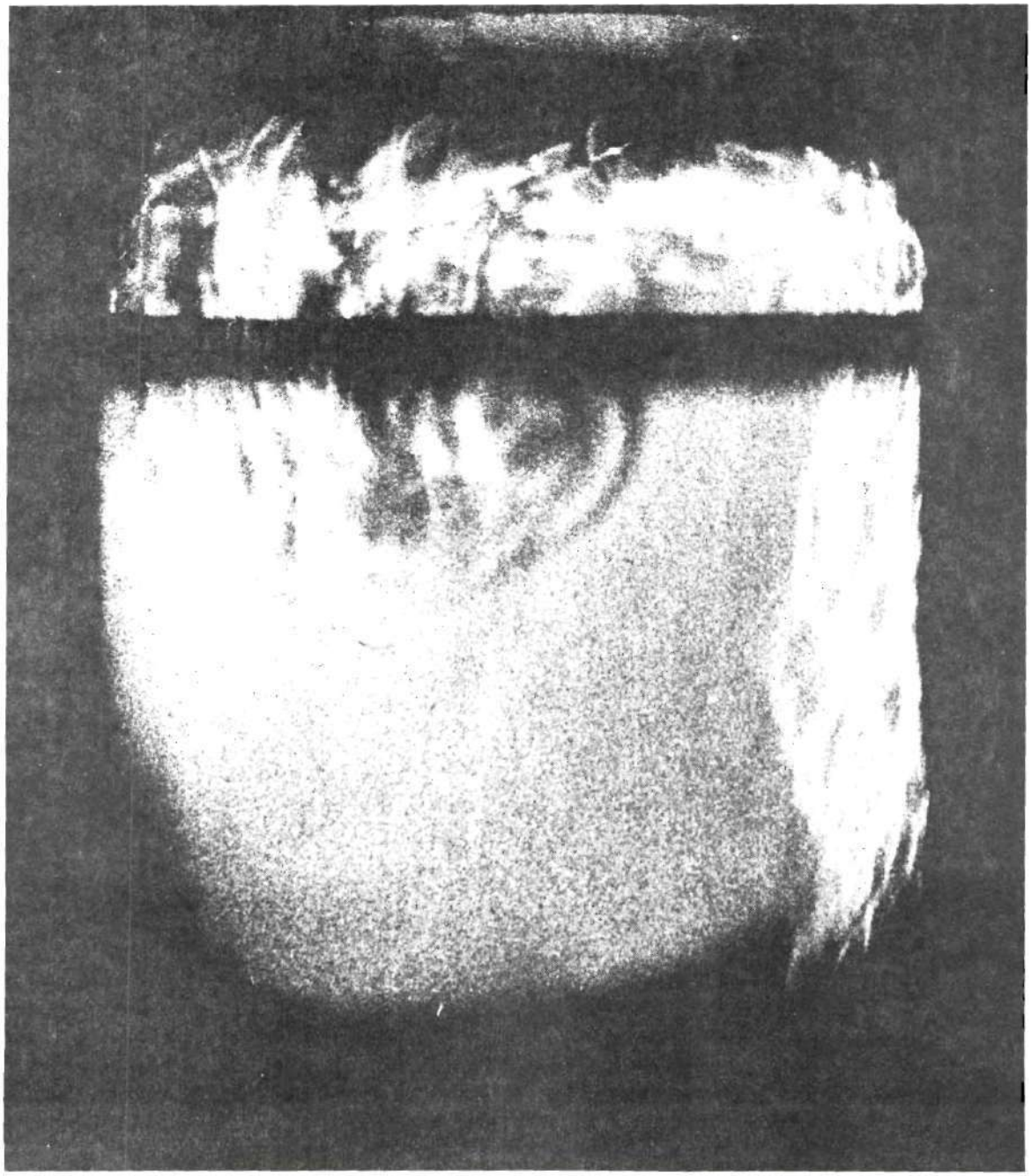

Figure 13. Schlieren Photograph Near the Surface Close to the Sidewalls with Side Heating Only. $Gr^* = 7 \times 10^{13}$, $\tau = 48$ sec.

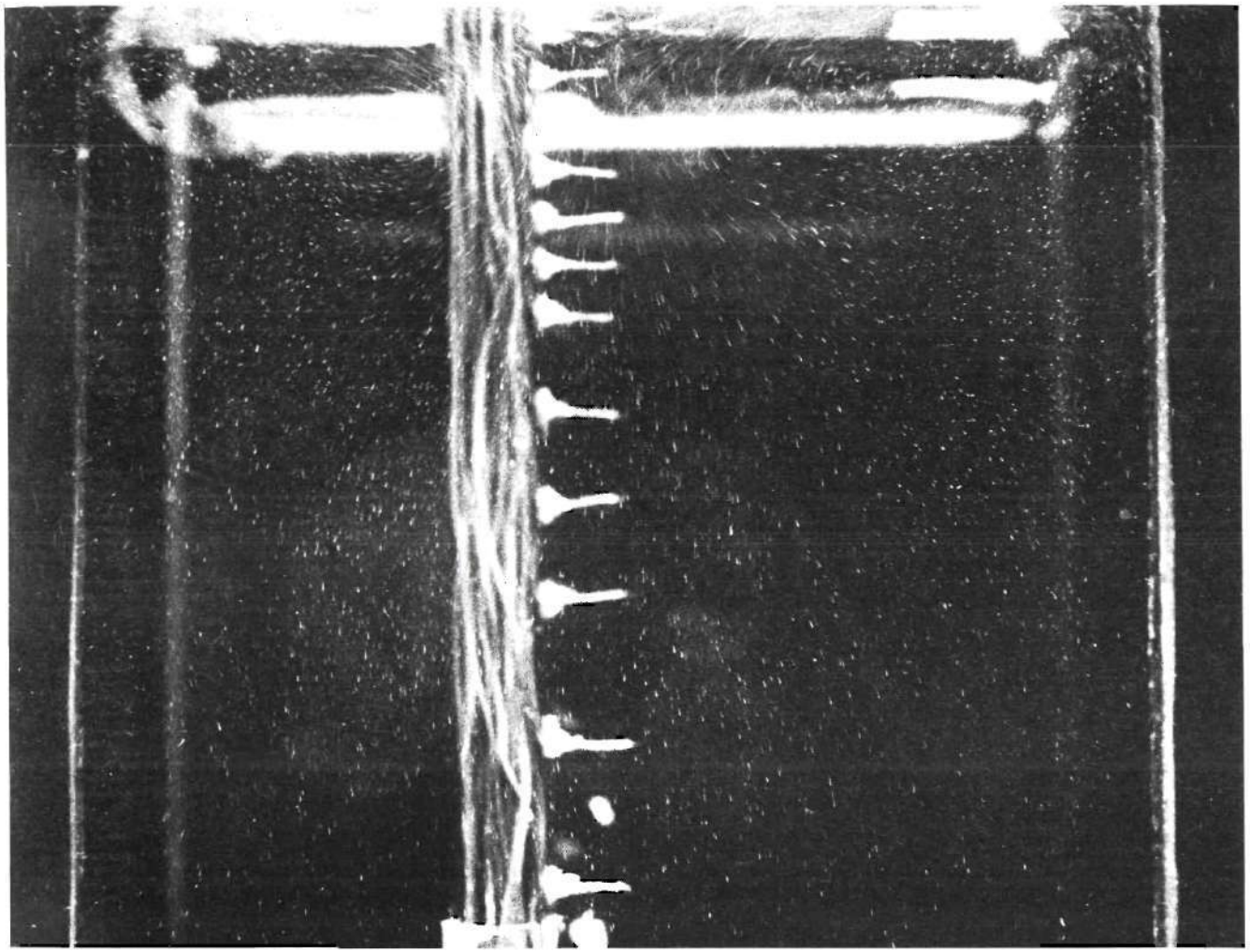

Figure 14. Particle Streak Photograph of Upper Region of Test Tank with Side Heating Only.
$Gr^* = 7 \times 10^{13}$, $\tau = 78$ sec.

CHAPTER IV

ANALYTICAL PROGRAM

Correlation of Test Data

To correlate the temperature data a thermal model and an analysis of the fluid behavior are needed. While the model previously discussed has its shortcomings, many of which are noted by Clark (29), for turbulent flow there seems at this time no way to avoid its simplifications and semi-empiricism and still obtain workable answers. Since no better model appears available, the present one has been adopted. Expanded and improved versions of the analyses of references 8 and 9 have been used, respectively, to correlate the data with side heating only and with combined side and bottom heating. In the latter case, K_o has been redefined as the fraction of the sidewall heating which is transfered through the boundary layer directly to the bulk liquid. Conveniently the change in the definition of K_o together with a few other necessary modifications can be made with hardly no increase in the complexity of the original analysis. A detailed description of these analyses is presented in Appendices A and B.

To compare the predicted results with the experimental data, Figures 15, 16, 7, and 17 are presented. In Figures 15, 16, and 17, as in Figure 7, the data are plotted using the ratio θ_2/θ_{2max}. This ratio allows a comparison between the predicted and the experimental results which illustrates the ability or inability of the analysis to predict

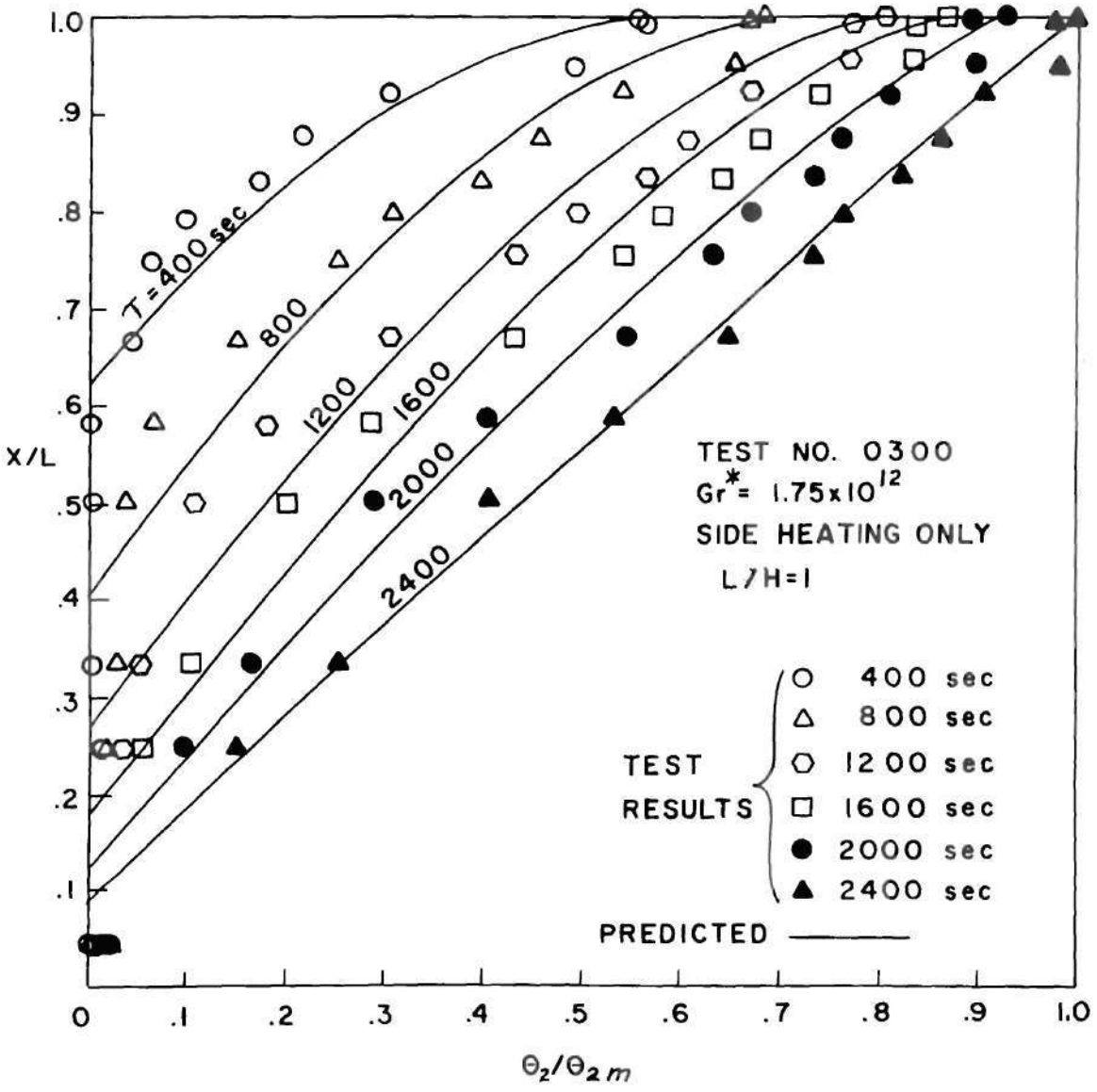

Figure 15. Temperature Profiles with Side Heating Only.

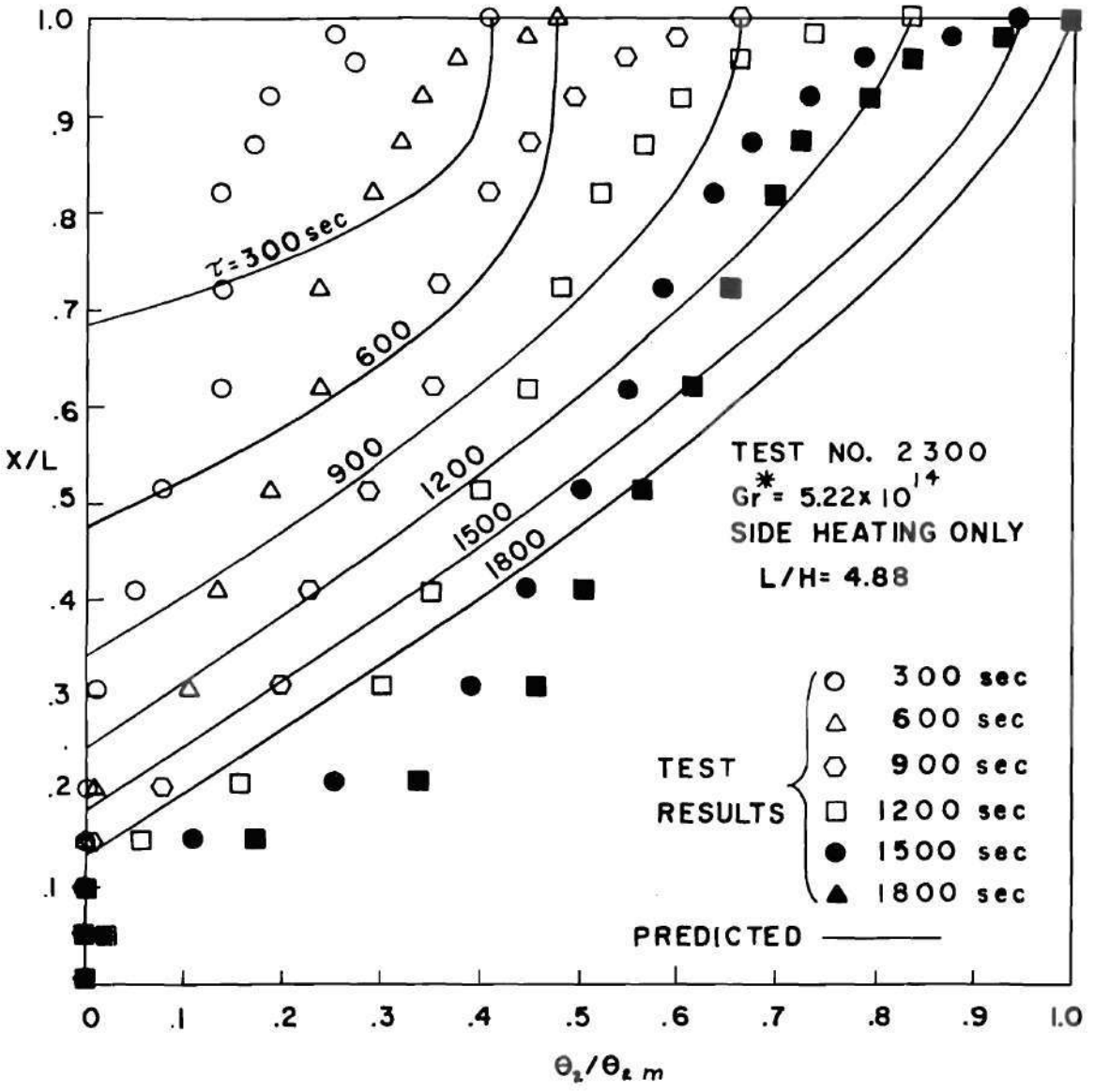

Figure 16. Temperature Profiles with Side Heating Only.

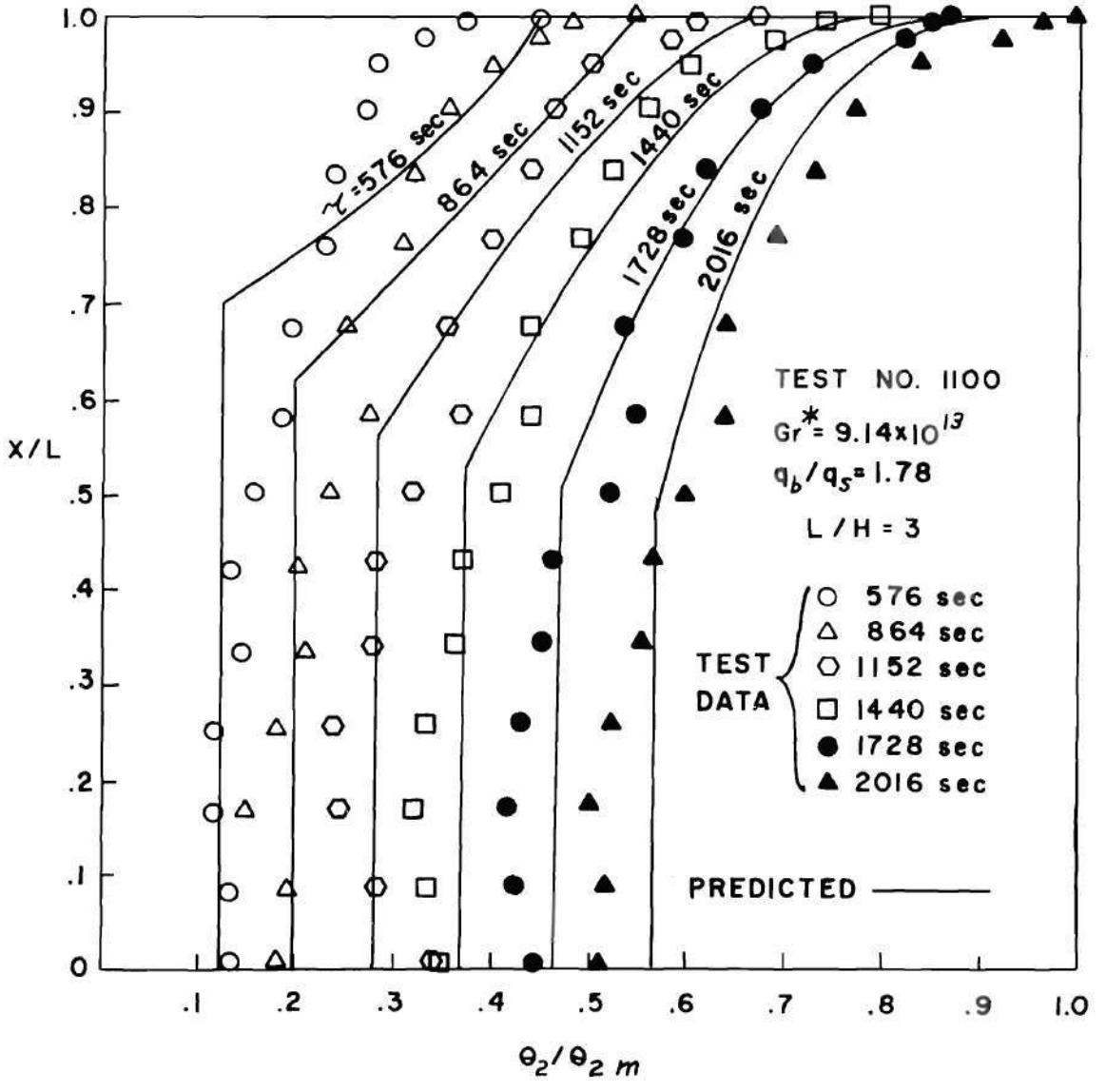

Figure 17. Temperature Profiles with Combined Bottom and Side Heating.

not only the shape of the profile but the temperature level as well. It also puts departures between the predicted and the experimental results in a fairer proportion. Figure 15 illustrates the ability of the analysis to accurately predict the experimental data at low values of Gr^* with side heating only. On the other hand, Figure 16 illustrates the inability of the analysis to predict the experimental results at large values of Gr^* with side heating only.

As seen from Figure 16, the actual rate of growth of the thermal layer is considerably greater than that indicated from the analysis. The predicted thermal layer thickness in Figure 15, however, checks nicely with the experimental data. In addition, the complex curvature of the temperature profile at large Gr^*, is only fairly represented by the analysis, while it works well at smaller Gr^*, as seen in Figure 15. This implies that the free convection flow at large Gr^* is fundamentally different than that at small Gr^*. This is again in agreement with the conclusions of Griffiths and Davis (35).

An investigation of the effects of changing the shape of the assumed turbulent free convection velocity profile has been made to determine if the rate of flow in the boundary layer can be increased sufficiently to explain the test results at large Gr^*. Following the method outlined in Appendix A, integral forms for the momentum and energy equations have been solved for several different velocity profiles and the results used to predict the rate of stratification. However, the effects of varying the profile are found to be small and quite insufficient to explain the test data.

Figures 7 and 17 illustrate the ability of the analysis with combined bottom and side heating using different values of q_b/q_s to predict the temperature profile, especially for large times, and lends confidence to the choice of this analysis as a means of correlating the data. Since the analysis with bottom heating requires knowledge of two previously defined empirical coefficients K_o and K_1, one of the objectives of the investigation has been to obtain a correlation of the test data which would allow prediction of K_o and K_1 as functions of Gr^*, L/H, and q_b/q_s. In addition, the overall success of the model in predicting the temperature profile in the liquid for given values for K_o and K_1 has been investigated.

A correlation of all the tests with combined bottom and side heating has been made. In the correlation, values of K_o and K_1 for each individual test have been obtained which minimize $\sigma_{Tx}/\bar{\theta}_2$, the time-space root mean square deviation between the predicted and experimental data expressed as a fraction of the mean temperature rise. The following expressions have been obtained for K_o and K_1:

$$K_o = \frac{3.3 \times 10^{-13}(q_b/q_s)Gr^*}{[(L/H)^4 + 3]} \quad \text{for all } Gr^*$$

For $Gr^* > 10^{13}$

$$K_1 = -(2)\left(\frac{q_s}{q_b}\right)\left(\frac{L}{H}\right)\ln\left\{1 - \left[\frac{K_o + \left(\frac{1}{2}\right)\left(\frac{q_b}{q_s}\right)\left(\frac{H}{L}\right)}{1 + \left(\frac{1}{2}\right)\left(\frac{q_b}{q_s}\right)\left(\frac{H}{L}\right)}\right]^{8/7}\right\} - .16 - .229[\log_{10}Gr^* - 13]^{3.59}$$

For $Gr^{*} < 10^{13}$

$$K_1 = -(2)\left(\frac{q_s}{q_b}\right)\left(\frac{L}{H}\right)\ln\left\{1 - \left[\frac{K_o + \left(\frac{1}{2}\right)\left(\frac{q_b}{q_s}\right)\left(\frac{H}{L}\right)}{1 + \left(\frac{1}{2}\right)\left(\frac{q_b}{q_s}\right)\left(\frac{H}{L}\right)}\right]^{8/7}\right\} - .16$$

These expressions have been shown to provide predictions of K_o and K_1 which allow correlation of the calculated and the experimental profiles to within a maximum error of 10 per cent of $\bar{\theta}_2$, the mean temperature rise of the test fluid. Since the minimum value of $\sigma_{Tx}/\bar{\theta}_2$ for any test with combined heating is 4.2 per cent and the average of all the minimums is 6.9 per cent, it is clear that even a perfect correlation of all the data would involve a certain amount of error. Hence a temperature deviation of 10 per cent of the bulk mean temperature rise is not felt to be excessive. In the use of these correlations some care should be made not to apply them to situations where $Gr^{*} > 10^{15}$. This is due to the presence of a substantial laminar and transitional flow region in the test tank which should make the effects of bottom heating more significant than would be expected in situations where, with side heating only, the flow is turbulent almost from the leading edge. In cases where a substantial portion of the natural convection flow is laminar with side heating only, the turbulence produced by bottom heating strongly disturbs the laminar flow and causes transition to occur close to the tank bottom. This results not only in a moderate increase in the heat diffusion in the already turbulent region, but in a significant transfer of heat to the bulk liquid in the previously laminar region due to turbulent mixing

which would not have occurred without bottom heating. This latter effect would not be present in case the flow with side heating only were turbulent almost from the leading edge.

Interpretation of Results

From the results of the present study and the conclusions of reference 35 a more complete understanding of the stratification process with side heating only begins to take form. It appears that the S-shape to the temperature profiles at large Gr^* is caused by eddy diffusion of heat across the boundary layer directly to the bulk liquid once the flow becomes turbulent. While a portion of the sidewall heat is carried away by the boundary layer and ultimately near the surface is transported out into the thermal layer, a significant percentage of the heat never reaches the surface, but is absorbed by the liquid directly. This explains the apparent agreement with the analytical model at low Gr^* where the amount of eddy diffusion is small because the flow is mainly laminar and it also explains the results at large Gr^* where the flow is primarily turbulent. Thus in the case of side heating only, the relatively simple temperature profile shape assumed in the analyses in Appendix B must somehow be modified to take into account the effects of increasing Gr^*. This problem is conveniently simplified, however, in the situation with combined heating because the bottom heat addition produces a fairly uniform temperature in the lower regions of the tank due to turbulent mixing in the vertical direction.

Analysis of Diffusion Effects on Bulk Liquid Thermal Behavior with Side Heating Only

In the situation with side heating only, an attempt has been made to determine a functional expression governing the mechanism of heat diffusion through the boundary layer by studying its effect on the bulk liquid thermal behavior in the lower region of the tank. In the analysis, the heat diffusion fraction K_o is considered primarily as a function of x alone. It is near zero along the laminar boundary layer, rises up rapidly during transition and approaches some asymptotic value between zero and unity as the Grashof number approaches infinity. This behavior is suggested from reference 35 and from the Schlieren and particle photographs, which in the laminar regime indicate no fluid motion out of the boundary layer. The pictures indicate that in the transitional region coarse turbulence begins to appear intermittently, and finally in the fully-developed turbulent regime the eddies forming and moving out into the bulk liquid are created almost continuously. Thus the diffusion of heat to the bulk liquid is primarily dependent on the degree of turbulence in the boundary layer, which is itself mainly a function of x.

In the analysis several assumptions are made, i.e.:

1. There is complete mixing of the bulk liquid in the horizontal plane.

2. The boundary layer thickness is small compared with the width of the tank.

3. The average velocity and the boundary layer thickness derived for a constant wall flux with a uniform fluid temperature for both laminar and turbulent free convection flow are sufficiently accurate to define

the boundary layer properties, even though in the latter derivation no consideration was given to the diffusion process. This implies that:

a. The product $\bar{U}\delta$ is a function of position x alone.

b. No allowance is made for the effects of changing bulk liquid temperature.

c. Starting transients in the boundary layer are negligible.

d. The downward velocity of the bulk liquid outside the boundary layer has no influence on the boundary layer properties.

Justification of assumption one comes from the test data which indicate that horizontal temperature gradients outside the boundary layer are negligible. Assumption two can be verified by simple calculation of δ in the lower region of the test tank. Assumption three is necessary to obtain an adequate expression for the boundary layer flow in both the laminar and turbulent regions which can be handled mathematically. It is verified to a large extent in the turbulent regions by the close agreement between predicted and observed values of $\bar{U}\delta$ in Figure 8. Concerning transients in the boundary layer growth, observations with the Schlieren system and the particles show that the boundary layer is essentially completely developed within one minute after application of side heating. Thus neglecting transient boundary layer effects should not cause any significant error in the results obtained.

With these assumptions, an analysis of the thermal behavior of an elemental bulk liquid control volume can be made. A sketch of the control volume is shown in Figure 18. From the sketch it can be seen that the control volume is assumed to gain heat by diffusion directly

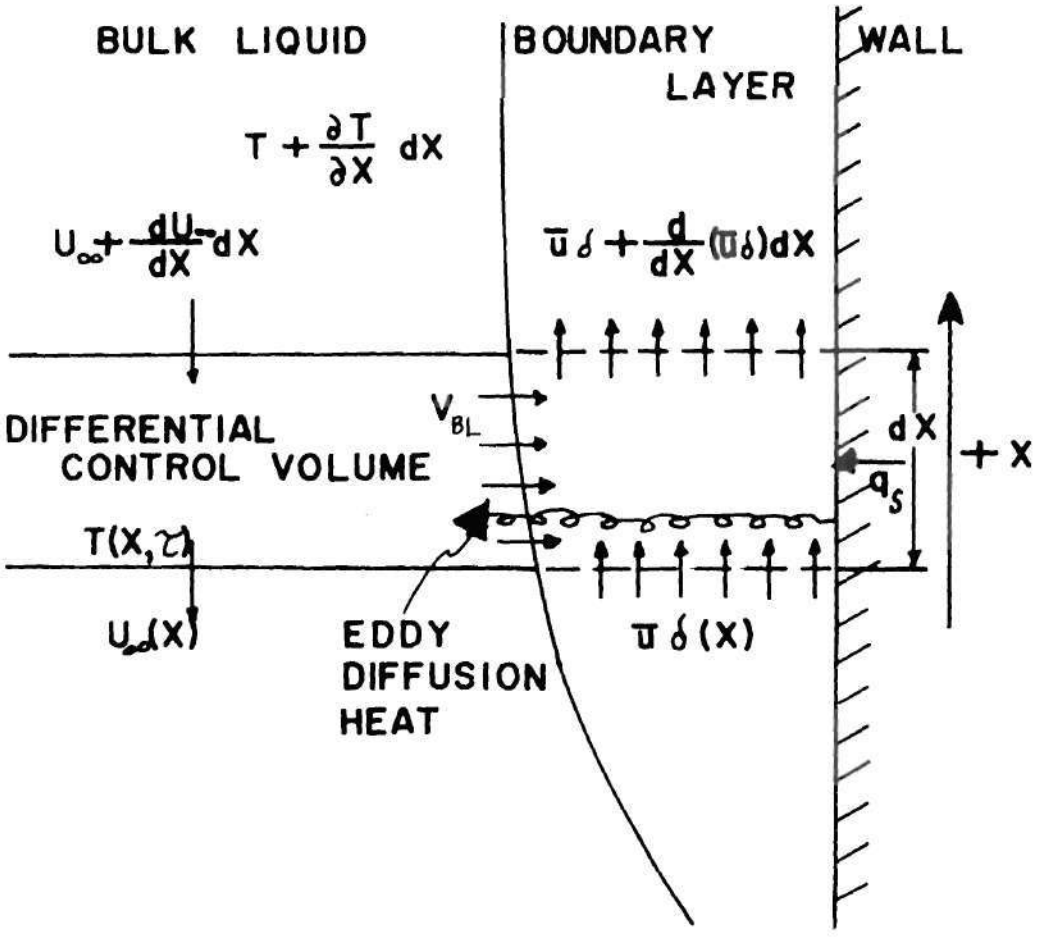

Figure 18. Boundary Layer Diffusion Analytical Model.

through the boundary layer and by convection from elements above. It loses heat by convection to elements below and by convection into the boundary layer which develops in thickness and velocity with increasing x. It should be recognized that the diffusion process pictured here must be studied in the relatively narrow domain in time and position during which there is no influence on the bulk liquid temperature due to the downward motion of warm stratified fluid from the surface. Thus the temperature rises measured in this regime are generally small and therefore experimental precision is limited.

Before making an energy balance, a realtion between U_∞ and V_{bl} must be obtained. It is clear from continuity that:

$$V_{bl} = \frac{\partial}{\partial x} (\bar{U}\delta) \tag{1}$$

In addition, neglecting the boundary layer thickness it follows from continuity that:

$$U_\infty = \frac{2}{H} \bar{U}\delta \tag{2}$$

Thus the result is obtained:

$$\frac{\partial U_\infty}{\partial x} = \frac{2}{H} \frac{\partial}{\partial x} (\bar{U}\delta) = \frac{2}{H} V_{bl} \tag{3}$$

Writing an energy balance during an elemental change in time:

$$WH\rho c dx \frac{\partial T}{\partial \tau} = WH\rho c(T + \frac{\partial T}{\partial x} dx)(U_\infty + \frac{\partial U_\infty}{\partial x} dx) + q_s K_o 2W dx \qquad (4)$$

$$- WH\rho c T U_\infty - 2W\rho c T \frac{\partial(\bar{U}\delta)}{\partial x} dx$$

Utilizing (2) and (3) and neglecting differential terms of a higher order the following equation is obtained:

$$\frac{\partial T}{\partial \tau} = \frac{2q_s}{H\rho c} K_o + \frac{2}{H} (\bar{U}\delta) \frac{\partial T}{\partial x} \qquad (5)$$

Initially the fluid is at a uniform temperature; thus

$$T(x,0) = T_{vo} \qquad (6)$$

It has been experimentally observed that

$$T(0,\tau) = T_{vo} \qquad (7)$$

Thus (5) must be solved subject to the boundary conditions (6) and (7). By making the substitution $\Theta_2 = T - T_{vo}$, the following more convenient differential equation is obtained:

$$\frac{\partial \Theta_2}{\partial \tau} = \frac{2q_s}{H\rho c} K_o + \frac{2}{H} (\bar{U}\delta) \frac{\partial \Theta_2}{\partial x} \qquad (8)$$

where: $\theta_2(0,\tau) = 0$

$\theta_2(x,0) = 0$.

Besides describing the thermal behavior of the bulk liquid, Equation (8) also provides one definition of the heat diffusion fraction K_o. Since the form of K_o is unknown, some means of determining it is necessary. There are two ways this can be done. The first method involves solving directly for K_o using the basic definition (8) and experimental data. The second involves solving the differential Equation (8) and then iterating in some manner for K_o by minimizing the error between the predicted and the experimental results. Both methods have advantages and disadvantages. The first method was chosen because it is more direct and is not influenced in any way by the analytical technique required to solve (8). There are, however, computational problems involved in the direct approach, since only a limited amount of data are available. For example, the formation of derivatives from the experimental results may involve large errors. To minimize these errors, time average values of K_o were determined by treating K_o as a function of x, (8) was rearranged and then integrated with respect to time to produce the result:

$$\bar{K}_o \tau = \frac{H\rho c}{2q_s} \theta_2 + c(x) - \frac{\rho c}{q_s} \bar{U}\delta \int_o^\tau \frac{\partial \theta_2}{\partial x} \, d\tau \qquad (9)$$

By noting that $\theta_2(0,x) = 0$, it can be shown that $c(x) = 0$. Thus an improved expression for K_o which involves only integrated quantities can be obtained:

$$\bar{K}_o = \frac{\frac{H\rho c}{2q_s}\theta_2 - \frac{\rho c}{q_s}\bar{U}\delta\int_o^\tau \frac{\partial\theta_2}{\partial x}\,d\tau}{\tau} \qquad (10)$$

To perform the operations indicated in the integral expression for $\bar{K}_o$, a computer program was written for use on the IBM 360 computer. A brief description of this program and a listing are presented in Appendix D. Numerical calculations for $\bar{K}_o$ using the data of a test identical to that of 1300 were made. Test 1300 was not used because sufficient data in the lower region of the test tank were unavailable. The results of the analysis are presented in Figure 19 where $\bar{K}_o$ is shown as a function of x at various times. From the figure it is seen that $\bar{K}_o$ does primarily vary with x, although there are evidently some effects of changing time. These effects will be discussed later. When it is considered that there are only 42 data points available in the ranges $0 < x < 4.5$ ft., and $0 < \tau < 660$ sec, it may be recognized that the apparent time dependence of K_o is at least partially due to errors produced by the coarseness of the computation grid.

The shape of the $\bar{K}_o$ curve in Figure 19 is interesting since for all times it shows an abrupt rise from zero to a maximum near unity at about 3.6 feet. Although sufficient data are not available, it is believed from the results of the photographic study and conclusions of reference 35 that the curve does not drop back to zero but takes on a constant value for large x. An explanation of the maximum point can be gained by considering what happens in the boundary layer during transition. In doing this, it becomes necessary to make a somewhat more general definition of K_o than has been used previously. Considering

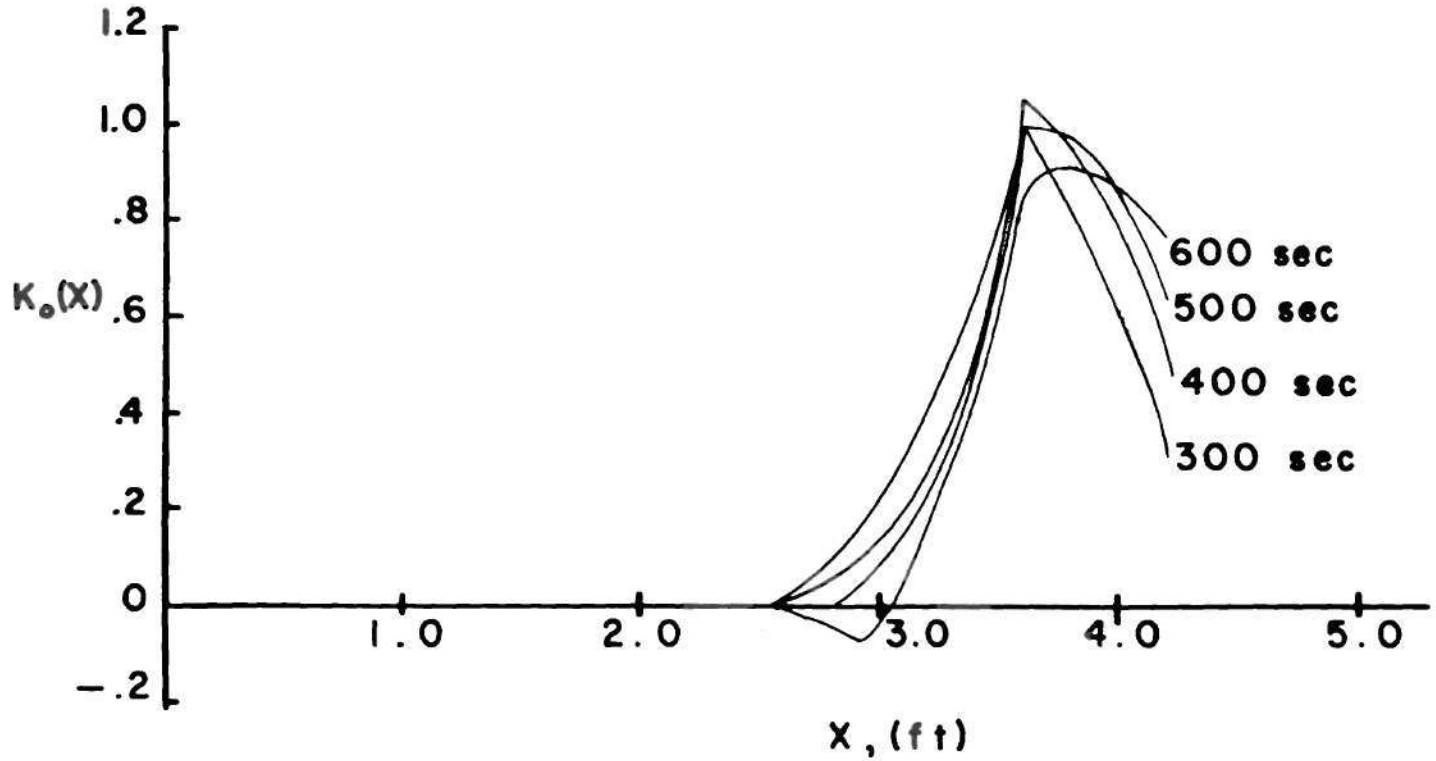

Figure 19. Experimental Values of K_o for Test 1300.

Figure 18 again, it is seen that the following expression can be written concerning the instantaneous change of the energy in the boundary layer:

$$q_s dx - q_d dx - \frac{\partial}{\partial x}\left[\int_o^\delta \rho c U T dy\right] dx = \frac{\partial}{\partial \tau}\left[\int_o^\delta \rho c T dy\right] dx \qquad (11)$$

Therefore:

$$q_d = q_s - \frac{\partial}{\partial x}\left[\int_o^\delta \rho c U T dy\right] - \frac{\partial}{\partial \tau}\left[\int_o^\delta \rho c T dy\right] \qquad (12)$$

Generalizing the previous definition of K_o, the following result is obtained:

$$K_o = 1 - \frac{1}{q_s}\frac{\partial}{\partial x}\left[\int_o^\delta \rho c U T dy\right] - \frac{1}{q_s}\frac{\partial}{\partial \tau}\left[\int_o^\delta \rho c T dy\right] \qquad (13)$$

If both sides of (13) are integrated with respect to time and then divided by time, a time average is obtained. Since the last term in (13) fluctuates strongly in the transitional regime, its time average should be small or near zero. Thus the result is obtained:

$$\overline{K_o(x)} \simeq 1 - \overline{\frac{1}{q_s}\frac{\partial}{\partial x}\left[\int_o^\delta \rho c U T dy\right]} \qquad (14)$$

where the bars indicate time average values. From this expression it can be seen that if the time average change with respect to x of the boundary layer energy integral is negative, $\bar{K}_o$ could conceivably take on values greater than or near unity.

In the process of transition to turbulence, Schlieren photographs indicate that large quantities of hot fluid abruptly and intermittently leave the boundary layer. Since the location of the transition point fluctuates in time it may be expected that this heat is released over a reasonably broad range of x and not just at a single point. This release of energy during transition indicates that the time average change with respect to x of the boundary layer energy drops sharply from its laminar flow value. Once a relatively stable condition is reached in the turbulent boundary layer, however, it would be expected that the change in the boundary layer energy would again take on a relatively constant positive value.

This, then, explains the presence of the maximum in the graph of K_o. For in a sense, the laminar boundary layer bursts during transition and releases a large amount of its energy to the bulk liquid. This energy then reflects large local values of K_o. After a stable condition is reached in the turbulent boundary layer, the amount of heat diffusion becomes nearly constant and K_o becomes more uniform and approaches an asymptotic value.

While the definition (13) of K_o based on boundary layer energy changes indicates that there is a time dependence to K_o, the results based on bulk liquid thermal response presented in Figure 19 demonstrate that this time dependence is not strong. Further, from the figure it is clear that the time average values of K_o do not differ greatly from the instantaneous values. Thus for purposes of the analysis, and to a reasonable precision, K_o is considered a unique function of x alone and therefore $\bar{K}_o \equiv K_o$.

Solution to the Boundary Layer Diffusion Equation

Once K_o is defined, a solution to (8) becomes of interest. Equation (8) is a linear first order non-homogeneous partial differential equation. It has been solved subject to certain constraints in two ways. The first involves a separation of variables technique; the second involves use of the Laplace Transform. The former solution is less general than the latter; however, it will be presented since to a certain extent it motivates the latter method. We have the differential equation

$$\frac{\partial \Theta_2}{\partial \tau} = \frac{2q_s K_o(x)}{H\rho c} + \frac{2}{H}(\bar{U}\delta)\frac{\partial \Theta_2}{\partial x} \tag{8}$$

Noting that K_o is considered a function of x alone, the following substitution is made:

$$\Theta_2(x,\tau) = w(x,\tau) - \psi(x) \tag{15}$$

Introducing this expression into (8) gives:

$$\frac{\partial w}{\partial \tau} = \left[\frac{2q_s K_o(x)}{H\rho c} - \frac{2}{H}(\bar{U}\delta)\frac{d\psi}{dx}\right] + \frac{2}{H}(\bar{U}\delta)\frac{\partial w}{\partial x} \tag{16}$$

where: $w(x,0) = \psi(x)$

$w(0,\tau) = \psi(0)$.

If ψ is chosen so that the bracketed term is zero, (16) can be converted into a simple linear homogeneous first order equation which can be solved

routinely. But the following relation between ψ, K_o, and $\bar{U}\delta$ must hold if this method of solution is followed:

$$\psi = \frac{q_s}{\rho c} \int \frac{K_o(x)}{\bar{U}\delta} dx \tag{17}$$

In solving the resulting homogeneous equation for $w(x,\tau)$ a product solution is assumed, i.e.,

$$w(x,\tau) = F(x) \cdot T(\tau) \tag{18}$$

Substituting this expression into (16), and dividing by $F \cdot T$, the following is obtained:

$$\frac{1}{T}\frac{\partial T}{\partial \tau} = \frac{2}{H}\frac{\bar{U}\delta}{F}\frac{\partial F}{\partial x} \tag{19}$$

Since the expression on the left is a pure function of time and that on the right is a pure function of x, both must equal some quantity λ, the separation constant. Thus the solution of (19) reduces to the solution of two ordinary differential equations:

$$\frac{dT}{d\tau} = \lambda T \tag{20}$$

$$\frac{dF}{dx} = \frac{H}{2}\frac{\lambda F}{\bar{U}\delta} \tag{21}$$

By simple integration the following results are obtained

$$T = C_1 e^{\lambda\tau} \tag{22}$$

$$F = C_2 e^{\frac{\lambda H}{2} \int \frac{dx}{\bar{U}\delta}} \tag{23}$$

Therefore:

$$w(x,\tau) = C_1 C_2 e^{\lambda\tau} \cdot e^{\frac{\lambda H}{2} \int \frac{dx}{\bar{U}\delta}} \tag{24}$$

and

$$\Theta_2 = C_1 C_2 e^{\lambda\tau} \cdot e^{\frac{\lambda H}{2} \int \frac{dx}{\bar{U}\delta}} - \psi(x) \tag{25}$$

In order that $\Theta_2(x,0)$ be zero the following condition must hold:

$$C_1 C_2 e^{\frac{\lambda H}{2} \int \frac{dx}{\bar{U}\delta}} = \frac{q_s}{\rho c} \int \frac{K_o(x)}{\bar{U}\delta} dx = \psi(x) \tag{26}$$

which also can be written:

$$C_1 F(x) = \frac{q_s}{\rho c} \int \frac{K_o(x)}{\bar{U}\delta} dx = \psi(x) \tag{27}$$

Differentiating both sides of (27) and utilizing (21), the following equation is obtained:

$$C_1 \frac{H}{2} \lambda F(x) = \frac{q_s}{\rho c} K_o(x) \tag{28}$$

This expression defines the basic relationship which must exist between K_o and $\bar{U}\delta$, if the form chosen in (16) is to be used. Written out more completely (28) becomes

$$K_o(x) = \left(\frac{\rho c\, H}{q_s\, 2}\right) C_1 C_2 \lambda e^{\frac{\lambda H}{2} \int \frac{dx}{\bar{U}\delta}} \tag{29}$$

and thus

$$\theta_2 = \frac{2q_s}{\rho c H \lambda} K_o(x) \left[e^{\lambda \tau} - 1\right] \tag{30}$$

Equation (29) is clearly a very restrictive relation between $K_o(x)$ and $\bar{U}\delta$. Even though some flexibility can be gained by the proper choice of λ, $C_1 C_2$ and suitable approximations to $\bar{U}\delta$, experience has shown that (30) does not adequately describe the test results. It should be emphasized, however, that the problem here is mathematical, not physical, and lies in the chosen method of solution which involves the substitution (15) with the inevitable result (30).

In order to obtain a more general solution to (8) a second method utilizing the Laplace Transform is presented. In this analysis, assumptions as to the commutability of certain limiting operations are made and often the derivation is not rigorous. Even though the solution is gained through formal mathematics, it can be shown that the result thus obtained satisfies the differential equation (8) and the boundary conditions. Questions concerning uniqueness of the solution have been ignored since

the agreement between the predicted and the experimental results appears to guarantee this property.

In the solution to (8), the Laplace Transform with respect to time is utilized. Thus each term in (8) is multiplied by $e^{-s\tau}$ and integrated with respect to τ from 0 to ∞ . The result of the transform of each term is indicated below:

$$\mathcal{L}_\tau\left[\frac{\partial \Theta_2}{\partial \tau}\right] = s\bar{\bar{\Theta}}_2(s,x) - \Theta_2(0,x) \tag{31}$$

$$\mathcal{L}_\tau\left[\frac{2q_s K_o(x)}{H\rho c}\right] = \left(\frac{1}{s}\right) \frac{2q_s K_o(x)}{H\rho c} \tag{32}$$

$$\mathcal{L}_\tau\left[\frac{2}{H} \bar{U}\delta \frac{\partial \Theta_2}{\partial x}\right] = \frac{2}{H} \bar{U}\delta \frac{d\bar{\bar{\Theta}}_2}{dx} \tag{33}$$

where

$$\mathcal{L}_\tau[\Theta_2(x,\tau)] = \bar{\bar{\Theta}}_2(x,s) \tag{34}$$

Hence (8) is transformed to the linear, first order, ordinary differential equation:

$$\frac{2}{H} \bar{U}\delta \frac{d\bar{\bar{\Theta}}_2}{dx} + \frac{1}{s} \frac{2q_s}{H\rho c} K_o(x) = s\bar{\bar{\Theta}}_2 \tag{35}$$

subject to the transformed boundary condition

$$\mathcal{L}_\tau[\Theta_2(0,\tau)] = \bar{\bar{\Theta}}_2(0,s) = 0 \ . \tag{36}$$

Rearranging and multiplying both sides by the integrating factor:

$$e^{-\frac{Hs}{2}\int \frac{dx}{\bar{U}\delta}}$$

the result is obtained:

$$\frac{d}{dx}\left[\bar{\bar{\Theta}}_2 e^{-\frac{Hs}{2}\int \frac{dx}{\bar{U}\delta}}\right] = - e^{-\frac{Hs}{2}\int \frac{dx}{\bar{U}\delta}} \cdot \frac{q_s}{\rho c} \frac{K_o(x)}{\bar{U}\delta} . \qquad (37)$$

This can be integrated directly, applying the transformed boundary conditions, to give:

$$\bar{\bar{\Theta}}_2 = (-) \frac{e^{\frac{Hs}{2}\int \frac{dx}{\bar{U}\delta}}}{s} \int_o^x \frac{e^{-\frac{Hs}{2}\int \frac{dx}{\bar{U}\delta}} \cdot q_s K_o(x)\, dx}{\rho c\, \bar{U}\delta} . \qquad (38)$$

At this point a new function g(x) is introduced with the property that

$$\bar{U}\delta = A\, g(x)/g'(x) \qquad (39)$$

and

$$g(0) = 0$$

where: $A = 1\ ft^2/sec$

$g(x)$ and $g'(x)$ are dimensionless.

Further it is assumed that $K_o(x)$ can be expanded as a power series in g(x). Thus

$$K_o = \sum_m C_m [g(x)]^m \qquad (40)$$

where C_m are dimensionless. Introducing (39) and (40) into (38) gives

$$\bar{\bar{\theta}}_2 = - \frac{q_s}{\rho c} \frac{[g(x)]^{\frac{HsB}{2A}}}{s} \int_o^x \frac{[g(x)]^{-\frac{HsB}{2A}} \sum_m C_m [g(x)]^m \, g'(x) \, dx}{A \, g(x)} \qquad (41)$$

where B = 1 ft.

Interchanging the operations of addition and integration, assuming $m > \frac{HsB}{2A}$, performing the indicated integration and noting that g(0) = 0 gives the result:

$$\bar{\bar{\theta}}_2 = - \left(\frac{2q_s}{H\rho c}\right) \frac{[g(x)]^{\frac{HsB}{2A}}}{s} \sum_m \frac{C_m [g(x)]^{m-\frac{HsB}{2A}}}{\frac{2Am}{BH} - s} \qquad (42)$$

which can be simplified to

$$\bar{\bar{\theta}}_2 = \left(\frac{1}{s}\right) \frac{2q_s}{H\rho c} \sum_m \frac{C_m [g(x)]^m}{s - \frac{2Am}{HB}} \, . \qquad (43)$$

The inverse transform of the summation term:

$$\mathcal{L}_\tau^{-1} \left[\left(\frac{2q_s}{H\rho C}\right) \sum_m \frac{C_m [g(x)]^m}{s - \frac{2mA}{HB}} \right] = \left(\frac{2q_s}{H\rho c}\right) \left[\sum_m C_m [g(x)]^m \right] e^{\frac{2mA}{HB} \tau} \qquad (44)$$

Utilizing the operational property:

$$\mathcal{L}_\tau^{-1} \left[\frac{1}{s} f(s)\right] = \int_o^\tau F(\tau) d\tau, \quad \text{where } f(s) = \mathcal{L}_\tau [F(\tau)] \qquad (45)$$

it is immediately seen that:

$$\Theta_2(x,\tau) = \frac{q_s B}{\rho c A} \sum_m C_m \frac{[g(x)]^m [e^{\frac{2mA}{HB}\tau} - 1]}{m} \tag{46}$$

Examination of this result shows that it satisfies (8) and the boundary conditions.

The introduction of g(x), as defined in (39), is suggested by (23) where F(x) plays the same role as g(x). Also, the expansion of $K_o(x)$ in powers of g(x) is suggested from (29). Examination of the solution to (8) using the separation of variables approach reveals that it is actually the first term in the series expansion of the solution using the Laplace Transform. If in (15) Θ_2 had been assumed as a series of the form

$$\Theta_2 = \sum_i \Theta_{2i} = \sum_i [w_i(x,\tau) - \psi_i(x)] \tag{47}$$

where: $\Theta_{2i}(0,\tau) = 0$

$\Theta_{2i}(x,0) = 0$,

a result identical to (46) would have resulted.

The only problem remaining is to find the proper g(x). From the defining relation it follows that

$$g(x) = e^{\frac{A}{B}\int \frac{dx}{\bar{U}\delta}} \tag{48}$$

Since the relation for $\bar{U}\delta$ must hold both in the laminar and the turbulent regions, a form which approaches the turbulent expression for large x but

is reasonably valid in the laminar region is desirable. Therefore utilizing Equations A-17 and A-19, an expression of the form

$$\bar{U}\delta = \frac{Kx^{8/7}}{1 + J/x^2} \tag{49}$$

where $J = 1\ ft^2$ seems plausible. A plot of this expression together with the computed values of $\bar{U}\delta$ for laminar and turbulent flow in the test under discussion is presented in Figure 20. Also plotted is a simpler expression for $\bar{U}\delta$ of the form

$$\bar{U}\delta = \frac{K'x}{1 + J/x^2} \tag{50}$$

where $J = 1\ ft^2$. It is seen that both expressions give an accurate fit to the computed curves of $\bar{U}\delta$. The latter expression, however, is of much greater usefulness, and has been used in the determination of $g(x)$. Thus to a close approximation

$$g(x) = \left[xe^{-\frac{J}{2x^2}}\right]^{\frac{A}{BK'}} \tag{51}$$

and

$$K_o(x) = \sum_m C_m \left[xe^{-\frac{J}{2x^2}}\right]^{\frac{mA}{BK'}} \tag{52}$$

It is convenient if the ratio $mA/K'B$ takes on integral values so that $K_o(x)$ can be expressed as a power series in $(xe^{-J/2x^2})$. Thus a new,

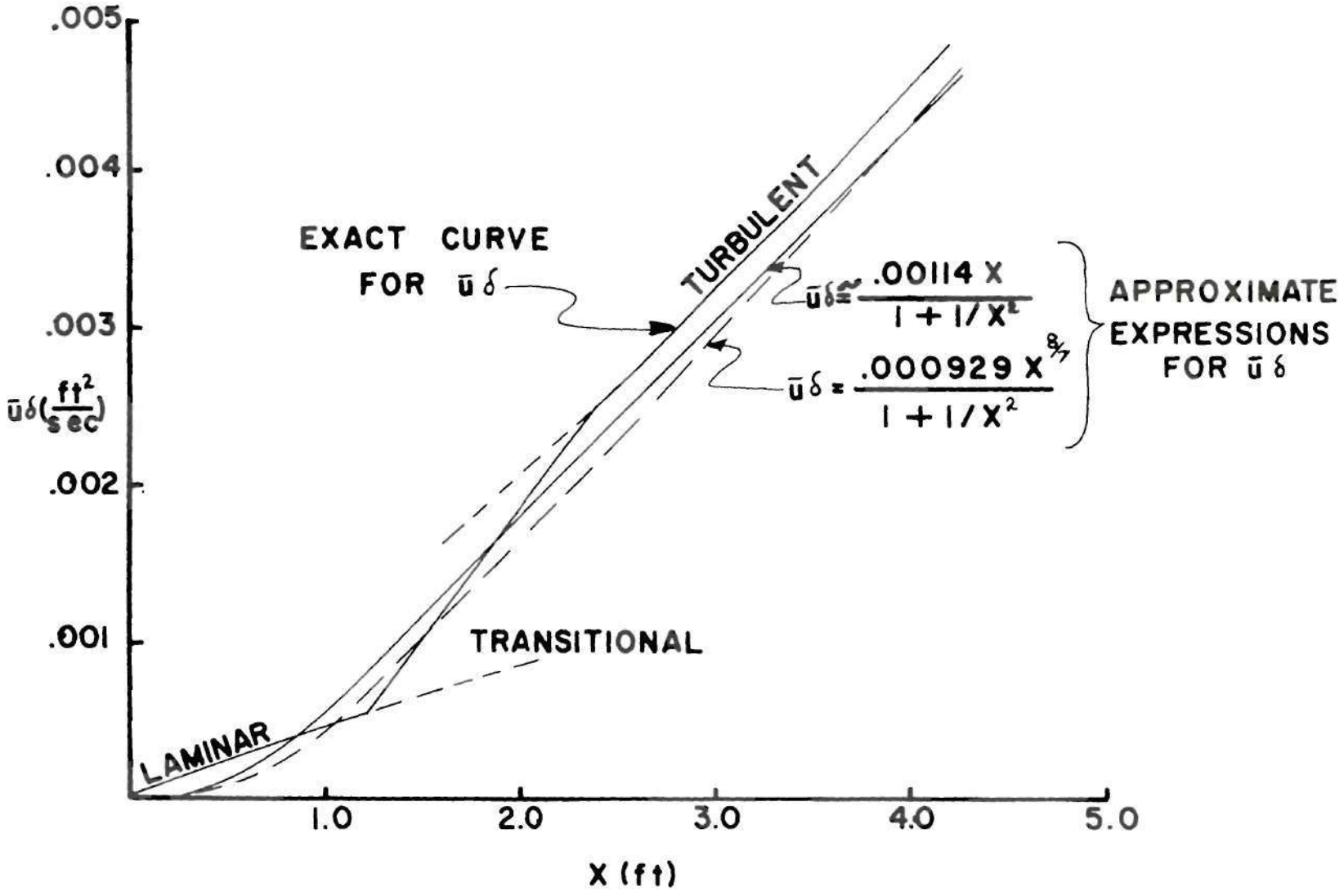

Figure 20. Graphs of $\bar{U}\delta$ for Test 1300.

dimensionless quantity

$$\eta = \frac{mA}{K'B} \tag{53}$$

is introduced, where η takes on positive integral values. Thus the final results are obtained:

$$K_o(x) = \sum_{\eta=1}^{\eta} C_\eta [xe^{-\frac{J}{2x^2}}]^\eta \tag{54}$$

and

$$\Theta_2(x,\tau) = \frac{q_s}{\rho c K'} \sum_{\eta=1}^{\eta} C_\eta \frac{[xe^{-\frac{J}{2x^2}}]^\eta [e^{\frac{2\eta K'\tau}{H}} - 1]}{\eta} \tag{55}$$

Using a least squares fit to the test data, the coefficients in the power series for Θ_2 have been determined by means of the computer program described in Appendix D. A comparison between the predicted results using an eighth order polynomial and the experimental results for Θ_2 is presented in Figure 21. Here it is seen that there is good agreement between the two families of curves. The rms deviation between the predicted and the test results is 0.023°F. Close examination of the predicted results, however, shows a waviness which is characteristic of power series fits. Unfortunately, beyond a certain point, the least squares technique to find the C_η's begins to produce erratic results as the order of the polynomial is continually increased. This is believed to be due to round-off error, even using double precision, in the cal-

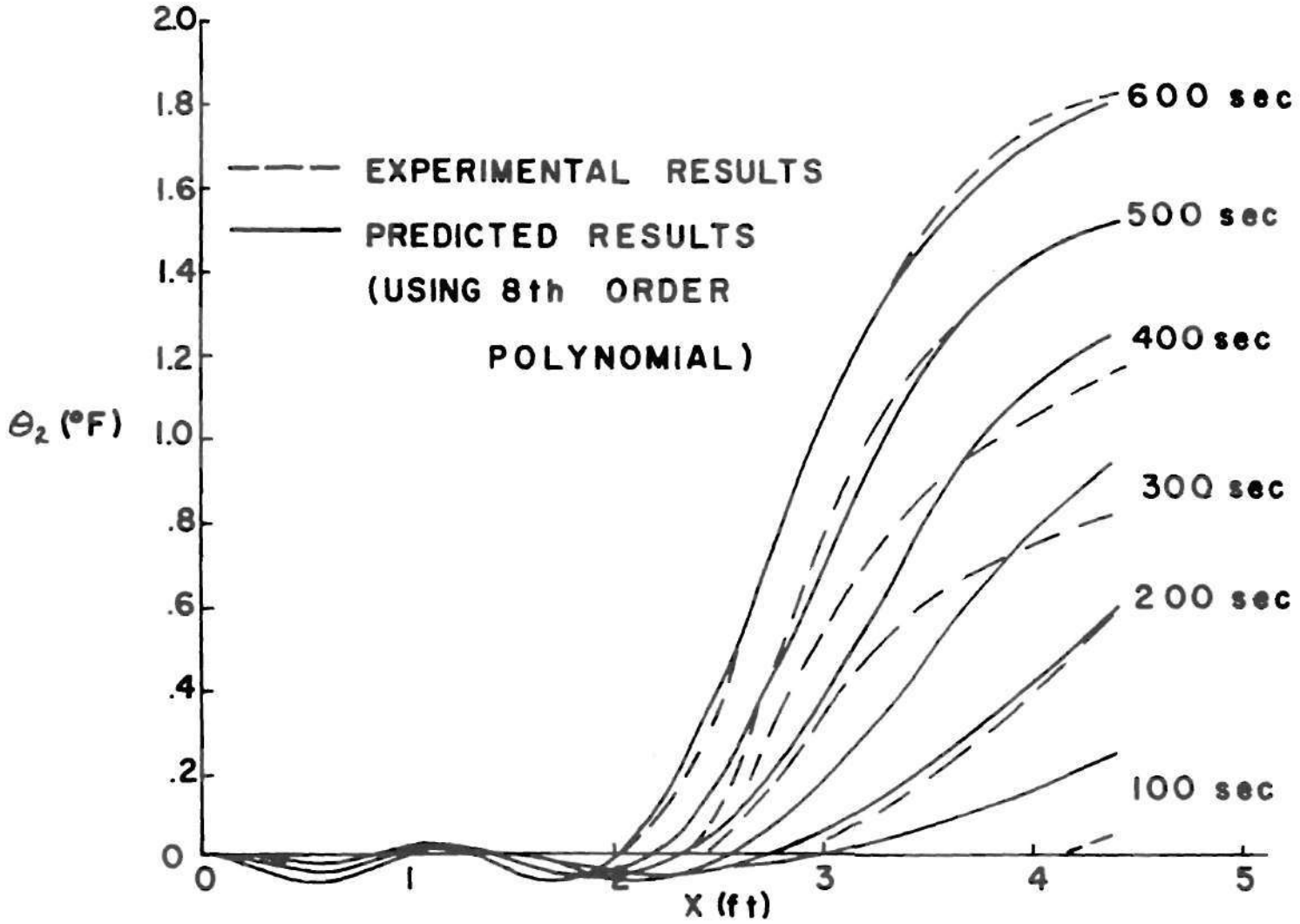

Figure 21. Experimental and Predicted Values of $\theta_2(x,\tau)$ for Test 1300.

culations. Thus there appears no way to significantly reduce the waviness of the results at the present time since power series fits of orders 8 or 9 are about the practical limit for the IBM 360 computer.

Corresponding to the eighth order polynomial for θ_2 a graph of $K_o(x)$ is presented in Figure 22, together with a graph of the time average $K_o(x)$ obtained from the test data. While both curves exhibit the same general shape, the agreement is not good. It was determined that as the order of the polynomial fit increases up to 8 or 9, both the peak predicted value of $K_o(x)$ and its location diminish. Using linear extrapolation, it was found that a 19th order polynomial should result in a maximum $K_o(x)$ of 1.0 at a value of x = 3.6 ft. This coincides with the peak value of $K_o(x)$ determined from the test results. Thus it is believed that if accurate, higher order fits to θ_2 were obtainable, the agreement for $K_o(x)$ would be significantly better.

The fact that much better accuracy can be obtained for $\theta_2(x,\tau)$ than for $K_o(x)$ using a certain order fit, perhaps needs some explanation. From Equation (10), the sensitivity of $K_o(x)$ to $\int_o^\tau \frac{\partial \theta_2}{\partial x} d\tau$ is seen. Thus while the expression for θ_2 using a certain order fit may oscillate about the experimental values and closely approximate it, the integral $\int_o^\tau \frac{\partial \theta_2}{\partial x} d\tau$ may significantly differ from the experimental values due to the waviness of the predicted curve. Hence it is seen that to produce satisfactory results, the expansion must not only closely approximate θ_2 but its derivatives as well.

While there are some shortcomings to the Laplace Transform technique, it clearly provides a much better way to solve (8) than the first method used. In addition, it appears that the effects of ignoring the

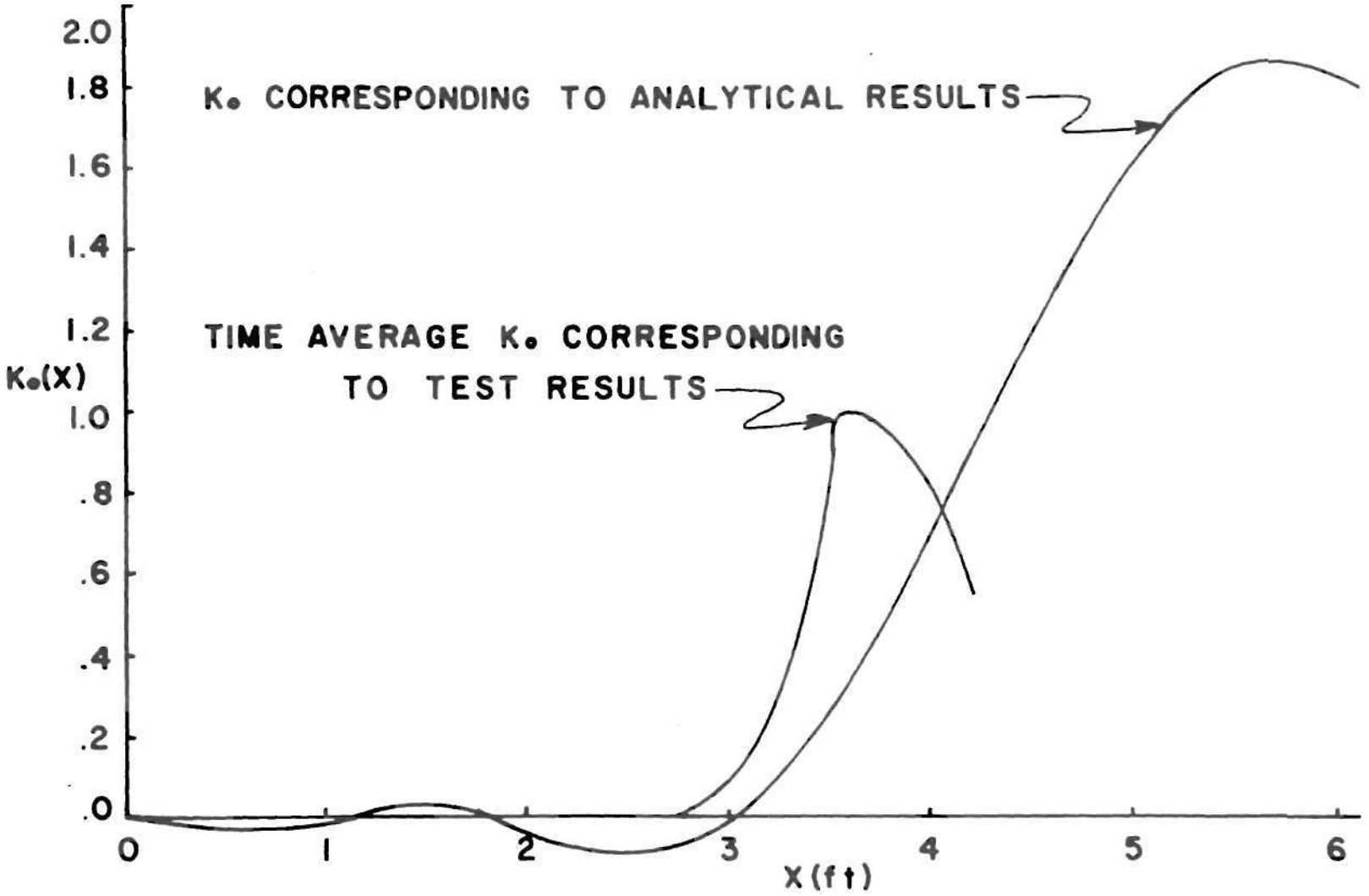

Figure 22. Experimental and Predicted Values of K_o for Test 1300.

time dependence of K_o and of the approximation involved in the expression for $\bar{U}\delta$ are negligible. Finally, since the results of the analysis and the testing show good agreement, the validity of the analytical model is fairly well established.

CHAPTER V

CONCLUSIONS

From the results of this investigation it appears that for enclosed liquids heated at the sides and/or at the bottom, a heat transfer eddy diffusion mechanism is present within the turbulent free convection boundary layer which allows heat to be transfered directly across the boundary layer to the bulk liquid. While the intensity of bottom heating and the liquid aspect ratio significantly influence the amount of heat transferred across the boundary layer, this heat transfer occurs even under conditions with side heating only, at large values of Gr^*. This implies that under these circumstances the turbulence itself present in the boundary layer is responsible for the heat transfer. Success of the boundary layer diffusion analysis supports this idea and provides a quantitative description of the heat transfer diffusion process.

Successful correlation of the data with combined side and bottom heating indicates that the analysis of reference 9 provides adequate predictions of liquid thermal behavior for most engineering purposes. Some improvement, however, might be made to give better predictions of the temperature profile, especially in the lower regions of the tank. The similarity of the temperature profiles perhaps might provide the basis for a more precise analysis. The limited success at large Gr^* of the analysis of reference 8, with side heating only, suggests that substantial improvement could be made perhaps by incorporating into the

analytical model the concept of heat diffusion across the turbulent boundary layer.

Although the photographic techniques used in the study could be improved by better lighting, the results of the study illustrate the usefulness of combined investigations of fluid motion with fluid thermal behavior. It is apparent that only a limited understanding of the boundary layer diffusion mechanism would have been possible from the temperature data alone.

CHAPTER VI

RECOMMENDATIONS

There are several ways in which the present test apparatus could be used, with some modifications, to extend the study of transient free convection effects. For example, the bottom shape could be varied to determine its influence on stratification phenomena. Also the test fluid might be changed to determine the effects of Prandtl number on stratification. In this case air might be used. Further, a study of the three dimensional effects of boundary layer and bulk liquid turbulence should be made to determine its role in the diffusion process. Without making any modifications to the test apparatus, however, an enormous amount of work could and should be done in additional investigation and quantitative study of stratification. More particle streak pictures and more Schlieren photographs together with axial temperature data would undoubtedly provide significant additional information concerning the process of stratification and boundary layer diffusion.

In addition to the above, a separate investigation of turbulent free convection should be made to obtain accurate boundary layer velocity and temperature profile data. Such information is vital to a final understanding of the diffusion process and may shed considerable light on the mechanics of turbulence itself. The definition of K_o from Equation (13) could be used to directly compute the diffusion fraction. In addition, the influence on the boundary layer of downward bulk liquid flow

could be investigated and transient phenomena could be studied. An investigation of the effects on stratification of the thermocouple probe diameter might also be made to confirm the implicit assumption that the relatively large probe diameter used had little if any influence on the experimental results obtained.

APPENDIX A

TURBULENT FREE CONVECTION WITH UNIFORM WALL HEAT FLUX*

An analysis of turbulent free convection with a uniform wall heat flux is presented. Following the approach of Eckert and Jackson (34), the Karman Integral Method is utilized. Integration of the Navier-Stokes equation and the energy equation across the boundary layer provides the following relations:

Momentum:

$$\frac{d}{dx}\left[\int_o^\delta U^2 dy\right] = g_o\beta \int_o^\delta \Theta dy - g_o \frac{\tau_w}{\rho} \qquad (A\text{-}1)$$

Energy:

$$\frac{d}{dx}\left[\int_o^\delta U\Theta dy\right] = \frac{q_s}{\rho c} \qquad (A\text{-}2)$$

The velocity and temperature profiles are assumed as

---

*While some of the results of the analyses discussed in Appendices A and B have been presented before (9), the details of the derivations are not available in the open literature. In addition, the analyses presented here are somewhat more general and improved over those in reference 9. It is felt, therefore, that to provide a proper discussion of the problem, derivation of these equations should be presented.

$$U = U_1(y/\delta)^{1/7}[1-y/\delta]^p \tag{A-3}$$

$$\Theta = \Theta_w[1 - (y/\delta)^{1/7}] \tag{A-4}$$

where p is considered a parameter whose value is chosen to give the best fit to experimental data. Also from (34), the wall shear stress is defined as

$$\tau_w = 0.0225 \frac{\rho}{g_o} U_1^2 \left(\frac{\nu}{U_1\delta}\right)^{1/4} \tag{A-5}$$

With the resulting relation for the Stanton number, using Reynolds Analogy for turbulent flow:

$$St = \frac{q_s}{\rho c U_1 \Theta_w} = 0.0225 \left(\frac{\nu}{U_1\delta}\right)^{1/4} Pr^{-2/3} \tag{A-6}$$

Introduction of the assumed velocity and temperature profiles into the integral terms appearing in (A-1), and (A-2) gives the results:

$$\int_o^\delta U^2 dy = \frac{U_1^2\delta\Gamma(9/7)\Gamma(1+2p)}{\Gamma(1 + 9/7 + 2p)} = U_1^2\delta J_1 \tag{A-7}$$

$$\int_o^\delta \Theta dy = \frac{\Theta_w\delta}{8} \tag{A-8}$$

$$\int_0^\delta U\Theta dy = U_1\Theta_w\delta\left[\frac{\Gamma(8/7)\Gamma(1+p)}{\Gamma(1+8/7+p)} - \frac{\Gamma(9/7)\Gamma(1+p)}{\Gamma(1+9/7+p)}\right] = U_1\Theta_w\delta J_2 \qquad (A-9)$$

In addition to these, the following integral is of interest

$$\bar{U} \triangleq \frac{1}{\delta}\int_0^\delta U dy = \frac{U_1\Gamma(8/7)\Gamma(1+p)}{\Gamma(1+8/7+p)} = U_1 J_3 \qquad (A-10)$$

Utilizing Equations (A-3) - (A-9), the energy equation becomes

$$\frac{d}{dx}[U_1\Theta_w\delta J_2] = \frac{q_s}{\rho c} = 0.0225\, U_1\Theta_w\left(\frac{\nu}{U_1\delta}\right)^{1/4}(Pr)^{-2/3} \qquad (A-11)$$

This can be integrated directly, noting that the right hand terms are constant to give:

$$\Theta_w = \frac{q_s x}{\rho c J_2 U_1 \delta} \qquad (A-12)$$

$$\delta = \left[\frac{.0225}{J_2}\right]^{4/5} Pr^{-8/15}\left(\frac{\nu}{U_1}\right)^{1/5} x^{4/5} \qquad (A-13)$$

Introduction of Equations (A-3) - (A-9) into the momentum equation leads to the relation:

$$\frac{d}{dx}[J_1 U_1^2\delta] = \frac{g_o\beta\Theta_w\delta}{8} - .0225\, U_1^2\left(\frac{\nu}{U_1\delta}\right)^{1/4} \qquad (A-14)$$

Substitution of the expressions for θ_w and δ into (A-14) produces, after rearrangement:

$$\frac{d}{dx}\left(U_1^{9/5}x^{4/5}\right) = A_1\left(\frac{x}{U_1}\right) - B_1\frac{x^{9/5}}{U_1^{1/5}} \qquad \text{(A-15)}$$

where $$A_1 = \left(\frac{g_o\beta q_s}{k\nu^2}\right)\frac{\nu^{14/5}}{Pr^{7/15}}\left[\frac{1}{8J_2^{1/5}J_1(.0225)^{4/5}}\right]$$

$$B_1 = Pr^{2/3}\frac{J_2}{J_1}$$

Following (34), it is assumed that

$$U_1(x) = C_3\,x^{\gamma} \qquad \text{(A-16)}$$

which after substitution into (A-15) allows the determination of C_3, and γ, with the result

$$U_1 = \left[\frac{A_1}{1.572 + B_1}\right]^{5/14\ \ 3/7} x \qquad \text{(A-17)}$$

The expression for U_1 can be written more descriptively as

$$U_1 = \left[\frac{1}{8^{5/14}J_2^{3/7}(.0225)^{2/7}}\right]\frac{\nu}{Pr^{1/6}}\left[\frac{Gr_x^*}{1.572\,\frac{J_1}{J_2} + Pr^{2/3}}\right]^{5/14}\left(\frac{1}{x}\right) \qquad \text{(A-18)}$$

Substitution of (A-17) into (A-12) and (A-13) leads to:

$$\delta = \left[\frac{(8^{1/14})(.0225)^{6/7}}{J_2^{5/7}}\right]\left(\frac{1}{Pr^{1/2}}\right)\left[\frac{Gr_x^*}{1.572\,\frac{J_1}{J_2} + Pr^{2/3}}\right]^{-1/14} x \qquad \text{(A-19)}$$

$$\Theta_w = \left[\frac{8^{2/7}J_2^{1/7}}{(.0225)^{4/7}}\right]\frac{q_s}{kPr^{1/3}}\left[\frac{Gr_x^*}{1.572\,\frac{J_1}{J_2} + Pr^{2/3}}\right]^{-2/7} x \qquad \text{(A-20)}$$

Finally, from the definition of the heat transfer coefficient, the following relation is obtained:

$$Nu_x = \left[\frac{(.0225)^{4/7}}{8^{2/7}J_2^{1/7}}\right]Pr^{1/3}\left[\frac{Gr_x^*}{1.572\,\frac{J_1}{J_2} + Pr^{2/3}}\right]^{2/7} \qquad \text{(A-21)}$$

APPENDIX B

STRATIFICATION ANALYSIS

In the general situation studied, heating of the test fluid occurs both at the sides of the container and at the bottom. The side heating causes the formation of a free convection flow of warm fluid upward with the resulting creation of a thermally stratified region near the surface. The thermal layer produced is stable and if side heating were to cease, the temperature profile would become static with the warmer less dense liquid floating above the colder, denser liquid. The bottom heating, in contrast, causes an unstable condition to exist since warm liquid is created beneath the cooler bulk liquid. The result is a strong mixing action which tends to equilize the temperature in the test tank.

With combined side and bottom heating the stabilizing effect of the side heating is opposed by the unstabilizing influence of bottom heating. Thus even though the thermal layer tends to grow due to side heating effects, simultaneously it also tends to diminish due to mixing effects caused by bottom heating. This mixing can be thought of analytically as an outward flow from the bottom of the thermal layer. In the analysis presented, it has been assumed that this mixing flow is a function only of the test conditions and not a function of time. In the case of side heating only, the mixing flow postulated would be zero. In the case of bottom heating only, the mixing flow would be such that no thermal layer can form. For intermediate values of bottom heating,

test results indicate that the thermal layer depth becomes constant at large test times. This indicates that the growth rate and the mixing rate must ultimately reach equilibrium and suggests that the latter can be expressed in terms of the former. In the analysis a form for this mixing flow has been chosen which automatically satisfies the two extreme conditions. In addition a constant K_1, to be determined experimentally, has been defined which allows intermediate values of the mixing flow to be calculated.

Besides K_1, another empirical constant is required in the analysis. This constant K_o, is defined here as the fraction of the total sidewall heating which passes directly to the bulk liquid. In the analysis of (9) K_o was considered as that fraction of the sidewall area over which no natural convection boundary layer is present. In the ideal case, a relation exists between the two constants K_o and K_1. This relation is discussed later. In the actual situation, however, K_o and K_1 must be considered independent of one another to allow individual selection of values which give a best fit of the test data to the analysis.

In the analysis of the motion and thermal behavior of the liquid within the container, the energy equation and the continuity equation are used primarily. The fluid in the tank is divided into two regions; the thermal layer and the bulk liquid. Certain assumptions and approximations are made concerning the interactions between these two regions. The main assumptions, however, have been stated in Chapter I and in the preceding paragraphs.

Mass Balance--Thermal Layer

Referring to Figure 1, the continuity equation can be written

$$\left(\begin{array}{c}\text{Rate of Change of}\\ \text{Mass in the Thermal}\\ \text{Layer}\end{array}\right) = \left(\begin{array}{c}\text{Rate of}\\ \text{Flow In}\end{array}\right) - \left(\begin{array}{c}\text{Rate of}\\ \text{Flow Out}\end{array}\right) \qquad \text{(B-1)}$$

Noting that the thermal layer control volume increases in size with time, an analytical expression for continuity can be written as:

$$\frac{d}{d\tau}(\rho HW\ell) = 2\delta W\rho[\bar{U} + \frac{d\ell}{d\tau}] - \rho U_{mix}[WH - 2W\delta] \qquad \text{(B-2)}$$

where $\bar{U}$ and δ are to be evaluated at the bottom of the thermal layer. Assuming incompressible flow, (B-2) becomes after rearranging terms:

$$\frac{d\ell}{d\tau} = \frac{2\bar{U}\delta}{H - 2\delta} - U_{mix} \qquad \text{(B-3)}$$

At this point an analytic expression for U_{mix} is needed. An expression satisfying the requirements stated previously has been chosen arbitrarily. This expression is

$$U_{mix} = \frac{2\bar{U}\delta(L)}{H - 2\delta(L)}\left[1 - e^{-K_1 Q_B/Q_S}\right] \qquad \text{(B-4)}$$

In addition to U_{mix}, a relation for $\bar{U}\delta$ is needed. From Appendix A,

expressions for $\bar{U}$ and δ can be obtained from Equations (A-10), (A-17) and (A-19). Thus Equation (B-3) becomes:

$$\frac{d\ell}{d\tau} = \frac{2K_2 x_t^{8/7}}{H - 2\delta(x_t)} - \frac{2K_2 L^{8/7}}{H - 2\delta(L)} \left[1 - e^{-K_1 \frac{Q_B}{Q_S}}\right] \qquad \text{(B-5)}$$

where x_t is defined in Figure 1 and

$$K_2 = \left[\frac{(.0225)^{4/7} J_3}{8^{2/7} J_2^{8/7}}\right] \frac{\nu}{Pr^{2/3}} \left[\frac{g_o \beta q_s / k\nu^2}{1.572 \frac{J_1}{J_2} + Pr^{2/3}}\right]^{2/7}$$

Energy Balance--Bulk Liquid

Noting that no work is done, an energy balance on the bulk liquid may be written in the form:

$$\left(\begin{array}{c}\text{Rate of Change}\\ \text{of Energy in}\\ \text{the Bulk}\\ \text{Liquid}\end{array}\right) = \left(\begin{array}{c}\text{Bottom}\\ \text{Heating}\\ \text{Rate}\end{array}\right) + \left(\begin{array}{c}\text{Partial Side}\\ \text{Heating Rate}\end{array}\right) - \left(\begin{array}{c}\text{Rate of Energy}\\ \text{Convected from}\\ \text{Bulk Liquid}\\ \text{Region}\end{array}\right) \qquad \text{(B-6)}$$

Since the bulk liquid is assumed always in thermal equilibrium, the first term becomes simply

$$WH\rho c \frac{d}{d\tau} [(L - \ell) \cdot T_v] \qquad \text{(B-7)}$$

The second term is

$$q_b WH \qquad \text{(B-8)}$$

The third term may be written as

$$2WLq_s K_o \tag{B-9}$$

The last term is

$$WH\rho cT_v \frac{d\ell}{d\tau} \tag{B-10}$$

By combination of the above relations, the bulk liquid energy balance can be written:

$$WH\rho c \frac{d}{d\tau}[(L - \ell) \cdot T_v] = WHq_b + 2WLq_s K_o - WH\rho cT_v \frac{d\ell}{d\tau} \tag{B-11}$$

This can be simplified to give:

$$\frac{dT_v}{d\tau} = \frac{q_b + 2q_s(L/H)K_o}{\rho c[L - \ell]} \tag{B-12}$$

Energy Balance--Thermal Layer

If heat transfer effects at the liquid surface are ignored, an energy balance on the thermal layer may be written in the form:

$$\int_o^\tau \left(\begin{array}{c}\text{Sidewall}\\ \text{Heating}\end{array}\right) d\tau + \int_o^\tau \left(\begin{array}{c}\text{Net Heat}\\ \text{Exchange by}\\ \text{Convected Mass}\\ \text{Transfer}\end{array}\right) d\tau = \left(\begin{array}{c}\text{Total Energy}\\ \text{Stored in the}\\ \text{Thermal Layer}\\ \text{at } \tau\end{array}\right) \tag{B-13}$$

The first term is simply:

$$2WLq_s(1 - K_o)\tau \qquad \text{(B-14)}$$

The second term can be written as:

$$WH\rho c \int_o^\tau T_v \frac{d\ell}{d\tau} d\tau \qquad \text{(B-15)}$$

Here it is assumed that the fluid leaves and enters the bulk liquid region at the bulk liquid temperature.

By combining (B-14) and (B-15) an expression for the total energy within the thermal layer can be obtained as a function of time alone. Unfortunately this does not provide sufficient information to determine the temperature profile, itself. However, besides the integral of the profile, the surface temperature and the bulk liquid temperature are also available using the results of both the tests and the analysis. Due to the nature of the problem and the limited information at hand, it appears then that an integral approach using an assumed temperature profile offers the best solution. After considerable trial and error an appropriate one parameter form for the thermal layer temperature profile which best fits all the test data has been chosen. This form is:

$$T_{t\ell} = T_s - (T_s - T_v)\,[1 - \varepsilon/\ell]^n \qquad \text{(B-16)}$$

where ε is defined in Figure 1 and n is a function of time alone. Thus, the total energy in the thermal layer at any time can be written as:

$$WH\rho c \int_{o}^{\ell} \{T_s - (T_s - T_v)[1 - \varepsilon/\ell]^n\} d\varepsilon \qquad \text{(B-17)}$$

After integration this becomes:

$$WH\rho c\ell \left[T_s - \frac{(T_s - T_v)}{n + 1} \right] \qquad \text{(B-18)}$$

T_v can be obtained analytically; however, T_s is not known in general and its value must be obtained from experimental measurements.*

Once the energy within the thermal layer is known, together with the bulk liquid and surface temperature, there exists a unique value of n. In general, n may vary with time from positive values near zero to values of the order of 10 to 20. An expression for n can be gained by combining Equations (B-13), (B-14), (B-15) and (B-18) to obtain:

$$n = \frac{(T_s - T_v)}{T_s - \frac{2L(1 - K_o)}{H\rho c\ell} q_s \tau - \frac{1}{\ell} \int_{o}^{\tau} T_v \frac{d\ell}{d\tau} d\tau} - 1 \qquad \text{(B-19)}$$

Equations (B-5), (B-12), (B-16) and (B-19) together with the assumptions made define the conditions within both the bulk liquid and

---

*In many cases of interest, however, where the liquid is pressurized with its own vapor, T_s is known, since the surface must be maintained at the saturation temperature corresponding to the tank pressure. Numerous investigators (38), (39), (40), have shown that the assumption of negligible heat and mass transfer at the surface is justified even under these conditions, where evaporation and/or condensation may be occurring.

the thermal layer as a function of time alone. In general a simultaneous solution to these equations must be obtained numerically since they are not readily amenable to analytic methods. If, however, the boundary layer thickness is ignored and the term $x_t^{8/7}$ in the expression for $\bar{U}\delta$ is linearized to the form $ax_t - b$, analytical solutions can be found for both ℓ and T_v. The solution for ℓ is

$$\ell = \ell_\infty[1 - \exp\ (-\frac{2aK_2}{H}\ \tau)] \qquad \text{(B-20)}$$

where $$\ell_\infty = L[1 - [1 - \exp\ (-K_1 Q_B/Q_S)]^{7/8}]$$

$$a = \frac{L^{8/7}}{\ell_\infty} \exp\ (-K_1 \frac{Q_B}{Q_S})$$

$$b = L^{8/7}[\frac{L}{\ell_\infty} \exp\ (-K_1 \frac{Q_B}{Q_S}) - 1]$$

The constants a and b are evaluated by equating $\bar{U}\delta$ and $ax_t - b$ at $x_t = L$ and $x_t = (L - \ell_\infty)$, respectively. The solution for T_v is

$$T_v = T_{vo} + \frac{Q_B + K_o Q_S}{WH\rho c[L - \ell_\infty]}\ [\tau + \frac{H}{2aK_2} \ln(1 - \frac{\ell}{L})] \qquad \text{(B-21)}$$

with the resulting expression for n:

$$n = \frac{WH\rho c\ell(T_s - T_v)}{\left\{WH\rho c\ell(T_s - T_v) - Q_S(1-K_o)\tau + \frac{Q_B + K_o Q_S}{(\frac{L}{\ell_\infty} - 1)}\left[\tau + \frac{HL}{2aK_2\ell_\infty}\ln(L - \frac{\ell}{L})\right]\right\}} - 1 \qquad \text{(B-22)}$$

Finally, if there is no bottom heating $T_v \equiv T_{vo}$, $U_{mix} = 0$ and a solution for ℓ can be obtained, neglecting the boundary layer thickness, with no linearization. This solution is

$$\ell = L\left[1 - \left(\frac{2K_2 L^{1/7}}{7H}\tau + 1\right)^{-7}\right] \qquad \text{(B-23)}$$

The corresponding expression for n is:

$$n = \frac{(T_s - T_{vo})}{(T_s - T_{vo}) - \frac{2Lq_s\tau}{H\rho c\ell}} - 1 \qquad \text{(B-24)}$$

Ideal Relation Between K_o and K_1

A relation between K_o and K_1 can be shown to exist in the ideal case, where the fluid behavior exactly follows that assumed in the analysis. In general, however, the derived relation between K_o and K_1 is displaced in various amounts from the results obtained from the testing. This displacement provides a measure of the departure of the actual fluid behavior from the ideal behavior.

To determine the relation between K_o and K_1, the behavior of the ideal system for large values of time is studied. Since ℓ approaches ℓ_∞

for large times, Equation (B-12) can be written

$$\left.\frac{dT_v}{d\tau}\right|_{\tau\to\infty} = \frac{q_b + 2q_s(L/H)K_o}{\rho c(L - \ell_\infty]} = \text{Constant} \tag{B-25}$$

By differentiating Equation (B-13) and by defining

$$\bar{T}_{t\ell} = \frac{1}{\ell}\int_o^{\ell} T_{t\ell}\, d\varepsilon \tag{B-26}$$

the following relation can be gained, noting that for large times ℓ becomes ℓ_∞:

$$\left.\frac{d\bar{T}_{t\ell}}{d\tau}\right|_{\tau\to\infty} = \frac{2Lq_s(1 - K_o)}{H\rho c\ell_\infty} = \text{Constant} \tag{B-27}$$

In addition, for large times the tank average temperature $\bar{T}$ is governed by the two relations

$$\left.\frac{d\bar{T}}{d\tau}\right|_{\tau\to\infty} = \frac{2q_s}{H\rho c} + \frac{q_b}{L\rho c} = \left(\frac{L - \ell_\infty}{L}\right)\frac{dT_v}{d\tau} + \frac{\ell_\infty}{L}\frac{d\bar{T}_{t\ell}}{d\tau} = \text{Constant} \tag{B-28}$$

Equations (B-25), (B-27) and (B-28) indicate that at large times all the temperature derivatives become constant. By combining these equations, it can be shown that

$$\left.\frac{d\bar{T}}{d\tau}\right|_{\tau\to\infty} = \left.\frac{d\bar{T}_{t\ell}}{d\tau}\right|_{\tau\to\infty} = \left.\frac{dT_v}{d\tau}\right|_{\tau\to\infty} = \frac{2q_s}{H\rho c} + \frac{q_b}{L\rho c} \tag{B-29}$$

Finally, using (B-25), (B-27) and the definition of ℓ_∞, the desired expression for K_1 can be written:

$$K_1 = -(2)\left(\frac{q_s}{q_b}\right)\left(\frac{L}{H}\right) \ln\left\{1 - \left[\frac{K_o + \left(\frac{1}{2}\right)\left(\frac{q_b}{q_s}\right)\left(\frac{H}{L}\right)}{1 + \left(\frac{1}{2}\right)\left(\frac{q_b}{q_s}\right)\left(\frac{H}{L}\right)}\right]^{8/7}\right\} \qquad \text{(B-30)}$$

This relation provides the basis for the correlation expression for K_1 presented in the section "Correlation of Test Data" in Chapter IV.

APPENDIX C

TEMPERATURE DATA CORRELATION COMPUTER PROGRAM

In the analysis presented in Appendix B two empirical constants, K_o and K_1, are required before any predictions of stratification can be made. One of the main objectives of the experimental program has been to supply data from which values of these constants can be gained under varying test conditions. To correlate the analytical model and the test data, a computer program has been written for use on the IBM 7094. Basically the objective of the program is to find the set of values for K_o and K_1 which give a "best fit" between the test data and the predicted results. The criterion used here for best fit is that family of predicted temperature profiles which minimizes the function:

$$(\sigma_{Tx}/\bar{\theta}_2) = \frac{1}{\bar{\theta}_2}\left[\frac{1}{L\tau_{max}}\int_o^{\tau_{max}}\int_o^{L}(T_p - T_{exp})^2 dx d\tau\right]^{1/2} \qquad (C\text{-}1)$$

where: T_p = predicted temperature, F

T_{exp} = experimental temperature, F

$\bar{\theta}_2$ = mean temperature rise of the test fluid.

The quantity $(\sigma_{Tx}/\bar{\theta}_2)$ is the root mean square temperature deviation in time and axial position between the test data and the predicted results expressed as a fraction of the test fluid mean temperature rise. It is a function of K_o and K_1 only. Thus the problem of determining a best

becomes that of finding the minimum point on a three-dimensional surface.

A minimization technique based on the definition of the gradient of a function of two independent variables was first tried unsuccessfully. During this phase, it was found that the $(\sigma_{Tx}/\bar{\theta}_2)$ surface is not shaped with a definite minimum but rather as a deep, narrow, slightly curved canoe whose keel is oriented at some angle between the positive K_o and K_1 axes. In retrospect, this shape is not too surprising when the ideal relation (B-30) between K_o and K_1 is studied. Because of this particular shape the gradient technique was found to converge extremely slowly. However, a second less elegant method was found which works very efficiently and consumes only a small amount of machine time. This method involves first finding the local minimum $(\sigma_{Tx}/\bar{\theta}_2)$ at a given K_o by successive calculation of the minimum of $(\sigma_{Tx}/\bar{\theta}_2)$ parabolas fitted through various guessed values of K_1. By continually decreasing the range of values of K_1 around the current local minimum, the desired least value of $(\sigma_{Tx}/\bar{\theta}_2)$ can be determined to arbitrary precision. Then using the value of K_1 obtained as a first guess, a new local minimum is found for a new value of K_o. This process is repeated over any desired range of K_o and K_1.

Figure 23 is presented to illustrate the shape of a typical $(\sigma_{Tx}/\bar{\theta}_2)$ surface together with the locus of local minimums. In addition, the ideal relation between K_o and K_1 is plotted. From study of the figures the elongated shape of the constant $(\sigma_{Tx}/\bar{\theta}_2)$ contours is observed and it is seen that $(\sigma_{Tx}/\bar{\theta}_2)$ varies only slightly from its minimum over a relatively broad range of values for K_o and K_1. In addition, the similarity between the actual and the ideal values for K_o and K_1 is noted.

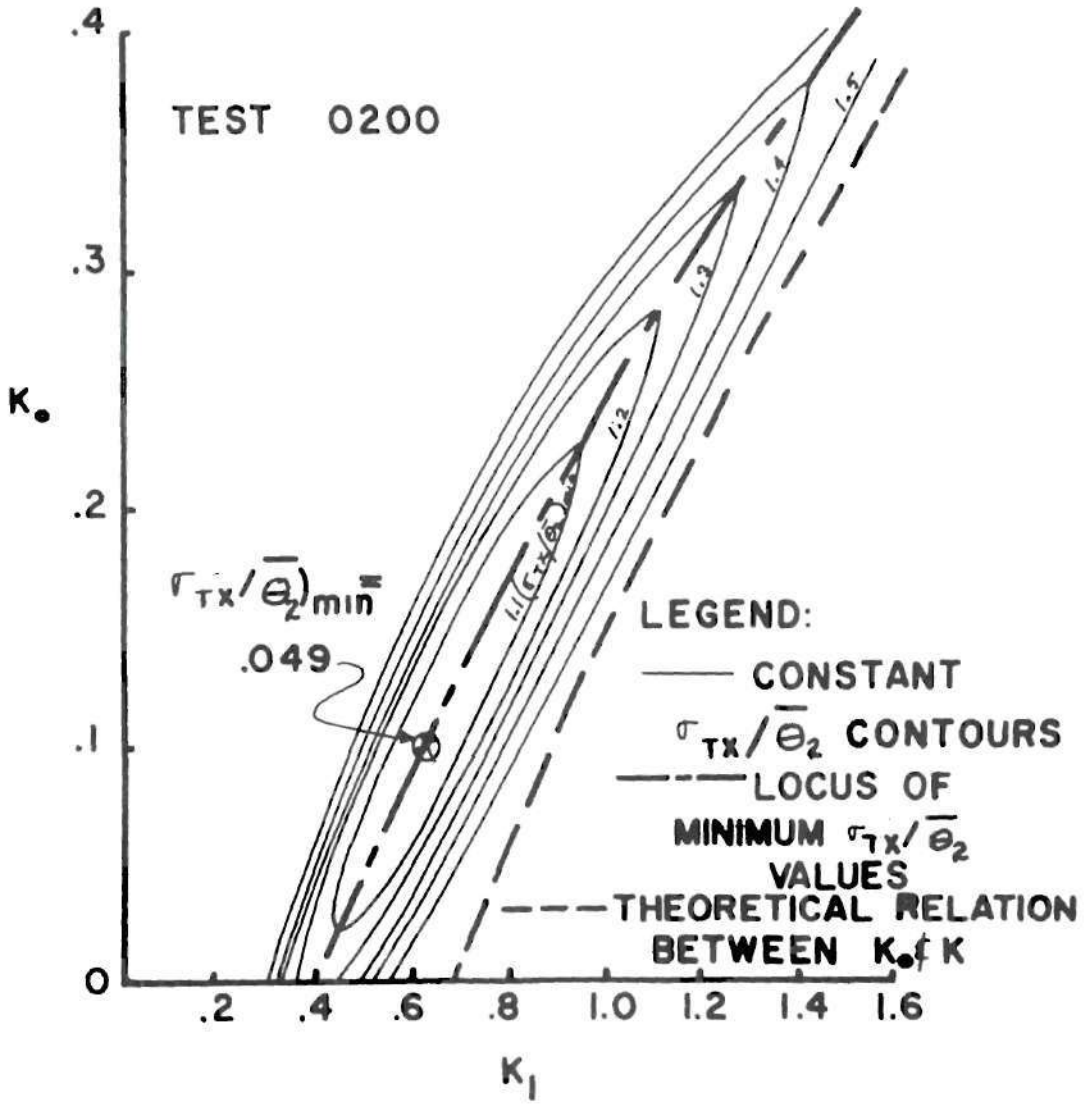

Figure 23. Constant $\sigma_{Tx}/\bar{\theta}_2$ Contours and Ideal Relation Between K_o and K_1, Test 0200.

In computing $(\sigma_{T_x}/\bar{\theta}_2)$, values of T_p for a given pair of K_o and K_1 must be obtained in some manner. The computer program is written so that the approximate analytical solutions presented in Equations (B-20), (B-21), and (B-22) can be used first to obtain approximate values for the desired locus of minimums. These $(\sigma_{T_x}/\bar{\theta}_2)$ values can then be used as first guesses to obtain even more precision by numerically solving Equations (B-5) and (B-12) for T_v and ℓ. It has been found that the numerical solutions give results insignificantly different from those corresponding to the approximate solutions. For this reason, and to save computer time, all of the correlations have been made using the approximate solutions.

Besides calculation of K_o and K_1, the computer program also converts the millivolt output from each test sensor to degrees Fahrenheit, using the calibration corrections, and produces temperature profiles at fixed values of time by interpolating parabolically in the raw test data. Further, it calculates various boundary layer characteristics and determines the bottom and side heat flux by integrating the temperature profile. Finally, the program has an option by use of which the predicted results and the test results are both plotted on the same graph allowing visual comparison of the theory and the experiment.

During the correlation of the test data with the analytical model an investigation was made of the effect on predicted thermal layer growth of the shape of the assumed velocity profile in the boundary layer. It was found that in Equation (A-3) a value of $p = 2$ gives most favorable results, although the effects of changes in the profile shape are relatively minor, generally being less than 10 per cent. Thus for

all the correlations presented, the velocity profile is assumed to be of the form

$$U = U_1(y/\delta)^{1/7}(1 - y/\delta)^2 \qquad (C\text{-}2)$$

This profile is different from that used by Eckert and Jackson which was chosen to give a best fit to existing heat transfer data for a vertical flat plate. It, however, is identical with that used by Fujii (37) in a more recent study of turbulent natural convection along vertical cylinders.

A complete listing of the computer program is presented in the following pages.

```
      DIMENSION TT(100),P(100),V(100),YK(100),XSE(16),TB(100),L2(8),          13/01/66

      DIMENSION TT(100),P(100),V(100),YK(100),XSE(16),TB(100),L2(8),
     1CP(100),PR(100),RET(100),ALP(100),TE(16,100),DTE(100),A(16),NA(4),
     2TEI(16,100),NS(16),XS(60),AA(6),LI(8),TI(100),DTAP(100),DUM(300),
     3ERP(100),GRC(100),QSC(100),QDSC(100),TTT(16,100),SIGMAX(100)
      DIMENSION YK0(5),YK1(5),YK2(5)
      COMMON XLL,XK1,QB,QS,XK0,NJ,DTIP,H,TV0,XK2,
     1PI,CPI,DLL,W,TE,XSE,SIGMAX,NA,TTT,TI,DUM,NTBLI,LI,BET,TT,P,V,YK,
     2CP,PR,ALP,DTE,G,Q,W,H,QDSC,DTIC
 1040 FORMAT(10E8.0)
      I=0
      IN=5
      IO=6
      IP=7
      IX=2
      IPP=3
      CALL LOOPEN(1,IPP)
C  READ POSITIONS OF 120 SENSORS
      READ INPUT TAPE IN,1040,XS
C  READ TABLE 1
 1    I=I+1
      READ INPUT TAPE IN,1000,TT(I),P(I),V(I),YK(I),CP(I),PR(I),BET(I),A
     1LP(I)
 1000 FORMAT(8E10.5)
      IF(TT(I))1,2,1
 2    NTBLI=I-1
      WRITE OUTPUT TAPE IO,2001
      WRITE OUTPUT TAPE IO,1090,(TT(I),P(I),
     1V(I),YK(I),CP(I),PR(I),BET(I),ALP(I),I=1,NTBLI)
 1090 FORMAT(14X,1HT,14X,1HP,14X,1HV,14X,
     11HK,13X,2HCP,13X,2HPR,11X,4HBETA,10X,
     25HALPHA//(8E15.5/))
C  READ TABLE 2
      REWIND IPP
 9999 READ INPUT TAPE IN,1010,W,H,XLL,QSA,
     1QBA,IMO,IDAY,IYEAR,NTEST,DLL,DTIP,
     2DTIC,TIM,EXK,TV0,G,NJ,NA
 1010 FORMAT(5E10.0,3I2,I4,2F10.0/5E10.0,6,I2,4I1)
      WRITE OUTPUT TAPE IO,2002
      WRITE OUTPUT TAPE IO,1100,W,H,XLL,
     1QSA,QBA,IMO,IDAY,IYEAR,NTEST,DLL,
     2DTIP,DTIC,TIM,NJ,EXK,TV0,G,NA
 1100 FORMAT(1X ,2HW=,E10.4/3H H=,F10.4/
     14H LL=,E10.4/5H QSA=,F10.4/5H QBA=,
     2E10.4/6H DATE=,I2,1H/,I2,1H/,I2/
     36H TEST=,I5/5H DLL=,F10.4/6H DTIP=,E10.4/
     46H DTIC=,F10.4/6H TIME=,F10.4/3H J=,
     5I5/5H EXK=,F10.4/5H TV0=,F10.4/3H G=,
     6E10.4/17H OPTION A,B,C,D =,4(I1,1H,))
C  READ TABLE 3
      READ INPUT TAPE IN,1020,((TE(I,J),TEI(I,J),I=1,16),J=1,NJ)
 1020 FORMAT(8E10.0)
      DO 3000 I=1,16
      DO 3000 J=1,NJ
 3000 TEI(I,J)=TEI(I,J)*PI
      DO 500 I=1,NJ
      WRITE OUTPUT TAPE IO,2003
```

```
      DIMENSION TT(100),P(100),V(100),YK(100),XSE(16),TR(100),L2(8),          13/01/66
 500  WRITE OUTPUT TAPE IO,1110,(TE(J,I),
     1TEI(J,I),J=1,16)
 1110 FORMAT(1X ,6X,4HTEMP,10X,4HTIME//
     1(F15.6,5X,F15.6/))
C  READ SENSOR NO.
      READ INPUT TAPE IN,1030,NS
 1030 FORMAT(16I5)
      WRITE OUTPUT TAPE IO,2004
C  READ READ TEMPERATURE POLY COEFF. FOR SENSORS
 3    READ INPUT TAPE IN,1050,AA,IIII
 1050 FORMAT(6E13.6,I5)
      IF(IIII)15,5,15
 15   DO 14 I=1,16
      IF(IIII-NS(I))14,4,14
 14   CONTINUE
      WRITE OUTPUT TAPE IO,1130,AA,IIII
 1130 FORMAT(6E13.6,1X,I5)
      GO TO 3
C  CORRECT SENSOR TEMP READING
 4    DO 51 J=1,NJ
 51   TE(I,J)=AA(1)+((((TE(I,J)*AA(6)+AA(5))*TE(I,J)+
     1AA(4))*TE(I,J)+AA(3))*TE(I,J)+AA(2))*TE(I,J)
      WRITE OUTPUT TAPE IO,1130,AA,IIII
      GO TO 3
 5    L1(4)=16
      L1(5)=16
      L1(6)=2
      L1(7)=NJ
      L1(1)=LOC(L1(1))
      DO 6 I=1,16
      L1(2)=LOC(TEI(I,1))
      L1(3)=LOC(TE(I,1))
      DO 6 J=1,NJ
      L1(8)=0
      XXJ=J
      TI(J)=XXJ*DTIP
 6    TE(I,J)=GIPIF(TI(J),L1(1))
      DO 7 I=1,16
      IIII=NS(I)
 7    XSE(I)=XS(IIII)
      WRITE OUTPUT TAPE IO,2005
 2001 FORMAT(1H1,16HINPUT TABLE 1 - ,
     116HFLUID PROPERTIES//)
 2002 FORMAT(1H1,16HINPUT TABLE 2 - ,
     119HTEST IDENTIFICATION//)
 2003 FORMAT(1H1,16HINPUT TABLE 3 - ,
     126HEXPERIMENTAL TEMPERATURES//)
 2004 FORMAT(1H1,16HINPUT TABLE 4 - ,
     131HSENSOR CALIBRATION COEFFICIENTS//)
 2005 FORMAT(1H1,16HINPUT TABLE 5 - ,
     128HLOCATIONS OF SENSORS//,
     21X,6HNUMBER,2X,15HSENSOR LOCATION//)
      WRITE OUTPUT TAPE IO,1140,(I,XSE(I),
     1I=1,16)
 1140 FORMAT(19X,I5,E15.6)
 100  CONTINUE
```

```
      DIMENSION TT(100),P(100),V(100),YK(100),XSF(16),TB(100),L2(8),          13701766

      L1(2)=LOC(TT(1))
      L1(3)=LOC(P(1))
      L1(4)=1
      L1(5)=1
      L1(6)=1
      L1(7)=NTBL1
      L2(1)=LOC(L2(1))
      L2(2)=L1(2)
      L2(3)=LOC(CP(1))
      L2(4)=1
      L2(5)=1
      L2(6)=1
      L2(7)=NTBL1
      NJJ=NJ+1
      DO 82 I=1,16
82    TE(I,NJJ)=TV0
      TI(NJJ)=0.
      DO 8 I=1,NJJ
      DO 81 III=1,16
81    A(III)=TE(III,I) - TVC
      DTE(I)=AREA(XSF,A,16,0.,XLL)/XLL
      TB(I)=TVC+DTE(I)
      L1(8)=0
      L2(8)=0
      XXI=TB(I)
      DTAP(I)=((QHA+QSA)*TI(I))/((XLL+DLL)*W*H*GIRIF(XXI,L1(1))*GIRIF(XX
     1I,L2(1)))
      EPR(I)=-(DTE(I)-DTAP(I))*100./DTAP(I)
      QHC(I)=QHA*(1.0-EPR(I)/100.)
      QSC(I)=QSA*(1.0-EPR(I)/100.)
8     QDSC(I)=QSC(I)/(2.0*W*XLL)
101   CONTINUE
      DO 9 I=1,NJJ
      L1(8)=0
      L1(2)=LOC(CP(1))
      CP1=GIRIF(TB(I),L1(1))
      L1(8)=0
      L1(3)=LOC(YK(1))
      YKI=GIRIF(TB(I),L1(1))
      L1(8)=0
      L1(3)=LOC(PR(1))
      PRI=GIRIF(TB(I),L1(1))
      L1(8)=0
      L1(3)=LOC(BLT(1))
      BLT1=GIRIF(TB(I),L1(1))
      L1(8)=0
      L1(3)=LOC(ALP(1))
      ALP1=GIRIF(TB(I),L1(1))
      L1(8)=0
      L1(2)=LOC(P(1))
      P1=GIRIF(TB(I),L1(1))
      L1(8)=0
      L1(2)=LOC(V(1))
      V1=GIRIF(TB(I),L1(1))
      DU=(1.0-0.**2)*(((BLT1*QDSC(I)*(G/YKI)*SQRTF(ALP1))/
     1(PR1+.8))**.4)
```

```
      DIMENSION TT(100),P(100),V(100),YK(100),XSE(16),TB(100),L2(8),          13/21/66

      C=  5.0*((G*BET1*QDSC(1)*(PR1**.53333333))/(P1*CP1*(V1**.2)*(3.30+
     1(PR1**.666666667)))**.3571428
      DL=(360.0**.2)*SQRTF(ALP1)*(((BET1*QDSC(I)
     1*(G/YK1)*SQRTF(ALP1))/(PR1+.8))**(-.2))
      DT=.512*(V1**.2)*(PR1**(-.5333333333))*(C**(-.2))
      THL=(QDSC(I)/(2.0*YK1))*(360.0**.2)*SQRTF(
     1ALP1)*(((BET1*QDSC(I)*(G/YK1)*SQRTF(ALP1))
     2/(PR1+.8))**(-.2))
      THT=37.7*QDSC(1)*(PR1**.5333333)*(C**
     1(-.8))/(P1*CP1*(V1**.2))
      XNTR=G*BET1*THT/(V1*V1)
      YNTR=G*BET1*QDSC(I)/(V1*V1*YK1)
      WRITE OUTPUT TAPE 10,1060,TT(I)
      DO 10 K=1,16
      XKK=11-K
      X=XKK*XLL*0.1
      X1=DIL*(X**.6)
      X2=C*(X**.42857143)
      X3=DL*(X**.2)
      X4=DT*(X**.71428571)
      X5=THL*(X**.2)
      X6=THT*(X**(-.14285714))
      X7=XNTR*(X**2.8571429)
      X8=YNTR*(X**4.0)
      XKK=XKK/16.0
102   CONTINUE
10    WRITE OUTPUT TAPE 10,1070,XKK,X,X1,X2,X3,X4,X5,X6,X7,X8
1060  FORMAT(8H1TABLE 1//1X,7HTIME = ,F8.1/14X,1HX,8X,
     1 3HDIL,7X,3HDIT,6X,6HDELTAL,4X,6HDELTAT,4X,
     2 6HTHLTAL,4X,6HTHETAT,6X,3HNGR,6X,4HNGR1/14X,2HFT,
     3 7X,6HFT/SEC,4X,6HFT/SEC,3X,2HFT,8X,2HFT,
     4 8X,1HF,9X,1HF)
1070  FORMAT(F5.1,2HLL,3X,7F10.6,2E16.4)
9     WRITE OUTPUT TAPE 10,1080,DTF(I),T3(I),DTAP(I),QDC(I),QSC(I),QDSC(
     1I),GR(I)
1080  FORMAT(////7H DTF = ,F14.7,5X,5HT3 = ,F14.7,
     1 5X,6HDTA = ,F14.7,5X,6HQDC = ,F14.7/
     2 7H QSC = ,F14.7,5X,7HQDSC = ,F10.7,3X,5HGRAD = ,F14.7)
      NJJJ=NJ-1
      XT=TVE+DTE(NJJ)/2.0
      SUM(2,7)=DTF(NJ)
      L1(2)=LOC(TT(1))
      L1(4)=1
      L1(5)=1
      L1(6)=1
      L1(7)=NTHL1
      L1(8)=
      L1(2)=LOC(BET)
      TT1=GIRLF(XT,L1(1))
      L1(8)=6
      L1(3)=LOC(DR)
      W=1.-GIRLF(XT,L1(1))
      L1(8)=
      L1(3)=LOC(V)
      V1    =GIRLF(XT,L1(1))
      L1(8)=
```

```
      DIMENSION TT(100),P(100),V(100),YK(100),XSE(16),TH(100),L2(8),          13/01/66

      L1(3)=LOC(CP)
      CP1  =GIR1F(XT,L1(1))
      L1(8)=0
      L1(3)=LOC(P)
      P1   =GIR1F(XT,L1(1))
      L1(8)=0
      L1(3)=LOC(ALP)
      ALP1=GIR1F(XT,L1(1))
      Q=QDSC(NJ)
      QB=QBC(NJ)
      QS=QSC(NJ)
      XK2=.966*(V1**.2)*(PR1**(-.53333333))*(((
     1G*RET1*Q*(PR1**.53333333))/(P1*CP1*(V1**.2)*
     2(3.30+(PR1**.66666666))))**.28571429)/H
      L1(2)=LOC(TE(1,NJ))
      L1(3)=LOC(XSE(1))
      L1(7)=16
      L1(8)=0
      X=GIR1F(.75*TE(1,NJ)+.25*TE(16,NJ),L1(1))
      XLI=XLL-X
      XKL=(((TE(1,NJ)-TVO)**N*P1*CP1*(XLL+DLL-XLI))/((TI(NJ)+
     1(1.G/(R**XK2   ))*LOGF(1.0-XLI/(XLL+DLL)))*QS))-QB/QS
      XKL=.15
      XLLP=XLL
103   XK1=-(QS/QB)*LOGF(1.0-(1.0-XLI/XLLP)**1.1428571)
      XK1=.1
      XK1=ABSF(XK1)
      IF(QB)110,111,110
110   NAIII=NA(1)
      GO TO(120,125,126),NAIII
125   CALL MINIMD(EXK,F,NITTD)
      GO TO 120
126   CALL MINIM(EXK,F,NITT)
      GO TO(120,125,125),NAIII
112   END FILE IPP
      END FILE IPP
      REWIND IPP
      CALL BRKOUT(1,4HPLOT,IPP)
13    GO TO 9999
111   XKL=0.
      XK1=0.
      C=((G*BET1*Q*(PR1**.53333333)/(P1*CP1*(V1**.2)))
     1**.28571428)*(V1**.2)*(PR1**(-.53333333))*
     2((.96)/((3.30+(PR1**.66666666))**.28571428))/H
      DO 113 I=1,NJ
      SUM(I)=XLL*(1.0-1.0/((C*(XLL**.14285714)*TI(I)/7.2+1.0)**7))
      SUM(I+100)=TVO
113   SUM(I+200)=(TE(16,I)-TVO)/((TE(16,I)-TVO)-2.0*QDSC(I)*XLL*TI(I)/(
     1H*M1*CP1*SUM(I)))-1.0
      NAIII=NA(1)
      GO TO(116,115,114),NAIII
114   CALL MINIM1(EXK,F,NITT)
115   CALL MINIM2(EXK,F,NITT)
      GO TO 120
116   CALL MINIM1(EXK,F,NITT)
120   IF(NA(3)-1)112,9999,112
```

```
DIMENSION TT(100),P(100),V(100),YK(100),XSE(16),TB(100),L2(8),          13/01/66
END(1,0,0,0,0,0,1,0,0,1,0,0,0,0,0)
```

```
      SUBROUTINE DIFC(XK0,XK1)                                          13/01/66

      SUBROUTINE DIFC(XK0,XK1)
      DIMENSION XSE(16),SIGMA(16),TE(16,100),SIGMAX(100),TI(100),NA(4),
     1TT(16,100),XL(100),TV(100),XN(100),L1(8),BET(100),TX(100),P(100),
     2V(100),YK(100),CP(100),PR(100),ALP(100),DTE(100),ODSC(100)
      COMMON XLL,XK1,DH,DS,XK0,NJ,DTIP,H,TV0,XK2,
     1PI,CP1,DLL,W,TE,XSE,SIGMAX,NA  ,TT,TI,XL,TV,XN,NTBL1,L1,BET,TX,P,
     2V,YK,CP,PR,ALP,DTE,G,Q,W,H,ODSC,HH
      CALL TAPE(2,IN,ID)
      KKKK=0
      NUPT=NUPT
      IF(NA(4)-2)12,12,13
12    WRITE OUTPUT TAPE 10,1010
1010 FORMAT(22H1DIFF. EQUATION VALUES//13X,1HT,13X,1HL,12X,2HTV,
     19X,5HDL/DT,8X,6HDTV/DT//)
13    SUM=0.
      L1(1)=LOC(L1(1))
      L1(2)=LOC(TX(1))
      L1(4)=I
      L1(5)=1
      L1(6)=1
      L1(7)=NTBL1
      XI=TV0*XN(97)/2.0
      L1(8)=0
      L1(3)=LOC(BET)
      BET1=GIR1F(XI,L1(1))
      L1(8)=0
      L1(3)=LOC(PR)
      PR1  =GIR1F(XI,L1(1))
      L1(8)=0
      L1(3)=LOC(V)
      V1   =GIR1F(XI,L1(1))
      L1(8)=0
      L1(3)=LOC(CP)
      CP1  =GIR1F(XI,L1(1))
      L1(8)=0
      L1(3)=LOC(P)
      P1   =GIR1F(XI,L1(1))
      L1(8)=0
      L1(3)=LOC(ALP)
      ALP1=GIR1F(XI,L1(1))
      C=5.0*((  6*BET1*U*(PR1**.53333333))/(P1*CP1*(V1**.2)*(3.30+
     1(PR1**.66666666))))**.35714286
      DT=.512*(V1**.2)*(PR1**(-0.53333333))*(C**(-.2))
      XLLP=XLL
      D=DT*(XLLP**.71428571)
      U1=C*(XLLP**.42857143)
      UM=.2590*(1.0-EXP(-XK1*DU/DS))*U1*D/(H/2.0-D)
      XN(98)=UM
      TM=TI(NJ)
      XK=1
      KL=0
      T=0.
      X=0.
      Y=TV0
      ERASE LIGHT 1
1     DO 2 I=1,4
```

```
      SUBROUTINE DIFC(XKG,XK1)                                          13/01/66

      XX=XLLP-X
      IF(KL-KK)51,52,52
51    XT=Y
      L1(8)=0
      L1(3)=LOC(BET)
      BET1=GIR1F(XT,L1(1))
      L1(8)=0
      L1(3)=LOC(PH)
      PH1 =GIR1F(XT,L1(1))
      L1(8)=0
      L1(3)=LOC(V)
      V1  =GIR1F(XT,L1(1))
      L1(8)=0
      L1(3)=LOC(CP)
      CP1 =GIR1F(XT,L1(1))
      L1(8)=0
      L1(3)=LOC(P)
      P1  =GIR1F(XT,L1(1))
      L1(8)=0
      L1(3)=LOC(ALP)
      ALP1=GIR1F(XT,L1(1))
      C=5.0*((  G*SET1*D*(PP1**.5333333))/(P1*CP1*(V1**.2)*(3.30+
     1(PR1**.6000000)))**.3571428
      DT=.512*(V1**.2)*(PR1**(-2.533333333))*(C**(-.2))
      KL=KL+1
52    T=DT*(XX**.71428571)
      U1=C*(XX**.42857142)
      DX=.2*SQ*U1*D/(H/2.0-D)-DM
      DY=(QP+XK.1*.5)/(W*H*P1*CP1*(XLL+DLL-X))
      T=INDV2F(T,HH)
      Y=INDV2F(Y,DY)
2     X=INDV2F(X,DX)
      KKKK=XMUDF(KKKK+1,51)
      SUM=SUM+DX*Y*HH
      IF(NA(4)-2)10,100,11
100   IF(KKKK-5)11,101,11
101   KKKK=0
11    WRITE OUTPUT TAPE 10,1000,T,X,Y,DX,DY
      IF(T-TI(KK))45,3,3
3     XL(KK)=X
      TV(KK)=Y
      XN(KK)=(TF(15,KK)-TV(KK))/(TE(15,KK)-2.0*XLLP*(1.-XKG)*
     1.5*C(KK)*TI(KK)/
     2(H*P1*CP1*XL(KK))-(1.5/XL(KK))*SUM              )-1.5
      KK=KK+1
45    IF(T-TM)1,9,9
9     DO 6 I=1,NJ
      T=TI(I)
      Y=XLL-XL(I)
      DO 7 J=1,16
      IF(XSP(J)-Y)7,7,8
7     CONTINUE
8     M=J
      DO 4 J=1,MM
      TT(J,I)=TV(I)
      YY=TV(I)-TL(J,I)
```

```
      SUBROUTINE DIFC(XKC,XKI)                                          13/01/66
9     SIGMA(J)=YY*YY
      DO 55 J=MM,16
      EL=XSE(J)*XL(I)-XLL
      YY=TE(16,I)-(TE(1c,I)-TV(I))*((1.0-EC/XL(I))**XN(I))
      IF(J-16)7c,75,75
75    YY=TE(16,I)
76    TT(J,I)=YY
      YY=YY-TE(J,I)
55    SIGMA(J)=YY*YY
6     SIGMAX(I)=SORTF(AREA(XSE,SIGMA,15,0.,XLL)/XLL)
      XN(10C)=XLI
      ZIFC=0.
      DO 66 I=1,NJ
66    ZIFC=ZIFC+SIGMAX(I)*SIGMAX(I)
      XNJ=NJ
      ZIFC=ZIFC/XNJ
1000  FORMAT(5E14.7)
      DIFC=SQRTF(ZIFC)
      RETURN
      END(1,2,0,0,0,0,1,0,0,1,0,0,0,0)
```

APPENDIX D

BOUNDARY LAYER DIFFUSION ANALYSIS COMPUTER PROGRAM

In the diffusion analysis presented in Chapter IV a computer program is required to correlate the test results with the analysis. This program, described here, makes the following operations:

1. Computation of a complete table of experimental values of θ_2 as a function of time and position, using parabolic interpolation between the data points taken.

2. Computation of a difference table for θ_2 as a function of time and position.

3. Computation of $\overline{K_o}(x)$ at different times from Equation (10) using the results of 1 and 2 above together with a numerical integration technique.

4. Computation of the coefficients C_η in Equation (55) for θ_2 using a least squares fit to the test data with the function

$$\left[-\frac{J}{xe^{2x^2}}\right]^\eta \left[\frac{e^{\frac{2\eta K'\tau}{H}} - 1}{\eta}\right]$$

used as the argument.

5. Computation of the predicted values of θ_2 as a function of position and time.

6. Computation of $K_o(x)$ corresponding to the C_η's and comparison with the time average $K_o(x)$ obtained in 3 above.

7. Check on the computed values of $K_o(x)$ from 6 by use of

Equation (10).

A complete listing of this program is presented in the following pages.

```
BPS FORTRAN D COMPILER    24/01/66                                          26/01/66
          C     INTERPOLATION TABLE FOR THETA
S.0001          DIMENSION X1(45),T1(7,5),TH1(7,5),TH(60,21),THP(60,20),X11(45),
               1UBD1(7),UBD(43),XBD1(7),XBD(43),ST(60),STHP(60),XK(19),XX(19),
               2FX(19),X(70),FX1(30),C1(19),CAL(19),ERR(70),FX2(70)
S.0002          DIMENSION BASIS(19,70),T2(7,10),TH2(7,10),X2(10)
S.0003          DIMENSION ZX(19)
S.0004          DOUBLE PRECISION BASIS,C1
S.0005          DOUBLE PRECISION ZZZ,XXX
S.0006          EQUIVALENCE (T1(1,1),T2(1,6)),(TH1(1,1),TH2(1,6)),(X1(1),X2(6))
S.0007          READ(5,100)(X2(J),J=1,10)
S.0008          DO 13 J=1,10
S.0009     13   READ(5,100)(T2(I,J),TH2(I,J),I=1,7)
S.0010     100  FORMAT(14F5.0)
S.0011          Q=.12
S.0012          H=2.
S.0013          P=62.4
S.0014          C=1.
S.0015          ZK=.00114
S.0016          HK2=2.*ZK/H
S.0017          CON=Q/(P*C*ZK)
S.0018          X2(1)=1.E-20
S.0019          DO 1510 II=1,19
S.0020          DO 1510 J=1,10
S.0021          DO 1510 I=1,7
S.0022          K=(J-1)*7.+I
S.0023     1510 BASIS(II,K)=(X2(J)*EXP(-.5/X2(J)**2))**II*(EXP(T2(I,J)*HK2*II)-1.)
               1/II*CON
S.0024          DO 1520 J=1,10
S.0025          DO 1520 I=1,7
S.0026          K=(J-1)*7.+I
S.0027     1520 FX2(K)=TH2(I,J)
S.0028          DO 34 J=1,5
S.0029          N=0
S.0030          JJ=5*(J-1)+1
S.0031          DO 34 I=1,5
S.0032          IF(TH1(I+1,J))15,15,20
S.0033     15   A=0.
S.0034          B=0.
S.0035          C=0.
S.0036          GO TO 26
S.0037     20   Z1=(TH1(I,J)-TH1(I+1,J))/(T1(I,J)-T1(I+1,J))
S.0038          Z2=(TH1(I,J)-TH1(I+2,J))/(T1(I,J)-T1(I+2,J))
S.0039          A=(Z1-Z2)/(T1(I+1,J)-T1(I+2,J))
S.0040          B=Z1-A*(T1(I,J)+T1(I+1,J))
S.0041          C=TH1(I,J)-A*T1(I,J)**2-B*T1(I,J)
S.0042     26   J1=N+1
S.0043          IF(I-5)28,27,28
S.0044     27   N=60
S.0045          GO TO 29
S.0046     28   N=T1(I+1,J)/10.
S.0047     29   DO 34 K=J1,N
S.0048          XK1=10*K
S.0049     30   TH(K,JJ)=A*XK1**2+B*XK1+C
S.0050          IF(TH(K,JJ))31,34,34
S.0051     31   TH(K,JJ)=0.
S.0052     34   CONTINUE
S.0053          DO 60 I=1,N
S.0054          II=0
S.0055          DO 60 J=1,11,5
S.0056          II=II+1
```

```
S.0057          IF(TH(I,J+5))45,35,45
S.0058       35 A=0.
S.0059          B=0.
S.0060          C=0.
S.0061          GO TO 56
S.0062       45 Z1=(TH(I,J)-TH(I,J+5))/(X1(II)-X1(II+1))
S.0063          Z2=(TH(I,J)-TH(I,J+10))/(X1(II)-X1(II+2))
S.0064          A=(Z1-Z2)/(X1(II+1)-X1(II+2))
S.0065          B=Z1-A*(X1(II)+X1(II+1))
S.0066          C=TH(I,J)-A*X1(II)**2-B*X1(II)
S.0067          IF(J1-17)56,55,56
S.0068       55 XK1=X1(II+1)
S.0069          GO TO 57
S.0070       56 J1=J+1
S.0071          J2=J+4
S.0072          XK1=X1(II)
S.0073       57 DO 59 K=J1,J2
S.0074          XK1=XK1+.1
S.0075       50 TH(I,K)=A*XK1**2+B*XK1+C
S.0076          IF(TH(I,K))58,59,59
S.0077       58 TH(I,K)=0.
S.0078       59 CONTINUE
S.0079          IF(J1-12)60,61,60
S.0080       61 J1=17
S.0081          J2=21
S.0082          GO TO 45
S.0083       60  J1=0
S.0084          J1=0
S.0085       64 DO 65 I=2,21
S.0086       65 X1(I)=X1(I-1)+.1
S.0087          WRITE(6,101)(X1(I),I=1,11)
S.0088      101 FORMAT(1H147X24HINTERPOLATED THETA TABLE
                1//1HO5HX =  4X11F10.1/)
S.0089          DO 70 I=1,N
S.0090          T=I*10
S.0091       70 WRITE(6,102)T,(TH(I,J),J=1,11)
S.0092      102 FORMAT(1H F9.0,11F10.3)
S.0093          WRITE(6,101)(X1(I),I=12,21)
S.0094          DO 80 I=1,N
S.0095          T=I*10
S.0096       80 WRITE(6,102) T,(TH(I,J),J=12,21)
           C    CALCULATION OF DIFFERENCES FOR THETA TABLE AT CONSTANT T
S.0097          DO 110 J=2,20
S.0098          DO 110 I=1,N
S.0099      110 THP(I,J)=(TH(I,J+1)-TH(I,J-1))/.2
S.0100          WRITE(6,103)(X1(I),I=2,11)
S.0101      103 FORMAT(1H151X16HDIFFERENCE TABLE//1HO5HX =  4X10F10.1/)
S.0102          DO 108 I=1,N
S.0103          T=I*10
S.0104      108 WRITE(6,102)T,(THP(I,J),J=2,11)
S.0105          WRITE(6,103)(X1(I),I=12,20)
S.0106          DO 109 I=1,N
S.0107          T=I*10
S.0108      109 WRITE(6,102)T,(THP(I,J),J=12,20)
S.0109          READ(5,106)(XBD1(I),I=1,7)
S.0110          READ(5,106)(UBD1(I),I=1,7)
S.0111      106 FORMAT(7F10.0)
S.0112          Z1=(UBD1(1)-UBD1(2))/(XBD1(1)-XBD1(2))
S.0113          Z2=(UBD1(1)-UBD1(3))/(XBD1(1)-XBD1(3))
S.0114          A=(Z1-Z2)/(XBD1(2)-XBD1(3))
S.0115          B=Z1-A*(XBD1(1)+XBD1(2))
```

```
S.0116           C=UBD1(1)-A*XBD1(I)**2-B*XBD1(1)
S.0117           DO 120 I=1,13
S.0118           XBD(I)=(I-1)/10.
S.0119      120  UBD(I)=A*XBD(I)**2+B*XBD(I)+C
S.0120           A=(UBD1(3)-UBD1(4))/(XBD1(3)-XBD1(4))
S.0121           B=UBD1(3)-A*XBD1(3)
S.0122           DO 130 I=14,25
S.0123           XBD(I)=(I-1)/10.
S.0124      130  UBD(I)=A*XBD(I)+B
S.0125           DO 140 I=4,5
S.0126           Z1=(UBD1(I)-UBD1(I+1))/(XBD1(I)-XBD1(I+1))
S.0127           Z2=(UBD1(I)-UBD1(I+2))/(XBD1(I)-XBD1(I+2))
S.0128           A=(Z1-Z2)/(XBD1(I+1)-XBD1(I+2))
S.0129           B=Z1-A*(XBD1(I)+XBD1(I+1))
S.0130           C=UBD1(I)-A*XBD1(I)**2-B*XBD1(I)
S.0131           IF(I-4)132,131,132
S.0132      131  J2=31
S.0133           J1=26
S.0134           GO TO 133
S.0135      132  J2=43
S.0136           J1=32
S.0137      133  DO 140 J=J1,J2
S.0138           XBD(J)=(J-1)/10.
S.0139      140  UBD(J)=A*XBD(J)**2+B*XBD(J)+C
S.0140           WRITE(6,104)(XBD(I),UBD(I),I=1,J2)
S.0141      104  FORMAT(1H1,51X,16HTABLE FOR UBD(X)/1H0,35X,1HX,18X,3HUBD//(1H ,30X,F10.3,
                 1,10XF10.6))
S.0142           NP1=70
S.0143           Q=.12
S.0144           H=2.
S.0145           P=62.4
S.0146           C=1.
S.0147           C11=2.*Q/(H*P*C)
S.0148           C2=2./H
S.0149           C1P=1./C11
S.0150           C2P=-C2/C11
S.0151           ZK=.00114
S.0152           HK2=2.*ZK/H
S.0153           CON=Q/(P*C*ZK)
S.0154           NP=19
S.0155           DO 141 I=1,NP
S.0156      141  FX(I)=0.
S.0157           DO 142 I=1,6
S.0158           X(I)=(I-1)*.5
S.0159           ZX(I)=X(I)
S.0160      142  XK(I)=0.
S.0161           DO 143 K=1,60
S.0162      143  ST(K)=10*K
S.0163           DO 144 I=7,NP
S.0164           X(I)=X1(I-1)
S.0165      144  ZX(I)=X(I)
S.0166           DO 170 JT=30,60
S.0167           DO 160 I=7,NP
S.0168           DO 155 K=1,JT
S.0169      155  STHP(K)=THP(K,I-1)
S.0170           XK(I)=(C1P*TH(JT,I-1)+C2P*UBD(I+24)*SINT(STHP,ST,JT))/(10.*JT)
S.0171      160  FX(I)=XK(I)+FX(I)
S.0172           T= JT*10
S.0173      170  WRITE (6,1007)T,( X(I),XK(I),I=1,NP)
S.0174           DO 180 I=1,NP
S.0175      180  FX(I)=FX(I)/31.
```

```
S.0176          IN=5
S.0177          IOT=6
S.0178          XX(1)=0.
S.0179          DO 300 I=2,NP
S.0180      300 XX(I)=X(I)*EXP(-.5/X(I)**2)
S.0181          DO 310 J=1,44
S.0182          X1(J)=J/10.
S.0183      310 X11(J)=X1(J)*EXP(-.5/X1(J)**2)
S.0184      185 DO 190 N=10,19
S.0185          N1=N
S.0186          WRITE(6,1006) N
S.0187          CALL LSQFIT(FX2,N,NP1,C1,BASIS)
S.0188          WRITE(IOT,2000)(C1(I),I=1,N1)
S.0189          RMS=0.
S.0190          DO 332 K=1,NP1
S.0191          X(K)=0.
S.0192          DO 331 I=1,N
S.0193      331 X(K)=C1(I)*BASIS(I,K)+X(K)
S.0194          ERR(K)=FX2(K)-X(K)
S.0195      332 RMS=RMS+ERR(K)**2
S.0196          RMS=SQRT(RMS/70.)
S.0197          WRITE(6,2003)(FX2(K),X(K),ERR(K),K=1,NP1)
S.0198          WRITE(6,1001)RMS
S.0199          RMS=0.
S.0200          WRITE(6,1003)
S.0201          X(1)=0.
S.0202          DO 8 I=2,NP
S.0203          X(I)=0.
S.0204          DO 7 J=1,N1
S.0205      7   X(I)=X(I)+C1(J)* XX(I)**J
S.0206          ERR(I)=FX(I)-X(I)
S.0207      8   RMS=ERR(I)**2+RMS
S.0208          RMS=SQRT(RMS/NP)
S.0209          WRITE(6,2004)(FX(K),X(K),ERR(K),K=1,NP)
S.0210          WRITE(6,1001) RMS
S.0211          RMS=0.
S.0212          DO 360 LK=1,44,11
S.0213          K10=LK+10
S.0214          WRITE(6,101)(X1(II),II=LK,K10)
S.0215          DO 360 LI=1,60
S.0216          T=10*LI
S.0217          EXT=EXP(HK2*T)
S.0218          DO 350 LJ=LK,K10
S.0219          THP(LJ,1)=0.
S.0220          DO 340 NI=1,N1
S.0221      340 THP(LJ,1)=C1(NI)*X11(LJ)**NI*(EXT**NI-1.)/NI +THP(LJ,1)
S.0222          THP(LJ,1)=CON*THP(LJ,1)
S.0223          IF(LJ-25)345,347,347
S.0224      345 RMS=THP(LJ,1)**2+RMS
S.0225          GO TO 350
S.0226      347 RMS=RMS+(THP(LJ,1)-TH(LI,LJ-24))**2
S.0227          IF(THP(LJ,1))349,349,348
S.0228     348  TH(LI,LJ-24)=THP(LJ,1)
S.0229          GO TO 350
S.0230      349 TH(LI,LJ-24)=0.
S.0231      350 CONTINUE
S.0232      360 WRITE(6,102)T,(THP(JJ,1),JJ=LK,K10)
S.0233          RMS=SQRT(RMS/(60.*44.))
S.0234          WRITE(6,1001)RMS
S.0235          DO 82 J=2,20
S.0236          DO 82 I=1,60
```

```
S.0237      82    THP(I,J)=(TH(I,J+1)-TH(I,J-1))/.2
S.0238            DO 89 JT=30,60
S.0239            DO 88 I=7,NP
S.0240            DO 87 K=1,JT
S.0241      87    STHP(K)=THP(K,I-1)
S.0242      88    XK(I)=(C1P*TH(JT,I-1)+C2P*UBD(I+24)*SINT(STHP,ST,JT))/(10.*JT)
S.0243            T=JT*10
S.0244      89    WRITE(6,1007)T,(ZX(I),XK(I),I=1,NP)
S.0245            WRITE(6,1005)
S.0246      1005  FORMAT(2HH1ADDITIONAL VALUES FOR KO(X)/1HO10X1HX18X2HKO)
S.0247            XXX=4.2
S.0248            DO 1600 I=1,50
S.0249            ZZZ=0.
S.0250            XXX=XXX+.1
S.0251            DO 1500 J=1,N1
S.0252      1500  ZZZ=ZZZ+C1(J)*(XXX*DEXP(-.5/XXX**2))**J
S.0253      1600  WRITE(6,1004) XXX,ZZZ
S.0254      1004  FORMAT(1HO2F20.8)
S.0255      190   CONTINUE
S.0256      1001  FORMAT(  6HORMS =F10.6)
S.0257      1002  FORMAT(  27HOPOINTS COMPUTED FROM POLY./1HO15X1HX18X5HKO(X)/
                 1(10XF10.3,10XF10.6))
S.0258      1003  FORMAT(16H1CHECK FOR KO(X)/1HO10X5HKO(X),15X3HCAL18X3HERR)
S.0259      1006  FORMAT(  27H1LEAST SQUARES FIT OF ORDERI3)
S.0260      1007  FORMAT(//39H1TABULATED VALUES FOR KO OF X AT TIME =F4.0/
                 11HO15X1HX18X5HKO(X)/(10XF10.3,10XF10.6))
S.0261     2000   FORMAT(13HOCOEFFICIENTS/(  6F16.7))
S.0262     2002   FORMAT(8X1HX13X4HF(X)5X10HCALCULATED6X5HERROR/(  4F14.5))
S.0263      2003  FORMAT(1HO10X2HFX17X4HCOMP16X3HERR/(3F20.6))
S.0264      2004  FORMAT(1HO(3F20.6))
S.0265      400   CALL EXIT
S.0266            END
```

```
BPS FORTRAN D COMPILER    24/01/66                                    26/01/66
 S.0001           SUBROUTINE LSQFIT(FX,N,NP,C,BASIS)
 S.0002           DOUBLE PRECISION AA(19,20),T1,BASIS(19,1),C(1)
 S.0003           DIMENSION FX(1)
 S.0004           N1=N+1
 S.0005           NM1=N-1
 S.0006           DO 2 I=1,N
 S.0007           DO 2 J=1,N1
 S.0008      2    AA(I,J)=0.
 S.0009           DO 4 K=1,NP
 S.0010           DO 4 J=1,N
 S.0011           DO 3 I=1,N
 S.0012      3    AA(J,I)=AA(J,I)+BASIS(I,K)*BASIS(J,K)
 S.0013      4    AA(J,N1)=AA(J,N1)-FX(K)*BASIS(J,K)
 S.0014           DO 5 K=1,NM1
 S.0015           DO 5 J=K,NM1
 S.0016           T1=AA(J+1,K)/AA(K,K)
 S.0017           DO 5 I=K,N1
 S.0018      5    AA(J+1,I)=AA(J+1,I)-AA(K,I)*T1
 S.0019           C(N)=-AA(N,N1)/AA(N,N)
 S.0020           DO 6 I=2,N
 S.0021           K=N1-I
 S.0022           C(K)=-AA(K,N1)/AA(K,K)
 S.0023           L=K+1
 S.0024           DO 6 J=L,N
 S.0025      6    C(K)=C(K)-C(J)*AA(K,J)/AA(K,K)
 S.0026           RETURN
 S.0027           END
```

APPENDIX E

CALIBRATION OF THERMOCOUPLES

Because the maximum temperature differences measured in the test fluid are only of the order of 10°F, an accurate knowledge of the true temperature at each sensor must be available. This requires that a precise calibration be made of the 60 thermocouples used in the vertical probe mounted in the tank. So that all thermocouple output voltages could be obtained under the same conditions, it was decided to calibrate all 60 at once, rather than in small batches. A constant temperature bath, catalogue number 6658D, with dimensions 15 in. x 15 in. x 15 in. manufactured by the Precision Scientific Company was used in the calibration. A rack containing 64 18 x 150mm test tubes filled with water was prepared. The rack was designed so that adjacent test tubes were separated by a minimum distance of 3/4 inches. Into the test tubes the thermocouples were inserted, all to the same depth. This arrangement was then immersed in the constant temperature bath. The use of the test tubes insured that each sensor would be subject to identically the same convective flow conditions and also insured that any small temperature variations in the bath would be strongly attenuated.

The leads near the thermocouple junctions were insulated from ambient conditions and thus reached a temperature near that of the sensors. This helped minimize any conduction effects which might be present. The leads were connected to a junction box and from there to

six rotary selector switches. The six switches in turn were linked to a single selector switch which also controlled the output voltage of a calibrated thermocouple connected directly to the constant temperature bath. This latter thermocouple was calibrated within a precision of ± 0.1°F at the calibration laboratory of the Lockheed-Georgia Company. The switching arrangement allowed a rapid comparison to be made between each thermocouple and the calibrated thermocouple.

The output voltages were measured on a Leeds and Northrup K-3 universal potentiometer. This potentiometer can be read to approximately 0.1 microvolts. It has an absolute accuracy, however, within ± 1 microvolt in the range investigated. Since a one-degree variation represents approximately 23 microvolts, temperature measurements within ± .05F can theoretically be made. However, reproducibility of the results to such a high precision could not usually be achieved. It is felt that this was due to thermal gradients present within the wiring circuit and across the terminal switches. For example, it was found that the cyclic 5°F variation in temperature caused by the air conditioning system in the room containing the calibration equipment resulted in a periodic apparent variation of approximately $\frac{1}{2}$ °F in the thermocouple output. This problem was solved by directing fans at the connections within the junction box to equalize temperatures. However, even opening the door to the room containing the equipment caused significant changes in apparent temperature. Thus in almost all the calibration test runs, some uncontrollable variations occurred.

The general calibration test procedure was

1. Establish the desired temperature level in the bath. This usually required 4 to 6 hours.

2. Read the values of the output voltages of each thermocouple and compare these with that of the calibrated thermocouple.

This procedure was followed at three different temperatures from slightly above ambient up to 140°F. At each temperature level three to five readings from each sensor were obtained and an average deviation from the calibrated thermocouple computed. To establish overall reproducibility of the results two additional calibrations were performed and average deviations for each thermocouple computed.

Upon study of the data it was found that a large majority of the thermocouples maintain a relatively constant error over the entire temperature range. This suggested the use of a constant correction for each thermocouple rather than an individual error curve. This correction for each thermocouple was obtained by averaging the deviations in all the readings at the three different temperature levels and rejecting any thermocouple with any deviation greater than 0.2°F from the average.

The average correction necessary to the standard for each thermocouple is presented in Table 3.

Table 3. Thermocouple Calibration Corrections

$$T_n)_{true} = C_n + T_{apparent}$$

where $T_{apparent}$ = Temperature of Standard Thermocouple corresponding to m.v. output of test sensor.

Sensor Number	Calibration Correction	Sensor Number	Calibration Correction
	C_n		C_n
1	-.0815	31	-.317
2	-.191	32	-.356
3	-.23	33	-.157
4	-.022	34	-.252
5	-.157	35	-.473
6	-.217	36	-.482
7	-.113	37	-.544
8	-.178	38	-.295
9	-.170	39	-.352
10	-.135	40	-.457
11	-.213	41	-.527
12	-.030	42	-.588
13	-.274	43	-.348
14	-.295	44	-.426
15	-.100	45	-.473
16	-.152	46	-.587
17	-.222	47	-.608
18	-.191	48	-.461
19	-.261	49	-.430
20	-.139	50	-.595
21	-.156	51	-.535
22	-.10	52	-.378
23	-.183	53	-.461
24	-.287	54	-.573
25	-.321	55	-.600
26	-.139	56	-.400
27	-.065	57	-.417
28	-.269	58	-.422
29	-.212	59	-.495
30	-.408	s	-.326

APPENDIX F

TABULATION OF AXIAL TEMPERATURE-TIME DATA FROM EXPERIMENTAL PROGRAM

In the data presented in the following tables, the computer program discussed in Appendix D was used to obtain from the original raw data axial temperature profiles at constant values of time.

Table 4. Experimental Temperatures

Test No. 0100 Initial Temperature 74.70°F

q_b = .1933 Btu/ft^{2}sec q_s = .150 Btu/ft^{2}sec

Gr^*_{max} = 1.55 x 10^{12}

Thermocouple Location (ft)	TEMPERATURES (°F) 350 (sec)	700 (sec)	1050 (sec)	1400 (sec)	1750 (sec)	2100 (sec)
0.0833	75.41	76.85	77.72	79.64	80.71	82.89
0.50	75.46	76.60	77.78	79.21	80.71	82.12
0.667	75.41	76.54	77.80	79.09	80.55	81.90
1.00	75.53	76.93	78.21	79.65	81.31	82.54
1.167	75.77	77.29	78.67	80.22	81.77	83.04
1.33	76.30	77.97	79.22	80.81	82.31	83.51
1.50	76.48	78.30	79.63	81.16	82.67	83.84
1.583	76.97	78.70	79.83	81.41	82.79	83.93
1.667	76.92	79.12	80.29	81.69	83.10	84.19
1.750	77.53	79.31	80.53	81.88	83.29	84.30
1.833	77.75	79.79	80.97	82.34	83.66	84.60
1.916	77.95	80.21	81.25	82.71	84.03	84.95
1.99	78.29	80.84	81.50	82.67	83.76	84.55
2.00	78.64	81.67	82.18	83.19	84.20	84.80

Table 5. Experimental Temperatures

Test No. 0200 Initial Temperature 83.55°F

q_b = .141 Btu/ft^{2}sec q_s = .153 Btu/ft^{2}sec

$Gr^*_{max} = 2.97 \times 10^{12}$

Thermocouple Location (ft)	TEMPERATURES (°F) 350 (sec)	700 (sec)	1050 (sec)	1400 (sec)	1750 (sec)	2100 (sec)	2450 (sec)
0.0833	84.29	85.19	85.98	87.54	88.39	89.56	90.85
0.500	84.03	85.04	86.05	87.18	88.16	89.36	90.64
0.667	83.96	84.89	85.96	87.11	88.09	89.27	90.74
1.00	83.99	85.29	86.86	88.19	89.42	90.72	92.17
1.167	84.54	86.06	87.48	88.81	90.00	91.22	92.81
1.333	84.94	86.71	88.09	89.41	90.56	91.78	93.53
1.50	85.29	87.15	88.58	89.91	91.06	92.32	94.02
1.583	85.67	87.36	88.79	90.11	91.24	92.60	94.16
1.667	85.84	87.61	89.22	90.55	91.66	92.90	94.56
1.75	85.93	87.85	89.68	90.86	91.89	93.14	94.72
1.833	86.46	88.18	89.94	91.12	92.14	93.34	94.89
1.916	86.57	88.55	90.31	91.50	92.48	93.59	94.98
1.99	86.60	88.37	90.15	91.31	92.25	93.34	94.69
2.00	88.23	89.80	91.54	92.46	93.17	94.12	95.29

Table 6. Experimental Temperatures

Test No. 0300 Initial Temperature 76.13°F

$q_b = 0$ $q_s = .171$ Btu/ft^{2}sec

$Gr^*_{max} = 1.75 \times 10^{12}$

Thermocouple Locations (ft)	TEMPERATURES (°F) 400 (sec)	800 (sec)	1200 (sec)	1600 (sec)	2000 (sec)	2400 (sec)
0.0833	76.11	76.20	76.26	76.30	76.39	76.45
0.50	76.32	76.40	76.53	76.93	77.54	78.36
0.667	76.24	76.48	76.92	77.62	78.52	79.84
1.000	76.22	76.71	77.78	79.01	80.39	82.13
1.167	76.20	77.02	78.73	80.27	82.04	84.00
1.333	76.71	78.31	80.63	82.43	84.14	85.76
1.50	77.15	79.86	82.55	84.06	85.43	86.91
1.583	77.52	80.65	83.37	84.74	86.02	87.43
1.667	78.69	81.95	84.46	85.63	86.87	88.27
1.750	79.31	82.90	85.16	86.23	87.37	88.78
1.833	80.59	84.02	86.01	86.97	88.09	89.46
1.916	83.31	85.85	87.48	88.35	89.39	90.65
1.99	84.41	85.93	87.53	88.37	89.26	90.46
2.00	84.32	86.27	88.04	88.86	89.79	90.91

Table 7. Experimental Temperatures

Test No. 0400 Initial Temperature 82.50°F

q_b = .197 Btu/ft^{2}sec q_s = .0536 Btu/ft^{2}sec

Gr^*_{max} = 6.86 x 10^{11}

Thermocouple Locations (ft)	TEMPERATURES (°F) 400 (sec)	800 (sec)	1200 (sec)	1600 (sec)	2000 (sec)	2400 (sec)
0.0833	83.30	84.23	85.32	86.28	87.49	88.57
0.50	83.01	84.03	85.04	86.22	87.14	88.05
0.667	83.14	84.14	85.12	86.11	87.29	87.93
1.000	83.23	84.27	85.19	86.24	87.43	88.05
1.167	83.30	84.50	85.34	86.30	87.53	88.13
1.333	83.26	84.40	85.36	86.28	87.50	88.21
1.500	83.51	84.59	85.51	86.39	87.46	88.50
1.583	83.57	84.71	85.70	86.59	87.52	88.66
1.667	83.65	84.72	85.67	86.63	87.43	89.23
1.75	83.75	84.83	85.76	86.89	87.57	89.26
1.833	84.17	85.06	85.99	87.02	87.81	89.17
1.916	84.12	85.42	86.38	87.16	87.96	89.19
1.99	84.09	85.33	86.28	87.05	87.85	89.07
2.00	83.89	85.35	86.33	87.03	87.95	89.27

Table 8. Experimental Temperatures

Test No. 0500 Initial Temperature 79.05°F

q_b = .0888 Btu/ft^{2}sec q_s = .0565 Btu/ft^{2}sec

Gr^*_{max} = 5.81 x 10^{11}

Thermocouple Locations (ft)	TEMPERATURES (°F) 400 (sec)	800 (sec)	1200 (sec)	1600 (sec)	2000 (sec)	2400 (sec)
0.0833	79.39	80.04	80.65	81.06	81.75	82.46
0.50	79.37	79.95	80.50	81.04	81.74	82.48
0.667	79.29	79.84	80.40	80.99	81.72	82.46
1.000	79.27	79.85	80.42	81.09	81.71	82.46
1.167	79.37	80.08	80.72	81.49	82.20	82.66
1.333	79.78	80.49	81.22	81.94	82.70	83.29
1.500	79.91	80.70	81.45	82.09	82.84	83.46
1.583	79.93	80.73	81.53	82.19	82.91	83.54
1.667	80.17	81.04	81.78	82.53	83.13	83.75
1.750	80.13	81.06	81.77	82.67	83.26	83.78
1.833	80.34	81.40	82.09	82.95	83.63	84.20
1.916	80.83	81.60	82.37	83.27	83.89	84.38
1.99	81.12	81.83	82.47	83.33	83.87	84.49
2.00	81.19	81.88	82.84	83.49	84.10	84.63

Table 9. Experimental Temperatures

Test No. 0600 Initial Temperature 76.70°F

q_b = .0473 Btu/ft^{2}sec q_s = .0587 Btu/ft^{2}sec

Gr^*_{max} = 5.68 x 10^{11}

Thermocouple Locations (ft)	TEMPERATURES (°F) 600 (sec)	1200 (sec)	1800 (sec)	2400 (sec)	3000 (sec)	3600 (sec)
0.0833	76.91	77.50	78.17	78.86	79.52	80.09
0.50	76.92	77.47	78.12	78.72	79.46	80.09
0.667	76.83	77.44	78.07	78.70	79.46	80.28
1.000	76.88	77.74	78.64	79.51	80.41	81.10
1.167	77.10	78.09	78.97	79.82	80.83	81.58
1.333	77.42	78.66	79.63	80.49	81.47	82.20
1.500	77.62	78.95	79.93	80.88	81.85	82.56
1.583	77.98	79.14	80.14	81.13	82.14	82.88
1.667	78.31	79.52	80.51	81.48	82.39	83.14
1.750	78.39	79.54	80.71	82.10	82.75	83.39
1.833	78.75	79.89	81.14	82.18	83.00	83.67
1.916	79.09	80.33	81.56	82.68	83.58	84.24
1.99	79.73	81.18	82.01	82.92	83.84	84.49
2.00	79.70	81.27	82.20	83.12	84.01	84.58

Table 10. Experimental Temperatures

Test No. 0700 Initial Temperature 75.24°F

$q_b = 0$ $q_s = 0.0632$ Btu/ft^{2}sec

$Gr^*_{max} = 5.48 \times 10^{11}$

Thermocouple Locations (ft)	TEMPERATURES (°F) 600 (sec)	1200 (sec)	1800 (sec)	2400 (sec)	3000 (sec)	3600 (sec)
0.0833	75.25	75.25	75.25	75.25	75.25	75.25
0.500	75.33	75.39	75.49	75.79	76.19	76.51
0.667	75.26	75.28	75.57	76.12	76.72	77.27
1.000	75.23	75.42	76.11	76.90	77.64	78.44
1.167	75.29	75.71	76.59	77.68	78.88	79.16
1.333	75.66	76.59	77.60	78.79	79.77	80.50
1.500	75.79	77.22	78.38	79.55	80.50	81.30
1.583	76.04	77.67	78.84	79.87	80.83	81.53
1.667	76.68	78.35	79.47	80.46	81.34	82.00
1.750	76.89	78.71	79.75	80.72	81.73	82.48
1.833	77.55	79.37	80.29	81.16	82.10	82.92
1.916	78.72	80.41	81.10	81.99	82.83	83.71
1.99	79.78	80.80	81.26	82.22	83.17	83.84
2.00	80.02	80.86	81.31	82.30	83.18	83.86

Table 11. Experimental Temperatures

Test No. 0800 Initial Temperature 73.80°F

$q_b = 0.144$ Btu/ft^{2}sec $q_s = 0.0177$ Btu/ft^{2}sec

$Gr^*_{max} = 1.54 \times 10^{11}$

Thermocouple Locations (ft)	TEMPERATURES (°F) 600 (sec)	1200 (sec)	1800 (sec)	2400 (sec)	3000 (sec)	3600 (sec)
0.0833	74.42	75.09	76.03	77.19	78.33	78.81
0.500	74.42	75.08	76.09	77.36	78.14	78.99
0.667	74.38	75.07	76.10	77.16	78.02	78.97
1.000	74.39	75.05	76.09	77.15	77.90	78.93
1.167	74.61	75.31	76.22	77.05	77.90	78.93
1.333	74.60	75.29	76.21	77.11	78.13	79.16
1.500	74.64	75.28	76.19	77.10	78.11	79.15
1.583	74.79	75.45	76.17	77.16	78.08	79.12
1.667	74.76	75.44	76.18	77.22	78.05	79.08
1.750	74.95	75.58	76.14	77.15	78.04	79.08
1.833	75.07	75.56	76.24	77.18	78.16	79.11
1.916	75.11	75.65	76.21	77.14	78.32	79.25
1.99	75.10	75.62	76.33	77.26	78.43	79.42
2.00	75.12	75.66	76.32	77.46	78.33	79.33

Table 12. Experimental Temperatures

Test No. 0900 Initial Temperature 79.00°F

$q_b = 0.0124$ Btu/ft^{2}sec $q_s = 0.0141$ Btu/ft^{2}sec

$Gr^*_{max} = 1.32 \times 10^{11}$

Thermocouple Locations (ft)	TEMPERATURES (°F) 600 (sec)	1200 (sec)	1800 (sec)	2400 (sec)	3000 (sec)	3600 (sec)	4200 (sec)	4800 (sec)
0.0833	79.09	79.17	79.35	79.43	79.67	79.88	79.89	80.12
0.500	79.09	79.16	79.37	79.56	79.75	79.81	79.90	80.19
0.667	79.06	79.13	79.29	79.48	79.65	79.82	79.88	80.06
1.000	78.99	79.21	79.49	79.62	79.82	80.02	80.16	80.41
1.167	79.01	79.21	79.57	79.80	79.99	80.21	80.37	80.54
1.333	79.35	79.63	79.94	80.13	80.31	80.54	80.67	80.88
1.500	79.33	79.71	79.99	80.23	80.41	80.58	80.71	80.88
1.583	79.34	79.71	80.02	80.27	80.45	80.63	80.80	80.93
1.667	79.47	79.85	80.19	80.39	80.54	80.72	80.89	81.09
1.750	79.49	79.84	80.19	80.40	80.61	80.72	80.93	81.17
1.833	79.66	80.02	80.39	80.57	80.79	80.95	81.19	81.37
1.916	79.82	80.28	80.48	80.70	80.92	81.12	81.36	81.54
1.99	80.12	80.28	80.56	80.69	80.92	81.13	81.45	81.57
2.00	80.56	80.67	80.86	80.87	81.22	81.36	81.53	81.66

Table 13. Experimental Temperatures

Test No. 1000 Initial Temperature 75.10°F

$q_b = 0$ $q_s = 0.0204$ Btu/ft^{2}sec

$Gr^*_{max} = 1.61 \times 10^{11}$

Thermocouple Locations (ft)	TEMPERATURES (°F) 600 (sec)	1200 (sec)	1800 (sec)	2400 (sec)	3000 (sec)	3600 (sec)	4200 (sec)	4800 (sec)	5400 (sec)
0.0833	75.10	75.10	75.10	75.10	75.11	75.12	75.12	75.12	75.12
0.500	75.11	75.15	75.13	75.25	75.44	75.62	75.76	75.85	76.03
0.667	75.11	75.14	75.17	75.36	75.54	75.81	75.98	76.08	76.33
1.000	75.09	75.20	75.39	75.59	75.82	76.09	76.30	76.57	76.78
1.167	75.07	75.23	75.53	75.76	75.99	76.32	76.56	76.83	77.04
1.333	75.32	75.53	75.86	76.22	76.52	76.86	77.11	77.31	77.55
1.500	75.28	75.68	76.12	76.48	76.82	77.16	77.41	77.61	77.86
1.583	75.33	75.89	76.28	76.60	76.90	77.28	77.50	77.74	77.98
1.667	75.57	76.12	76.57	76.86	77.25	77.57	77.72	78.00	78.18
1.750	75.62	76.29	76.74	76.94	77.28	77.62	77.84	78.04	78.21
1.833	75.99	76.57	76.96	77.29	77.57	77.83	78.05	78.21	78.38
1.916	76.45	76.96	77.30	77.55	77.78	78.00	78.22	78.34	78.56
1.99	76.69	77.33	77.43	77.67	77.82	78.04	78.26	78.34	78.55
2.00	76.65	77.32	77.55	77.67	77.81	78.03	78.26	78.34	78.54

Table 14. Experimental Temperatures

Test No. 1100 Initial Temperature 74.72°F

q_b = .22 Btu/ft^{2}sec q_s = .124 Btu/ft^{2}sec

$Gr^*_{max} = 9.14 \times 10^{13}$

Thermocouple Locations (ft)	TEMPERATURES (°F) 288 (sec)	576 (sec)	864 (sec)	1152 (sec)	1440 (sec)	1728 (sec)	2016 (sec)
0.0833	75.76	75.86	76.16	77.56	77.61	78.41	79.01
0.50	75.19	75.90	76.35	77.09	77.55	78.29	79.09
1.00	75.02	75.74	76.00	76.77	77.43	78.23	78.93
1.50	75.01	75.72	76.22	76.72	77.50	78.31	79.11
2.00	75.08	75.90	76.42	77.05	77.74	78.53	79.38
2.50	75.07	75.84	76.40	77.08	77.78	78.56	79.45
3.00	75.37	76.07	76.67	77.40	78.19	79.09	79.73
3.50	75.48	76.29	76.95	77.77	78.40	79.26	80.07
4.042	75.37	76.32	76.81	77.64	78.41	79.20	80.06
4.56	75.84	76.65	77.31	78.04	78.78	79.70	80.51
5.00	76.02	76.69	77.41	78.36	79.08	79.93	80.80
5.40	76.31	76.97	77.72	78.60	79.41	80.37	81.20
5.68	76.10	77.06	78.05	78.93	79.77	80.81	81.76
5.833	76.50	77.44	78.42	79.63	80.53	81.61	82.44
5.926	76.53	77.80	78.73	79.81	80.91	81.91	82.83
6.000	77.00	78.44	79.26	80.31	81.41	82.05	83.11

Table 15. Experimental Temperatures

Test No. 1200 Initial Temperature 80.45°F

q_b = .1115 Btu/ft^{2}sec q_s = .1183 Btu/ft^{2}sec

Gr^*_{max} = 1.09 x 10^{14}

Thermocouple Locations (ft)	TEMPERATURES (°F) 288 (sec)	576 (sec)	864 (sec)	1152 (sec)	1440 (sec)	1728 (sec)	2016 (sec)	2304 (sec)
0.0833	80.61	81.06	81.36	81.66	82.16	83.56	83.36	84.66
0.50	80.70	81.00	81.35	81.65	82.15	82.89	83.40	84.00
1.00	80.60	80.90	81.20	81.64	82.19	82.74	83.24	83.93
1.50	80.57	81.08	81.44	81.99	82.66	83.18	83.86	84.47
2.00	80.65	81.31	81.91	82.41	83.05	83.65	84.30	84.90
2.50	80.68	81.39	82.04	82.55	83.14	83.83	84.40	85.03
3.00	80.98	81.63	82.22	82.91	83.48	84.16	84.86	85.47
3.50	81.20	81.90	82.51	83.19	83.76	84.48	85.19	85.77
4.042	80.96	81.93	82.38	83.11	83.78	84.43	85.16	85.79
4.56	81.31	82.24	82.87	83.59	84.25	85.12	85.69	86.34
5.00	81.53	82.36	83.16	83.79	84.55	85.35	86.12	86.74
5.40	82.10	82.78	83.46	84.15	84.84	85.70	86.48	87.22
5.68	81.89	82.88	83.78	84.55	85.38	86.22	87.16	87.87
5.83	82.16	83.05	84.00	84.95	85.95	86.88	87.70	88.54
5.926	82.52	83.43	84.31	85.15	86.18	87.16	88.13	88.91
6.000	83.28	83.53	84.20	85.15	86.14	87.31	88.03	89.00

Table 16. Experimental Temperatures

Test No. 1300 Initial Temperature 78.13°F

$q_b = 0$ $q_s = .1295$ Btu/ft^{2}sec

$Gr^*_{max} = 1.078 \times 10^{14}$

Thermocouple Locations (ft)	TEMPERATURES (°F) 288 (sec)	576 (sec)	864 (sec)	1152 (sec)	1440 (sec)	1728 (sec)	2016 (sec)	2304 (sec)
0.0833	78.16	78.16	78.16	78.16	78.16	78.16	78.16	78.16
0.50	78.31	78.26	78.36	78.36	78.41	78.41	78.56	78.76
1.00	78.21	78.21	78.21	78.26	78.26	78.73	79.24	79.55
1.50	78.21	78.21	78.35	78.59	79.02	79.76	80.51	81.35
2.00	78.34	78.29	78.89	79.59	80.34	81.37	82.01	82.56
2.50	78.54	78.90	79.66	80.47	80.95	81.81	82.40	82.99
3.00	78.68	79.40	80.29	80.93	81.43	82.24	82.87	83.55
3.50	78.87	79.77	80.58	81.30	81.73	82.69	83.27	84.01
4.042	78.94	79.70	80.63	81.29	82.01	82.76	83.47	84.16
4.56	79.28	80.03	80.99	81.75	82.32	83.20	83.94	84.75
5.00	79.47	80.35	81.19	82.01	82.64	83.53	84.23	85.02
5.40	79.64	80.57	81.45	82.28	82.95	83.92	84.77	85.55
5.68	79.71	80.83	81.87	82.86	83.53	84.52	85.45	86.36
5.83	79.81	80.99	82.02	83.23	84.16	85.29	86.26	87.15
5.93	79.93	81.04	82.25	83.54	84.70	85.81	86.81	87.79
6.00	80.16	81.22	82.33	83.66	84.75	86.11	87.18	88.30

Table 17. Experimental Temperatures

Test No. 1400 Initial Temperature 84.7°F

q_b = .204 Btu/ft^{2}sec q_s = .052 Btu/ft^{2}sec

Gr^*_{max} = 5.7 x 10^{13}

Thermocouple Locations (ft)	TEMPERATURES (°F) 600 (sec)	1200 (sec)	1800 (sec)	2400 (sec)	3000 (sec)	3600 (sec)
0.0833	85.61	86.83	87.92	88.37	88.88	89.42
0.50	85.35	86.05	86.94	87.84	88.56	89.23
1.00	85.24	86.02	86.92	87.80	88.55	89.43
1.50	85.23	86.02	86.94	87.82	88.61	89.38
2.00	85.31	86.09	87.02	87.96	88.72	89.32
2.50	85.52	86.28	87.03	88.02	88.86	89.49
3.016	85.40	86.23	87.09	87.98	88.83	89.63
3.50	85.43	86.30	87.12	88.03	88.89	89.65
4.00	85.58	86.44	87.25	88.08	89.06	89.80
4.50	85.76	86.53	87.39	88.35	89.21	89.99
5.00	85.87	86.70	87.54	88.44	89.31	90.30
5.31	85.88	86.90	87.74	88.74	89.70	90.32
5.67	86.02	87.02	88.02	88.83	89.80	90.57
5.83	86.10	87.13	88.14	88.98	89.91	90.64
5.916	86.30	87.27	88.17	89.00	89.94	90.73
6.000	86.41	87.56	88.76	89.50	90.28	90.75

Table 18. Experimental Temperatures

Test No. 1500 Initial Temperature 85.78°F

q_b = 0.101 Btu/ft^{2}sec q_s = 0.053 Btu/ft^{2}sec

Gr^*_{max} = 5.67 x 10^{13}

Thermocouple Locations (ft)	TEMPERATURES (°F) 400 (sec)	800 (sec)	1200 (sec)	1600 (sec)	2000 (sec)	2400 (sec)	2800 (sec)	3200 (sec)
0.0833	86.05	86.38	86.82	87.27	87.77	88.07	88.67	88.70
0.50	86.07	86.35	86.81	87.23	87.63	88.03	88.44	88.69
1.00	86.01	86.36	86.82	87.22	87.66	88.02	88.44	88.73
1.50	86.12	86.42	86.86	87.36	87.81	88.17	88.59	88.88
2.00	86.14	86.54	87.02	87.45	87.88	88.30	88.68	89.03
2.50	86.09	86.56	87.13	87.57	88.03	88.37	88.79	89.15
3.016	86.07	86.62	87.20	87.64	88.06	88.48	88.90	89.29
3.50	86.11	86.69	87.28	87.74	88.19	88.63	88.99	89.36
4.00	86.36	86.88	87.47	87.98	88.36	88.77	89.21	89.57
4.50	86.47	86.92	87.41	87.97	88.37	88.79	89.23	89.62
5.00	86.57	87.13	87.69	88.17	88.60	89.11	89.61	90.04
5.31	86.68	87.28	87.76	88.32	88.74	89.21	89.77	90.21
5.67	86.76	87.44	88.03	88.56	88.97	89.54	90.12	90.51
5.83	86.91	87.42	88.06	88.65	89.10	89.56	90.19	90.63
5.916	86.91	87.61	88.25	88.80	89.26	89.65	90.25	90.75
6.00	87.12	87.75	88.67	89.07	89.46	89.81	90.56	91.00

Table 19. Experimental Temperatures

Test No. 1600 Initial Temperature 87.45°F

q_b = .0502 Btu/ft^{2}sec q_s = .046 Btu/ft^{2}sec

Gr^*_{max} = 5.28 x 10^{13}

Thermo-couple Locations (ft)	TEMPERATURES (°F) 400 (sec)	800 (sec)	1200 (sec)	1600 (sec)	2000 (sec)	2400 (sec)	2800 (sec)	3200 (sec)
0.0833	87.46	87.48	87.53	87.88	88.07	88.25	88.67	89.03
0.50	87.45	87.46	87.53	87.77	88.03	88.29	88.61	88.97
1.00	87.45	87.45	87.50	87.76	87.97	88.17	88.55	88.82
1.50	87.45	87.54	87.68	88.03	88.33	88.65	89.10	89.45
2.00	87.44	87.68	87.95	88.27	88.59	88.94	89.38	89.76
2.50	87.46	87.73	88.07	88.42	88.79	89.20	89.50	89.91
3.016	87.61	87.91	88.25	88.65	89.03	89.42	89.81	90.17
3.50	87.64	88.06	88.43	88.80	89.19	89.62	89.97	90.36
4.00	87.79	88.11	88.46	88.89	89.40	89.53	90.24	90.57
4.50	88.20	88.34	88.81	89.24	89.68	90.14	90.51	90.84
5.00	88.73	89.13	89.56	90.08	90.49	91.02	91.46	91.75
5.31	88.82	89.22	89.74	90.19	90.60	91.09	91.51	91.81
5.67	88.87	89.38	89.88	90.35	90.87	91.39	91.77	92.05
5.83	88.99	89.54	90.04	90.54	91.14	91.63	92.03	92.30
5.916	88.99	89.65	90.22	90.65	91.20	91.77	92.19	92.42
6.00	89.02	89.66	90.48	91.09	91.45	91.90	92.32	92.53

Table 20. Experimental Temperatures

Test No. 1700 Initial Temperature 84.46°F

$q_b = 0.0$ $q_s = 0.052$ Btu/ft^{2}sec

$Gr^*_{max} = 5.14 \times 10^{14}$

Thermocouple Locations (ft)	TEMPERATURES (°F) 400 (sec)	800 (sec)	1200 (sec)	1600 (sec)	2000 (sec)	2400 (sec)	2800 (sec)	3200 (sec)
0.0833	84.45	84.45	84.45	84.44	84.46	84.46	84.47	84.48
0.50	84.56	84.54	84.49	84.48	84.56	84.64	84.64	84.90
1.00	84.49	84.49	84.48	84.52	84.77	84.97	85.06	85.34
1.50	84.55	84.57	84.64	84.83	85.14	85.42	85.73	86.16
2.00	84.52	84.70	84.95	85.19	85.67	86.11	86.54	86.93
2.50	84.57	84.85	85.24	85.66	86.21	86.65	86.93	87.27
3.016	84.67	85.15	85.70	86.20	86.60	86.94	87.34	87.66
3.50	84.76	85.27	85.88	86.31	86.79	87.00	87.46	87.81
4.00	84.94	84.45	86.02	86.38	86.87	87.28	87.65	87.97
4.50	85.09	85.65	86.24	86.67	87.14	87.56	87.93	88.24
5.00	85.20	85.78	86.33	86.91	87.42	87.84	88.21	88.44
5.31	85.30	85.97	86.47	87.01	87.51	87.92	88.29	88.49
5.67	85.32	85.97	86.63	87.24	87.76	88.18	88.58	88.76
5.83	85.54	86.16	86.86	87.51	88.06	88.42	88.79	88.94
5.916	85.53	86.22	86.84	87.45	88.06	88.44	88.77	88.88
6.00	85.69	86.50	87.00	87.68	87.93	88.38	88.78	88.87

Table 21. Experimental Temperatures

Test No. 1800 Initial Temperature 76.65°F

q_b = .1385 Btu/ft^{2}sec q_s = 0.0147 Btu/ft^{2}sec

$Gr^*_{max} = 1.07 \times 10^{13}$

Thermocouple Locations (ft)	TEMPERATURES (°F) 750 (sec)	1500 (sec)	2250 (sec)	3000 (sec)	3750 (sec)	4500 (sec)	5250 (sec)
0.0833	77.14	77.50	78.02	78.61	79.18	79.88	80.11
0.50	76.97	77.34	77.82	78.34	78.82	79.44	79.82
1.00	77.00	77.31	77.78	78.30	78.70	79.32	79.74
1.50	77.04	77.40	77.88	78.39	78.82	79.34	79.76
2.00	77.07	77.47	77.93	78.44	78.89	79.37	79.88
2.50	77.05	77.52	78.01	78.48	78.82	79.26	79.75
3.016	77.10	77.57	78.06	78.56	78.90	79.42	79.83
3.50	77.14	77.69	78.15	78.59	78.90	79.40	79.81
4.00	77.13	77.68	78.14	78.59	78.93	79.44	79.81
4.50	77.16	77.68	78.15	78.62	78.88	79.36	79.82
5.00	77.14	77.71	78.19	78.69	78.96	79.40	79.79
5.31	77.24	77.81	78.25	78.76	79.22	79.55	79.92
5.67	77.18	77.74	78.21	78.74	79.12	79.44	79.81
5.83	77.29	77.84	78.25	78.78	79.16	79.51	79.86
5.916	77.35	77.88	78.31	78.78	79.19	79.62	79.93
6.00	77.73	78.27	78.70	79.17	79.58	80.00	80.31

Table 22. Experimental Temperatures

Test No. 1900 Initial Temperature 83.50°F

$q_b = 0.144$ Btu/ft^{2}sec $q_s = 0.0148$ Btu/ft^{2}sec

$Gr^*_{max} = 1.35 \times 10^{13}$

Thermocouple Locations (ft)	TEMPERATURES (°F) 1000 (sec)	2000 (sec)	3000 (sec)	4000 (sec)	5000 (sec)	6000 (sec)
0.0833	83.60	83.57	83.65	83.91	84.10	84.31
0.50	83.53	83.62	83.77	84.00	84.18	84.43
1.00	83.50	83.57	83.74	84.00	84.18	84.43
1.50	83.47	83.64	83.86	84.14	84.45	84.66
2.00	83.52	83.77	84.05	84.34	84.58	84.89
2.50	83.84	84.15	84.38	84.65	84.97	85.25
3.016	83.75	84.05	84.31	84.65	85.01	85.30
3.50	83.86	84.14	84.36	84.74	85.09	85.41
4.00	84.00	84.34	84.58	84.94	85.26	85.51
4.50	83.96	84.34	84.57	84.95	85.35	85.61
5.00	83.92	84.31	84.57	84.94	85.34	85.60
5.31	83.88	84.23	84.43	84.98	85.38	85.73
5.67	84.02	84.47	84.69	85.06	85.46	85.81
5.83	84.00	84.50	84.77	85.11	85.41	85.78
5.916	84.10	84.58	84.85	85.19	85.49	85.60
6.00	84.48	84.81	85.18	85.58	85.80	86.07

Table 23. Experimental Temperatures

Test No. 2000 Initial Temperature 79.60°F

$q_b = 0$ $q_s = .0179$ Btu/ft^{2}sec

$Gr^*_{max} = 1.41 \times 10^{13}$

Thermocouple Locations (ft)	TEMPERATURES (°F) 1200 (sec)	2400 (sec)	3600 (sec)	4800 (sec)	6000 (sec)	7200 (sec)
0.083	79.61	79.59	79.60	79.61	79.61	79.61
0.50	79.59	79.62	79.64	79.66	79.68	79.83
1.00	79.58	79.64	79.78	80.06	80.25	80.54
1.50	79.63	79.82	80.02	80.44	80.78	81.12
2.00	79.71	79.98	80.36	80.88	81.17	81.56
2.50	79.80	80.14	80.60	81.00	81.30	81.73
3.016	79.92	80.39	80.77	81.17	81.47	81.95
3.50	80.09	80.56	80.94	81.39	81.69	82.16
4.00	80.17	80.68	81.03	81.52	81.86	82.33
4.50	80.30	80.81	81.21	81.73	81.99	82.50
5.00	80.51	80.98	81.33	81.85	82.08	82.58
5.31	80.54	81.07	81.45	81.95	82.24	82.71
5.67	80.54	81.07	81.54	82.07	82.29	82.78
5.83	80.67	81.14	81.55	82.15	82.30	82.82
5.916	80.61	81.14	81.58	82.11	82.33	82.69
6.00	80.75	81.23	81.62	82.19	82.34	82.68

Table 24. Experimental Temperatures

Test No. 2100 Initial Temperature 71.20°F

q_b = .1635 Btu/ft^{2}sec q_s = .121 Btu/ft^{2}sec

Gr^*_{max} = 5.01 x 10^{14}

Thermocouple Locations (ft)	TEMPERATURES (°F) 300 (sec)	600 (sec)	900 (sec)	1200 (sec)	1500 (sec)	1800 (sec)
0.0833	71.81	72.14	72.79	73.55	74.06	74.69
0.500	71.53	72.01	72.57	73.14	73.74	74.37
1.00	71.39	71.85	72.50	73.09	73.58	74.19
1.50	71.40	71.91	72.43	73.01	73.58	74.24
2.00	71.33	71.90	72.46	73.06	73.56	74.22
3.00	71.47	72.15	72.74	73.39	74.03	74.67
4.00	71.56	72.33	72.90	73.52	74.27	74.90
5.00	71.67	72.52	73.10	73.75	74.39	75.02
6.00	71.80	72.55	73.23	74.00	74.68	75.31
7.00	71.88	72.63	73.39	74.20	74.88	75.50
8.00	72.10	72.93	73.68	74.40	75.20	75.86
8.50	72.22	73.21	73.98	74.68	75.44	76.11
9.00	72.63	73.65	74.33	75.14	75.89	76.54
9.33	72.98	73.86	74.77	75.65	76.50	77.17
9.58	73.53	74.28	75.35	76.36	77.38	78.09
9.75	73.88	75.17	76.16	77.28	78.33	78.92

Table 25. Experimental Temperatures

Test No. 2200 Initial Temperature 74.10°F

q_b = 0.1082 Btu/ft^{2}sec q_s = .114 Btu/ft^{2}sec

Gr^*_{max} = 5.28 x 10^{14}

Thermocouple Locations (ft)	TEMPERATURES (°F) 300 (sec)	600 (sec)	900 (sec)	1200 (sec)	1500 (sec)	1800 (sec)
0.0833	74.34	74.53	75.02	75.60	75.89	76.31
0.50	74.20	74.47	74.90	75.38	75.89	76.38
1.00	74.26	74.60	75.07	75.54	75.87	76.35
1.50	74.36	74.66	75.09	75.61	76.05	76.53
2.00	74.39	74.84	75.34	75.84	76.35	76.89
3.00	74.35	74.99	75.53	76.09	76.60	77.13
4.00	74.45	75.11	75.71	76.32	76.86	77.41
5.00	74.76	75.42	76.01	76.61	77.29	77.83
6.00	74.82	75.50	76.17	76.88	77.46	78.02
7.00	74.79	75.53	76.27	76.96	77.64	78.23
8.00	75.02	75.68	76.47	77.15	77.86	78.46
8.50	75.10	75.90	76.73	77.48	78.15	78.75
9.00	75.12	76.12	76.97	77.78	78.59	79.15
9.33	75.49	76.45	77.38	78.22	78.92	79.54
9.58	76.12	76.62	77.71	78.79	79.66	80.33
9.75	76.28	77.79	78.99	79.36	80.00	80.62

Table 26. Experimental Temperatures

Test No. 2300 Initial Temperature 75.50°F

$q_b = 0$ $q_s = 0.108$ Btu/ft^{2}sec

$Gr^*_{max} = 5.22 \times 10^{14}$

Thermocouple Locations (ft)	TEMPERATURES (°F) 300 (sec)	600 (sec)	900 (sec)	1200 (sec)	1500 (sec)	1800 (sec)
0.0833	75.59	75.59	75.62	75.61	75.61	75.61
0.50	75.54	75.59	75.62	75.61	75.61	75.72
1.00	75.54	75.59	75.61	75.63	75.79	76.04
1.50	75.54	75.57	75.68	75.97	76.28	76.65
2.00	75.56	75.68	76.08	76.54	77.15	77.63
3.00	75.66	76.23	76.81	77.44	77.96	78.34
4.00	75.90	76.38	76.97	77.69	78.28	78.62
5.00	76.09	76.75	77.35	78.03	78.64	78.99
6.00	76.43	77.03	77.73	78.33	78.92	79.28
7.00	76.45	77.06	77.80	78.52	79.12	79.47
8.00	76.43	77.36	78.08	78.76	79.44	79.79
8.50	76.62	77.51	78.32	79.05	79.66	79.98
9.00	76.71	77.66	78.59	79.32	80.05	80.37
9.33	77.25	77.93	78.90	79.63	80.38	80.69
9.58	77.08	78.33	79.25	80.04	80.93	81.20
9.75	78.09	78.52	79.67	80.64	81.51	81.69

Table 27. Experimental Temperatures

Test No. 2400 Initial Temperature 76.20°F

q_b = .1775 Btu/ft^{2}sec q_s = 0.043 Btu/ft^{2}sec

Gr^*_{max} = 2.11 x 10^{14}

Thermocouple Locations (ft)	TEMPERATURES (°F) 450 (sec)	900 (sec)	1350 (sec)	1800 (sec)	2250 (sec)	2700 (sec)
0.0833	76.44	76.86	77.44	77.90	78.33	78.91
0.500	76.36	76.80	77.38	77.89	78.35	78.89
1.00	76.37	76.81	77.28	77.78	78.25	78.72
1.50	76.18	76.65	77.23	77.62	78.07	78.54
2.00	76.23	76.74	77.13	77.67	78.10	78.59
3.00	76.51	76.83	77.27	77.77	78.15	78.63
4.00	76.34	76.81	77.23	77.70	78.15	78.60
5.00	76.64	77.08	77.54	77.93	78.37	78.80
6.00	76.68	77.11	77.59	78.01	78.45	78.91
7.00	76.87	77.29	77.76	78.18	78.61	79.06
8.00	76.87	77.27	77.74	78.16	78.57	79.04
8.50	76.86	77.26	77.71	78.19	78.61	79.07
9.00	77.07	77.49	77.93	78.40	78.81	79.26
9.33	77.14	77.70	78.19	78.60	79.01	79.42
9.58	77.18	77.91	78.38	78.80	79.26	79.65
9.75	77.50	78.44	78.79	79.16	79.54	79.99

Table 28. Experimental Temperatures

Test No. 2500 Initial Temperature 76.40°F

$q_b = 0.077$ Btu/ft^{2}sec $q_s = 0.041$ Btu/ft^{2}sec

$Gr^*_{max} = 1.97 \times 10^{14}$

Thermocouple Locations (ft)	TEMPERATURES (°F)					
	450 (sec)	900 (sec)	1350 (sec)	1800 (sec)	2250 (sec)	2700 (sec)
0.0833	76.73	77.06	77.32	77.76	78.09	78.48
0.50	75.52	76.73	77.07	77.49	77.82	78.25
1.00	76.35	76.59	76.97	77.35	77.72	77.98
1.50	76.41	76.68	77.05	77.40	77.78	78.03
2.00	76.53	76.84	77.12	77.56	77.93	78.22
3.00	76.63	76.90	77.39	77.84	78.12	78.38
4.00	76.70	77.03	77.41	77.84	78.17	78.41
5.00	76.70	77.10	77.48	77.91	78.25	78.48
6.00	76.87	77.26	77.65	78.06	78.37	78.59
7.00	76.86	77.25	77.63	78.03	78.38	78.59
8.00	76.92	77.44	77.90	78.30	78.61	78.80
8.50	77.04	77.51	77.99	78.41	78.73	78.91
9.00	77.12	77.70	78.15	78.58	78.89	79.05
9.33	77.27	77.97	78.45	78.85	79.16	79.28
9.58	77.66	78.18	78.56	78.93	79.24	79.34
9.75	77.92	78.59	79.02	79.44	79.75	79.79

Table 29. Experimental Temperatures

Test No. 2600 Initial Temperature 74.39°F

$q_b = 0.047$ Btu/ft^{2}sec $q_s = 0.049$ Btu/ft^{2}sec

$Gr^*_{max} = 2.24 \times 10^{14}$

Thermocouple Locations (ft)	TEMPERATURES (°F) 600 (sec)	1200 (sec)	1800 (sec)	2400 (sec)	3000 (sec)	3600 (sec)
0.0833	74.65	74.93	75.18	75.56	75.94	76.49
0.50	74.60	74.92	75.12	75.55	75.94	76.40
1.00	74.59	74.75	75.12	75.54	75.90	76.27
1.50	74.52	74.76	75.24	75.67	76.17	76.57
2.00	74.42	74.85	75.36	75.83	76.29	76.78
3.00	74.61	75.06	75.57	76.12	76.63	77.06
4.00	74.73	75.19	75.73	76.33	76.80	77.25
5.00	74.83	75.36	75.93	76.53	77.01	77.48
6.00	74.92	75.48	76.13	76.66	77.19	77.65
7.00	75.04	75.60	76.25	76.85	77.42	77.89
8.00	75.22	75.86	76.54	77.10	77.69	78.21
8.50	75.34	76.11	76.75	77.37	77.97	78.51
9.00	75.46	76.26	76.98	77.61	78.24	78.76
9.33	75.81	76.47	77.32	77.95	78.57	79.10
9.58	75.86	76.63	77.35	78.11	78.87	79.42
9.75	76.20	76.93	77.49	78.38	79.10	79.56

Table 30. Experimental Temperatures

Test No. 2700 Initial Temperature 75.30°F

$q_b = 0$ $q_s = 0.045$ Btu/ft^{2}sec

$Gr^*_{max} = 2.15 \times 10^{14}$

Thermocouple Locations (ft)	TEMPERATURES (°F) 600 (sec)	1200 (sec)	1800 (sec)	2400 (sec)	3000 (sec)	3600 (sec)
0.0833	75.30	75.31	75.30	75.30	75.31	75.31
0.50	75.31	75.32	75.36	75.37	75.45	75.63
1.00	75.34	75.37	75.40	75.42	75.65	75.89
1.50	75.35	75.43	75.58	75.95	76.34	76.68
2.00	75.26	75.45	75.85	76.44	76.88	77.18
3.00	75.47	76.04	76.63	77.04	77.47	77.73
4.00	75.69	76.29	76.84	77.28	77.73	78.01
5.00	75.83	76.37	76.99	77.48	77.90	78.17
6.00	75.95	76.63	77.21	77.75	78.14	78.42
7.00	75.98	76.62	77.19	77.79	78.23	78.53
8.00	76.08	76.69	77.40	78.03	78.48	78.75
8.50	76.29	76.90	77.60	78.25	78.71	78.98
9.00	76.38	77.06	77.80	78.44	78.87	79.12
9.33	76.51	77.31	78.01	78.66	79.15	79.39
9.58	76.67	77.47	78.20	78.88	79.36	79.57
9.75	76.95	77.58	78.35	79.14	79.69	79.89

Table 31. Experimental Temperatures

Test No. 2800 Initial Temperature 76.23°F

$q_b = 0.0289$ Btu/ft^{2}sec $q_s = 0.016$ Btu/ft^{2}sec

$Gr^*_{max} = 7.33 \times 10^{13}$

Thermocouple Locations (ft)	TEMPERATURES (°F) 900 (sec)	1800 (sec)	2700 (sec)	3600 (sec)	4500 (sec)	5400 (sec)
0.0833	76.25	76.36	76.66	76.95	77.12	77.43
0.500	76.25	76.36	76.62	76.88	77.12	77.43
1.00	76.24	76.36	76.62	76.85	77.03	77.42
1.50	76.30	76.46	76.78	76.98	77.23	77.62
2.00	76.38	76.56	76.78	76.98	77.22	77.57
3.00	76.37	76.59	76.92	77.20	77.39	77.66
4.00	76.40	76.67	77.01	77.26	77.39	77.73
5.00	76.55	76.81	77.03	77.26	77.39	77.80
6.00	76.53	76.87	77.19	77.42	77.69	77.96
7.00	76.56	76.85	77.21	77.49	77.69	77.99
8.00	76.68	76.99	77.25	77.58	77.77	78.15
8.50	76.76	77.10	77.40	77.68	77.99	78.30
9.00	76.84	77.19	77.48	77.72	78.03	78.37
9.33	76.93	77.31	77.60	77.93	78.16	78.53
9.58	76.97	77.30	77.59	77.94	78.25	78.58
9.75	77.04	77.32	77.67	77.98	78.33	78.63

Table 32. Experimental Temperatures

Test No. 2900 Initial Temperature 75.90°F

$q_b = 0.0164$ Btu/ft^{2}sec $q_s = 0.0176$ Btu/ft^{2}sec

$Gr^*_{max} = 8.12 \times 10^{13}$

Thermocouple Locations (ft)	TEMPERATURES (°F) 900 (sec)	1800 (sec)	2700 (sec)	3600 (sec)	4500 (sec)	5400 (sec)
0.0833	75.92	75.94	76.11	76.29	76.60	76.79
0.50	75.92	75.91	76.13	76.36	76.53	76.85
1.00	75.91	75.97	76.28	76.58	76.57	76.84
1.50	75.93	76.10	76.41	76.75	76.71	76.97
2.00	75.94	76.17	76.45	76.80	76.86	77.07
3.00	75.92	76.22	76.58	77.01	77.16	77.37
4.00	75.97	76.37	76.79	77.10	77.23	77.52
5.00	76.10	76.49	76.92	77.32	77.39	77.61
6.00	76.16	76.53	76.96	77.40	77.51	77.80
7.00	76.30	76.71	77.20	77.53	77.64	77.83
8.00	76.52	76.97	77.41	77.79	77.85	77.98
8.50	76.62	77.14	77.58	77.96	77.98	78.17
9.00	76.65	77.13	77.62	78.07	78.18	78.35
9.33	76.72	77.26	77.79	78.20	78.32	78.42
9.58	76.82	77.35	77.95	78.42	78.39	78.44
9.75	76.83	77.39	77.98	78.49	78.47	78.57

Table 33. Experimental Temperatures

Test No. 3000 Initial Temperature 76.15°F

$q_b = 0$ $q_s = 0.019$ Btu/ft^{2}sec

$Gr^*_{max} = 8.7 \times 10^{13}$

Thermocouple Locations (ft)	TEMPERATURES (°F) 900 (sec)	1800 (sec)	2700 (sec)	3600 (sec)	4500 (sec)	5400 (sec)
0.0833	76.15	76.16	76.14	76.16	76.15	76.17
0.50	76.25	76.22	76.27	76.31	76.44	76.49
1.00	76.25	76.22	77.22	76.43	76.57	76.76
1.50	76.16	76.22	76.22	76.50	76.74	76.97
2.00	76.16	76.26	76.34	76.63	76.99	77.24
3.00	76.25	76.43	76.72	77.10	77.31	77.50
4.00	76.36	76.69	76.90	77.19	77.51	77.76
5.00	76.44	76.77	77.06	77.40	77.73	77.94
6.00	76.53	76.85	77.11	77.51	77.85	78.07
7.00	76.54	76.94	77.19	77.59	77.93	78.24
8.00	76.57	77.06	77.29	77.60	78.03	78.37
8.50	76.56	77.09	77.40	77.69	78.14	78.52
9.00	76.68	77.18	77.48	77.80	78.30	78.61
9.33	76.69	77.25	77.60	77.93	78.39	78.71
9.58	76.70	77.34	77.61	77.95	78.45	78.76
9.75	76.87	77.37	77.71	78.00	78.48	78.84

APPENDIX G

ANALYSIS OF VELOCITY MEASUREMENTS USING A PHOTOGRAPHIC SYSTEM

While the photographic technique used here to measure the motion of the test fluid has numerous advantages, there are certain corrections which must be applied to the data and certain factors regarding the use of the suspended particles, which must be studied before the results obtained can be properly interpreted. These factors are:

1. The relation between the actual fluid motion and the particle motion, i.e., inertia and buoyancy effects.

2. The relation between the apparent particle motion and the true particle motion, i.e., light refraction effects.

In this appendix these considerations are discussed and a computer program for correcting and correlating the photographic velocity data is presented.

Particle Response to Buoyant Forces and Unsteady Accelerations

Since the trajectories of the spherical particles suspended in the test fluid, rather than the true fluid motion itself, are what is actually obtained from the photographic technique, some investigation of the departure between the particle velocity and the true velocity is necessary. There are two main sources of possible error that should be considered. The first is that error resulting from the rising or

settling of the individual particles due to differences between their density and that of the test fluid. Since the particles are extremely small, the flow Reynolds number is of the order unity and thus Stokes equation for the drag of a sphere in creeping motion is valid. Hence the terminal velocity of a particle can be obtained by equating the buoyant force to the drag force acting on it. It follows that:

$$\frac{\pi}{6} D_p^3(\rho - \rho_p) = 3\pi\mu D_p U_p \qquad \text{(G-1)}$$

where: D_p = particle diameter, ft

ρ = density of test fluid, lbm/ft^3

ρ_p = density of particles, lbm/ft^3

μ = viscosity of test fluid, lbm/ft sec

U_p = rising or settling velocity, ft/sec

Thus

$$U_p = \frac{D_p^2}{18\nu}(1 - \rho_p/\rho) \qquad \text{(G-2)}$$

For water at 80°F:

$$\nu = .93 \times 10^{-5} \text{ ft}^2/\text{sec}, \qquad \rho = 62.4 \text{ lbm/ft}^3$$

For the average particle:

$$D_p = 0.000167 \text{ ft}, \qquad \rho_p = 26 \text{ lbm/ft}^3$$

$$\therefore U_p = .965 \times 10^{-4} \text{ ft/sec}$$

Since velocities in the boundary layer are of the order of 0.1 ft/sec and experimental observations indicate that velocities (U) in the range .01 ft/sec < U < .1 ft/sec are common it appears that the maximum errors present due to buoyant effects are only of the order of 1 per cent.

The second possible type of error is that which may occur when the suspended particles move into regions of accelerated fluid flow. To evaluate the particle response to acceleration, two simple cases are considered. In each case the gross motion of the fluid is assumed to be independent of the presence of the particles and Stokes equation for the drag on a sphere in creeping motion is used. Justification for this latter assumption becomes evident when the results are studied.

The first problem considered is that of a steady flow in the x direction with a superimposed oscillating flow of frequency ω in the y direction. It is assumed that the particle is at rest with respect to the flow at time zero. The basic equations of motion for the particle are:

$$3\pi\mu D_p(U - U_p) = \frac{\pi D_p^3}{6}\rho_p \frac{dU_p}{d\tau} \qquad (G\text{-}3)$$

$$3\pi\mu D_p(V - V_p) = \frac{\pi D_p^3}{6}\rho_p \frac{dV_p}{d\tau} \qquad (G\text{-}4)$$

where: $U = U_o$

$V = V_o \sin\omega\tau$

Substituting

$$\zeta = U - U_p, \qquad \zeta(0) = U_o \tag{G-5}$$

$$\phi = V - V_p, \qquad \phi(0) = 0$$

The above equations become

$$\frac{d\zeta}{d\tau} = -\frac{18\mu}{D_p^2\rho_p}\zeta \tag{G-6}$$

$$\frac{d\phi}{d\tau} = \omega V_o \cos\omega\tau - \frac{18\mu}{D_p^2\rho_p}\phi \tag{G-7}$$

Since the equations are not coupled, they can be solved independently.

Therefore:

$$\zeta = U_o \exp\left(-\frac{18\mu}{D_p^2\rho_p}\tau\right) \tag{G-8}$$

$$\phi = \frac{V_o\omega}{\omega^2 + \left(\frac{18\mu}{D_p^2\rho_p}\right)^2}\left[\frac{18\mu}{D_p^2\rho_p}\cos\omega\tau + \omega\sin\omega\tau - \frac{18\mu}{D_p^2\rho_p}\exp\left(-\frac{18\mu}{D_p^2\rho_p}\tau\right)\right] \tag{G-9}$$

For water at 80°F, using 2 mil particles, the coefficient

$$\frac{18\mu}{D_p^2\rho_p} = 10^4 \tag{G-10}$$

Thus in 10^{-4} seconds, the particle x velocity is within e^{-1} of the

steady state condition. It is clear then that ζ approaches zero and ϕ approaches its asymptotic state very rapidly. Of interest also is the maximum value of ϕ after the quasi-steady state is reached. Conveniently this value is independent of the initial conditions. Taking the derivative of the asymptotic relation for ϕ, and equating it to zero, the maximum value of ϕ is found to be

$$\phi_\infty\Big|_{max} = \frac{V_o}{\sqrt{1 + (\frac{1}{\omega})^2(\frac{18\mu}{\rho_p D_p^2})^2}} \qquad \text{(G-11)}$$

For water at 80°F with ω = 100 radians/sec

$$\frac{\phi_\infty\Big|_{max}}{V_o} = \frac{1}{\sqrt{1 + 10^4}}$$

$$= 10^{-2}$$

Thus even with a flow oscillating at 16 cps the maximum velocity error is only 1 per cent.

The second case considered is that of the motion of a particle within a potential vortex. In this case it is also assumed that the particle is completely at rest at time zero. The basic equations of motion for the spherical particle are

$$(\frac{\pi D_p^3}{6}\rho_p)\left[\frac{d^2R_p}{d\tau^2} - R_p(\frac{d\theta_p}{d\tau})^2\right] = -3\pi\mu D_p \frac{dR_p}{d\tau} \qquad \text{(G-12)}$$

$$\left(\frac{\pi D_p^3}{6}\rho_p\right)\frac{1}{R_p}\frac{d}{d\tau}\left(R_p^2\frac{d\theta_p}{d\tau}\right) = 3\pi\mu D_p\left[\frac{\Gamma}{2\pi R_p} - R_p\frac{d\theta_p}{d\tau}\right] \qquad \text{(G-13)}$$

Multiplying the second equation by $6\,R_p/\pi D_p^3\rho_p$, substituting $Z = R_p^2\frac{d\theta_p}{dt}$, rearranging, and using the integrating factor $\exp(\frac{18\mu\tau}{D_p^2\rho_p})$ gives the equation:

$$\frac{d}{d\tau}\left(e^{\frac{18\mu\tau}{D_p^2\rho_p}}Z\right) = \frac{18\mu}{D_p^2\rho_p}\left(\frac{\Gamma}{2\pi}\right)e^{\frac{18\mu\tau}{D_p^2\rho_p}} \qquad \text{(G-14)}$$

Integrating directly and applying the initial conditions produce the result:

$$Z = R_p^2\frac{d\theta_p}{d\tau} = \frac{\Gamma}{2\pi}\left[1 - e^{-\frac{18\mu}{D_p^2\rho_p}\tau}\right] \qquad \text{(G-15)}$$

Thus the tangential velocity

$$V_{tan} = R_p\frac{d\theta_p}{d\tau} = \left(\frac{\Gamma}{2\pi R_p}\right)\left[1 - e^{-\frac{18\mu}{D_p^2\rho_p}\tau}\right] \qquad \text{(G-16)}$$

The first term in (G-16) is recognized as the tangential velocity of the vortex. The second term using Equation (G-10) is unity except for extremely short times. Thus, the particle tangential motion is essentially that of the vortex. Using the relation (G-15) obtained for Z, Equation G-12 can be written

$$\frac{d^2R_p}{d\tau^2} - \frac{\Gamma^2}{4\pi^2 R_p^3}\left[1 - e^{-\frac{18\mu}{D_p^2\rho_p}\tau}\right]^2 = -\frac{18\mu}{D_p^2\rho_p}\frac{dR_p}{d\tau} \qquad \text{(G-17)}$$

Let

$$P = \frac{dR_p}{d\tau}\ ,\ \therefore\ \frac{d^2R_p}{d\tau^2} = \frac{dP}{dR_p}\frac{dR_p}{d\tau} = P\frac{dP}{dR_p} \qquad \text{(G-18)}$$

Thus (G-17) becomes:

$$P\left[\frac{dP}{dR_p} + \frac{18\mu}{D_p^2\rho_p}\right] = \frac{\Gamma^2}{4\pi^2 R_p^3}\left[1 - e^{-\frac{18\mu}{D_p^2\rho_p}\tau}\right]^2 \qquad \text{(G-19)}$$

Solving directly for P produces the relation:

$$P = \frac{dR_p}{d\tau} = \left(\frac{\Gamma^2}{4\pi^2 R_p^3}\right)\frac{\left[1 - e^{-\frac{18\mu}{D_p^2\rho_p}\tau}\right]^2}{\frac{dP}{dR_p} + \frac{18\mu}{D_p^2\rho_p}} \qquad \text{(G-20)}$$

The largest possible value the right-hand term can have is when $R_p = R_o$, $\tau \to \infty$, and $\frac{dP}{dR_p} = 0$. Thus

$$\frac{dR_p}{d\tau} < \left(\frac{\Gamma}{2\pi R_o}\right)^2\left(\frac{1}{R_o}\right)\left(\frac{D_p^2\rho_p}{18\mu}\right) \qquad \text{(G-21)}$$

Since

$$\Gamma = 2\omega\pi R_c^2 \quad , \tag{G-22}$$

where R_c is the vortex radius,

$$\frac{dR_p}{d\tau} < \frac{\omega^2 R_c^4}{R_o^3} \left(\frac{D^2 \rho_p}{18\mu}\right) \tag{G-23}$$

A typical value of ω has been found to be 1 radian/sec. A typical vortex radius is 0.07 feet. Thus for water at 80°F with R_o = .01 ft,

$$\frac{dR_p}{d\tau} < .24 \times 10^{-2} \text{ ft/sec}$$

The above values indicate that for both types of motion only a negligible velocity error between the particle and the fluid motion should be present.

Light Refraction Effects on Position and Velocity Measurements

In using the photographic technique, consideration must also be given to inherent distortions and velocity errors produced by light refraction in passing through the water and the glass panels to the camera lens. The basic expression which governs these effects is called the general equation for refraction which can be written:

$$\frac{\sin\alpha_1}{\sin\alpha_2} = \frac{\mu_{r2}}{\mu_{r1}} \qquad \text{(G-24)}$$

where α_1 and α_2 are the angles between the normal to a surface and an arriving and leaving ray of light, respectively; μ_{r1} and μ_{r2} are the refractive indices of the media through which the light passes.

Typical values of μ_r are shown below:

Medium	Refraction Index
Pure Water	1.33
Air	1.0003
Plate Glass (Libby Owens Ford)	1.523

An interesting feature of the problem considered here is that distortions in apparent position and velocity due to light refraction are symmetric about the optical axis of the camera, if the camera is focused normally to the glass sides of the tank. Since this camera orientation provides such a simplification to the corrections required, all the photographs presented were taken with the optical axis of the camera perpendicular to the glass sides. Figure 24 presents a typical situation.

From a study of the figure, the following equation can be written:

$$\overline{pq} = (\varepsilon_1 + \varepsilon_2) = \frac{t_1 + t_2}{\cos\alpha_g} \cdot \sin(\beta_r - \alpha_g) \qquad \text{(G-25)}$$

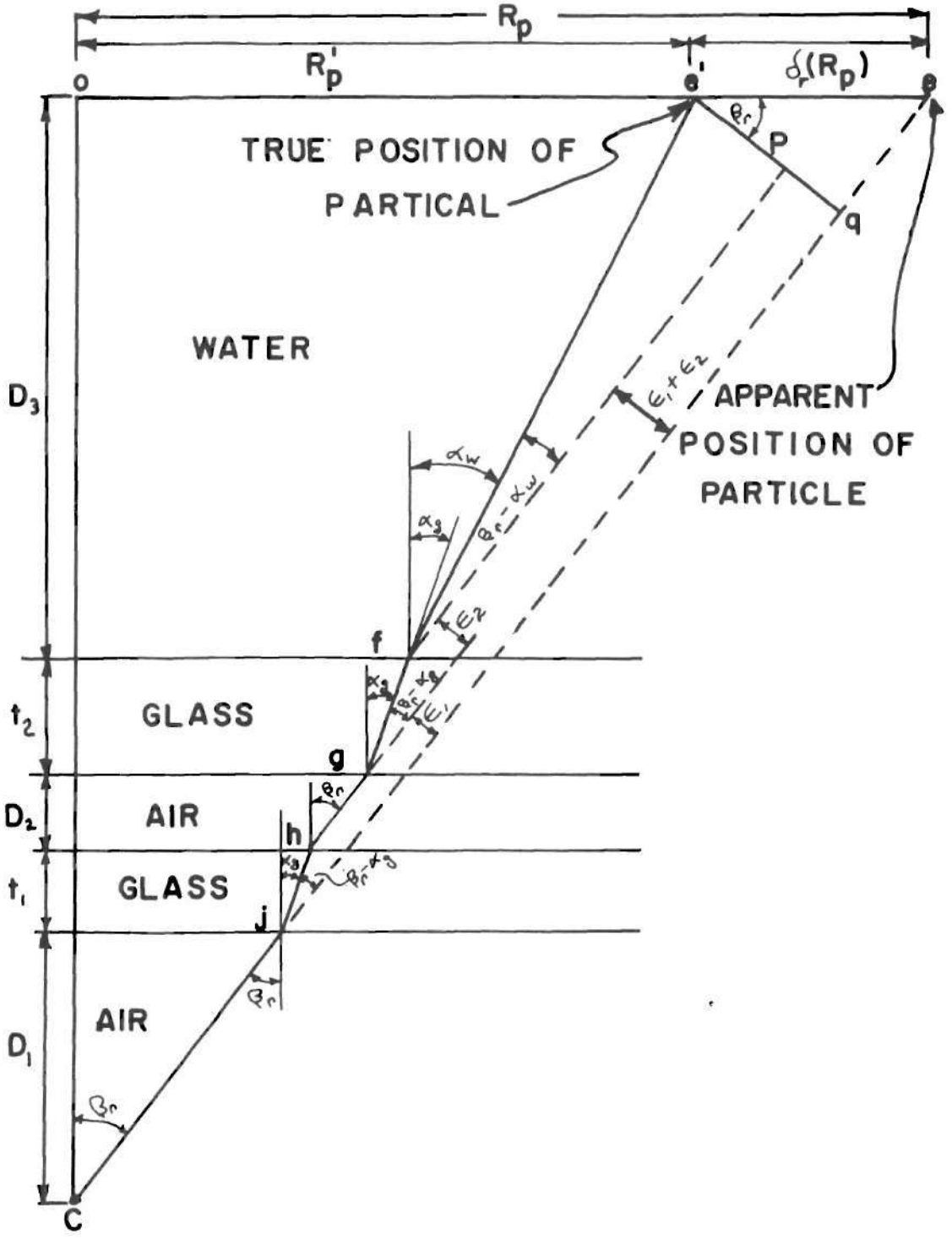

Figure 24. Schematic Diagram of Light Refraction Effects on Radial Position of Particles.

Using the general law of refraction, (G-25) becomes:

$$\overline{pq} = (t_1 + t_2)(\sin \beta_r)\left[1 - \sqrt{\frac{1 - \sin^2\beta_r}{\mu_{rg}^2 - \sin^2\beta_r}} \right] \qquad \text{(G-26)}$$

Also from study of the figure, an expression for $\overline{e'p}$ is found:

$$\overline{e'p} = \frac{D_3}{\cos\alpha_w} \sin(\beta_r - \alpha_w) \qquad \text{(G-27)}$$

Again the general equation for refraction gives:

$$\overline{e'p} = D_3(\sin\beta_r)\left[1 - \sqrt{\frac{1 - \sin^2\beta_r}{\mu_{rw}^2 - \sin^2\beta_r}} \right] \qquad \text{(G-28)}$$

Noting that $\overline{e'e} = \overline{eq}/\cos\beta_r$ and $\beta_r = \tan^{-1} R_p/\overline{oc}$, a relation for $\delta_r(R_p)$ can be found:

$$\delta_r(R_p) = \frac{R_p}{\overline{oc}} \left\{ (D_3 + t_1 + t_2) - \frac{D_3}{\sqrt{(\frac{R_p}{\overline{oc}})^2 (\mu_{rw}^2 - 1) - \mu_{rw}^2}} - \frac{(t_1 + t_2)}{\sqrt{(\frac{R_p}{\overline{oc}})^2 (\mu_{rg}^2 - 1) - \mu_{rg}^2}} \right\} \qquad \text{(G-29)}$$

Thus an expression for the radial error in apparent position is gained as a function of the apparent position of a particle which is what is usually known. To obtain velocity information it is convenient, due to the symmetry of $\delta_r(R_p)$ about the optical axis, to make the necessary calculations using a polar coordinate system. The origin of this coordinate system is taken at the intersection of the optical axis of the camera

and the plane of the motion. In polar coordinates:

$$|V_t| = \sqrt{\left(\frac{dR_p'}{d\tau}\right)^2 + R_p'^2\left(\frac{d\Theta_p}{d\tau}\right)^2} \qquad \text{(G-30)}$$

where V_t = true velocity. From Figure 24, it is seen that:

$$R_p' = R_p - \delta_r(R_p) \qquad \text{(G-31)}$$

From symmetry,

$$\Theta_p = \Theta_p(\tau), \text{ alone} \qquad \text{(G-32)}$$

Using the chain rule, it follows that

$$\frac{dR_p'}{d\tau} = \frac{dR_p}{d\tau}\left[1 - \frac{d\delta_r}{dR_p}\right] \qquad \text{(G-33)}$$

Thus the expression for the true velocity becomes

$$|V_t| = \frac{dR_p}{d\tau}\sqrt{\left(1 - \frac{d\delta_r}{dR_p}\right)^2 + (R_p - \delta)^2\left(\frac{d\Theta_p}{dR_p}\right)^2} \qquad \text{(G-34)}$$

where

$$\frac{d\delta_r}{dR_p} = \frac{D_3}{\overline{oc}}\left\{1 - \frac{\mu_{rw}^2}{\left[\left(\frac{R_p}{\overline{oc}}\right)^2 (\mu_{rw}^2 - 1) - \mu_{rw}^2\right]^{3/2}}\right\} \qquad \text{(G-35)}$$

$$+ \frac{(t_1 + t_2)}{\overline{oc}}\left\{1 - \frac{\mu_{rg}^2}{\left[\left(\frac{R_p}{\overline{oc}}\right)^2 (\mu_{rg}^2 - 1) - \mu_{rg}^2\right]^{3/2}}\right\}$$

In order to obtain velocity data from the photographs, an approximation using finite differences must be made to (G-34). In addition, it is convenient to make a transformation from the polar coordinate system to a cartesian coordinate system with the origin located at the lower left-hand corner of the photograph. Thus in the new coordinate system:

$$R_p = \sqrt{(x_p - x_o)^2 + (y_p - y_o)^2} \qquad \text{(G-36)}$$

$$\Theta_r = \tan^{-1}\left(\frac{y_p - y_o}{x_p - x_o}\right) \qquad \text{(G-37)}$$

where: x_o = x coordinate of optical axis

y_o = y coordinate of optical axis.

Therefore, the final result for V_t is obtained:

$$|V_t| = \left(\frac{R_{PB} - R_{PA}}{\Delta\tau}\right)\left\{\left[1 - \frac{d\delta_r(\bar{R}_p)}{dR_p}\right]^2 + \{\bar{R}_p - \delta_r(\bar{R}_p)\}^2\left[\frac{\Theta_{PB} - \Theta_{PA}}{R_{PB} - R_{PA}}\right]^2\right\}^{1/2} \qquad \text{(G-38)}$$

where: R_{PA} = initial apparent radial position, ft

R_{PB} = final apparent radial position, ft

θ_{PA} = initial angular position, radions

θ_{PB} = final angular position, radians

$\Delta\tau$ = exposure time, seconds

Equations (G-29), (G-31), and (G-38) have been used to calculate the particle positions and velocities in the Velocity Data Correlation and Analysis Computer Program which is listed later in this appendix. In this computer program, written for the IBM 7094, the initial and final apparent positions for up to 900 particles are used as input data, together with pertinent physical constants and identification information. The computer calculates the value of various quantities including δ_r, R_p, and V_t for each particle and also calculates the average velocity in nine subregions of each photograph.

Besides the average velocity in each subregion, the computer also calculates an intensity parameter defined as:

$$I = \frac{\sum_n \left[1/2(\bar{U}_t - U_{tn})^2 + 1/2\,(\bar{V}_t - V_{tn})^2\right]^{1/2}}{|\bar{V}_t|} \qquad \text{(G-39)}$$

where: $\bar{U}_t = \frac{1}{m} \sum_{n=1}^{m} U_{tn}$

$\bar{V}_t = \frac{1}{m} \sum_{n=1}^{m} V_{tn}$

U_{tn} = x component of n the particle true velocity

V_{tn} = y component of n the particle true velocity

$$|\bar{V}_t| = \sqrt{\bar{U}_{tn}^2 + \bar{V}_{tn}^2}$$

This parameter, analogous to a turbulent intensity, provides a quantitative means to judge the degree of turbulence present in a given region.

In the next pages a complete listing of this program is presented.

```
      CALL TAPE(2,IN,IO)                                                    07/10/65

      CALL TAPE(2,IN,IO)
      DIMENSION S(100,12,9),NPR(9),UTK(9),SVTK(9),VTK(9),XI(9),BN(9),
     1XXX(3),YYY(3),KKKK(100,9),XX(9),YY(9)
      KKK=0
C     INPUT TABLE 2
 1000 FORMAT(3E10.0,4I5,3E10.0/8E10.0/8E10.0/8E10.0)
      READ INPUT TAPE IN,1000,XM,YM,DTI,
     1IMO,IDAY,IYEAR,NTEST,QSA,QBA,TV0,XLL,
     2TI,XCL,YCL,OC,T1,T2,UG,UW,
     3D3,(XXX(I),YYY(I),I=1,3),X0,Y0,SCALE
      XM=XM*SCALE
      YM=YM*SCALE
      X0=X0*SCALE
      Y0=Y0*SCALE
      XXX(1)=XXX(1)*SCALE
      XXX(2)=XXX(2)*SCALE
      XXX(3)=XXX(3)*SCALE
      YYY(1)=YYY(1)*SCALE
      YYY(2)=YYY(2)*SCALE
      YYY(3)=YYY(3)*SCALE
      DO 111 I=1,3
      DO 111 J=1,3
      II=I+(J-1)*3
      XX(II)=XXX(I)
  111 YY(II)=YYY(J)
      WRITE OUTPUT TAPE IO,1050,XM,YM,DTI,
     1IMO,IDAY,IYEAR,NTEST,QSA,QBA,TV0,XLL,
     2TI,XCL,YCL,OC,T1,T2,UG,UW,
     3D3,(I,I,XX(I),YY(I),I=1,9),X0,Y0,SCALE
 1050 FORMAT(38H1INPUT DATA TABLE 1 - SYSTEM CONSTANTS//
     18H XMAX = ,E14.7/
     18H YMAX = ,E14.7/7H EXT = ,E14.7/8H DATE = ,I2,1H/,I2,1H/,I2/
     212H TEST NO. = ,I5/7H QSA = ,E14.7/7H QBA = ,E14.7/
     37H TV0 = ,E14.7/6H LL = ,E14.7/8H TIME = ,E14.7/7H XCL = ,E14.7/
     47H YCL = ,E14.7/6H OC = ,E14.7/6H T1 = ,E14.7/6H T2 = ,E14.7/
     56H UG = ,E14.7/6H UW = ,E14.7/6H D3 = ,E14.7/
     69(1X,1HX,I1,2H,Y,I1,3H = ,2E14.7/),
     89H X0,Y0 = ,E14.7,E14.7/
     99H SCALE = ,E14.7)
      DO 9998 I=1,9
 9998 NPR(I)=0
      WRITE OUTPUT TAPE IO,1060
 1060 FORMAT(49H1INPUT DATA TABLE 2 - APPARENT PARTICLE POSITIONS//
     13H  N,11X,4HXAAN,11X,4HYAAN,11X,4HXBAN,11X,4HYBAN//)
 9999 READ INPUT TAPE IN,1010,X,Y,Z,W
      X=X*SCALE
      Y=Y*SCALE
      Z=Z*SCALE
      W=W*SCALE
      IF(SIGNF(1.,X)+1.+X)9997.5,9997
 1010 FORMAT(4F7.0)
 9997 RAAN=SQRTF((X-X0)*(X-X0)+(Y-Y0)*(Y-Y0))
      KKK=KKK+1
      WRITE OUTPUT TAPE IO,1070,KKK,X,Y,Z,W
 1070 FORMAT(I4,5X,E10.4,5X,E10.4,5X,E10.4,5X,E10.4)
      RBAN=SQRTF((Z-X0)*(Z-X0)+(W-Y0)*(W-Y0))
```

```
      CALL TAPE(2,IN,IO)                                                    07/10/65

      DAN=RAAN*((D3+T1+T2)-D3/SQRTF((RAAN/OC)*(RAAN/OC)*(UW*UW-1.0)
     1+UW*UW)-(T1+T2)/SQRTF((RAAN/OC)*(RAAN/OC)*(UG*UG-1.0)+UG*UG))/OC
      DBN=RBAN*((D3+T1+T2)-D3/SQRTF((RBAN/OC)*(RBAN/OC)*(UW*UW-
     11.0)+UW*UW)-(T1+T2)/SQRTF((RBAN/OC)*
     2(RBAN/OC)*(UG*UG-1.0)+UG*UG))/OC
      RRRR=ABSF(RBAN-RAAN)
      TAN=ATANF(Y-Y0,X-X0)
      TBN=ATANF(W-Y0,Z-X0)
21    XA=X-DAN*COSF(TAN)
      YA=Y-DAN*SINF(TAN)
      XB=Z-DBN*COSF(TBN)
      YB=W-DBN*SINF(TBN)
      RN=(RAAN+RBAN)/2.0
      DDDR=((T1+T2)/OC)*(1.0-UG*UG/((
     1(RN/OC)*(RN/OC)*(UG*UG-1.0)+UG*UG)**1.5))+(D3/OC)*(1.0-UW*UW/(((RN
     2/OC)*(RN/OC)*(UW*UW-1.0)+UW*UW)**1.5))
      DN=(DAN+DBN)/2.0
      PI=3.14.59265
      TH2=ABSF(TBN-TAN)
100   IF(TH2-PI)102,102,101
101   TH2=TH2-PI
      GO TO 100
102   CONTINUE
      VT=((RRRR       )/DTI)*SQRTF((1.0-DDDR)**2+
     1((RN-DN)**2)*(((TH2      )/(RBAN-RAAN)
     2)**2))
      U=ATANF(YB-YA,XB-XA)
      UT=VT*COSF(U)
      SVTI=VT*SINF(U)
      VAN=((RRRR       )/DTI)*SQRTF(1.0+RN*RN*
     1((TH2      )/(RBAN-RAAN))**2)
      ZN=ATANF(W-Y,Z-X)
      UAN=VAN*COSF(ZN)
20    SVAN=VAN*SINF(ZN)
      DO 1 I=1,3
      IF(XA-XXX(I))2,1,1
1     CONTINUE
2     NR=I
      DO 3 I=1,3
      IF(YA-YYY(I))4,3,3
3     CONTINUE
4     NR=NR*3(I-1)
      NPR(NR)=NPR(NR)+1
      KK=NPR(NR)
      KKKK(KK,NR)=KKK
      S(KK,1,NR)=DAN
      S(KK,2,NR)=DBN
      S(KK,3,NR)=XA
      S(KK,4,NR)=YA
      S(KK,5,NR)=XB
      S(KK,6,NR)=YB
      S(KK,7,NR)=UT
      S(KK,8,NR)=SVTI
      S(KK,9,NR)=VT
      S(KK,10,NR)=UAN
      S(KK,11,NR)=SVAN
```

```
      CALL TAPE(2,IN,IO)                                                    07/10/65

      S(KK,12,NR)=VAN
      GO TO 9999
5     DO 6 I=1,9
      KK=NPR(I)
6     WRITE OUTPUT TAPE IO,1030,I,(
     1S(JJ,J,I),J=1,12),KKKK(JJ,I),JJ=1,KK)
1030 FORMAT(56H1OUTPUT TABLE 1 - PARTICLE POSITION, DISPLACEMENT, VELOC
     115HITY INFORMATION//1H0,
     113HREGION NO. = ,I1/7X,3HDAN,7X,3HDBN,6X,4HXATN,6X,4HYATN,
     16X,4HXBTN,6X,4HYBTN,6X,4HVXTN,6X,4HVYTN,7X,3HVTN,
     26X,4HVXAN,6X,4HVYAW,7X,3HVAN,4X,1HN/
     3(12F10.5,2X,I3))
      DO 10 KK=1,9
      UTK(KK)=0.
      SVTK(KK)=0.
      VTK(KK)=0.
      XI(KK)=0.
      N=NPR(KK)
      DO 7 I=1,N
      UTK(KK)=UTK(KK)+S(I,7,KK)
7     SVTK(KK)=SVTK(KK)+S(I,8,KK)
      XN=N
      UTK(KK)=UTK(KK)/XN
      SVTK(KK)=SVTK(KK)/XN
      VTK(KK)=SQRTF(UTK(KK)*UTK(KK)+SVTK(KK)*SVTK(KK))
      BN(KK)=ATANF(SVTK(KK),UTK(KK))
      DO 8 I=1,N
8     XI(KK)=XI(KK)+(S(I,7,KK)-UTK(KK))**2+
     1(S(I,8,KK)-SVTK(KK))**2
10    XI(KK)=SQRTF(.5*XI(KK))/VTK(KK)
      WRITE OUTPUT TAPE IO,1040,(I,I=1,9),(XI(I),I=1,9),(
     1UTK(I),I=1,9),(SVTK(I),I=1,9),(VTK(I),I=1,9),(BN(I),I=1,9)
1040 FORMAT(56H1OUTPUT TABLE 2 - MEAN PARTICLE VELOCITIES AND INTENSITI
     12HES//
     211H  REGION = ,8(I1,12X),I1/6H  I = ,9(E13.6)//
     26H  VX= ,9E(13.6)//
     36H  VY= ,9E(13.6)//
     46H  V = ,9E(13.6)//
     56H ETA= ,9E(13.6))
      CALL EXIT
      END(1,0,0,0,0,0,1,0,0,1,0,0,0,0,0)
```

BIBLIOGRAPHY

1. Lighthill, M. J., "Theoretical Considerations on Free Convection in Tubes." Quarterly of Mechanics and Applied Mathematics, 6, pp. 398-439, 953.

2. Martin, B. W., "Free Convection in an Open Thomosyphon with Special Reference to Turbulent Flow," Proceedings Royal Society A., 230, pp. 502-530, 955.

3. Hammitt, F. B., *Heat and Mass Transfer in Closed, Vertical, Cylindrical Vessels with Internal Heat Sources for Homogenous Reactors*, Ph.D. Thesis, University of Michigan, Dec., 1957.

4. Hammitt, F. G., et al., "Free-Convection Heat Transfer and Fluid Flow in Closed Vessels with Internal Heat Source, University of Michigan Report IP-399, Nov., 1959.

5. Hammitt, F. G. and Chu, P. T., "Transient Internal Natural Convection Heating and Cooling of Closed Vertical Cylindrical Vessels." University of Michigan Report IP-452, 1960.

6. Neff, R., "A Survey of Stratification in a Cryogenic Liquid," *Advances in Cyrogenic Engineering*, Vol. 5, pp. 460-466, Plenum Press, New York, 1959.

7. Huntley, S. C., "Temperature-Pressure-Time Relations in a Closed Container," NACA TN 4259 (1959).

8. "Main Tank Pressurization System Study and Test Program," Lockheed-Georgia Company, Marietta, Georgia, Engineering Report 5296, Vol. 1, (December, 1961) Confidential.

9. Tatom, J. W., Brown, W. H., Knight, L. H. and Coxe, E. F., "Analysis of Thermal Stratification of Liquid Hydrogen in Rocket Propellant Tanks," *Advances in Cyrogenic Engineering*, Vol. 9, pp. 265-272, Plenum Press, New York, 1963.

10. Tellep, D. M. and Harper, E. T., "Approximate Analysis of Propellant Stratification," American Institute of Aeronautics and Astronautics Journal, Vol. 1, No. 8, August, 1963, pp. 1954.

11. "Analytical and Experimental Study of Liquid Orientation and Reduced Gravity Fields," Lockheed Missiles and Space Company Report 2.05-64.1, July, 1964.

12. Harper, E. T., Hurd, S. E., Levy, A. M. and Tellep, D. M., "Analytical and Experimental Study of Stratification in Standard and Reduced Gravity Fields," *Proceedings of the Conference on Propellant Tank Pressurization and Stratification,* NASA, Huntsville, Alabama, January 20, 21, 1965.

13. Bailey, T. E., Vandekoppel, R. and Skartvedt, G., "Cryogenic Propellant Stratification and Test Data Correlation," AIAA Journal, Vol. 1, No. 1, pp. 1657-1659, January, 1963.

14. Bailey, T. E. and Fern, R. F., "Analytical and Experimental Determination of Liquid Hydrogen Temperature Stratification," *Advances in Cryogenic Engineering,* Vol. 9, pp. 254-264, Plenum Press, New York, 1963.

15. Ruder, J. M., "Stratification in a Pressurized Container with Sidewall Heating," AIAA Journal, Vo. II, No. 1, pp. 135-137, January, 1964.

16. Barnett, D. O., Winstead, T. W., and McReynolds, L. S., "An Investigation of Liquid Hydrogen Stratification in a Large Cylindrical Tank of the Saturn Configuration," *International Advances in Cryogenic Engineering,* Vol. 10, pp. 314-324, Plenum Press, New York, 1964.

17. Vliet, C. G., Brogan, J. J., Sheppard, T. S., Morse, F. H. and Hines, F. L., "Stratified Layer Flow Model--A Numerical Approach to Temperature Stratification in Liquids Contained in Heated Vessels." Presented before 1964 AIAA Aerospace Sciences Meeting, New York, January 20-22, 1964.

18. Robbins, J. H. and Rogers, A. C., Jr., "An Analysis on Predicting Thermal Stratification in Liquid Hydrogen," Presented before AIAA First Annual Meeting, June 29-July 2, 1964.

19. Anderson, B. H. and Kolar, M. J., "Experimental Investigation of the Behavior of a Confined Fluid Subjected to Nonuniform Source and Wall Heating," NASA TN D-2079, November, 1963.

20. Clark, J. A. and Barakat, H. Z., "Transient Laminar Free Convection Heat and Mass Transfer in Closed, Partially-Filled Liquid Containers," Technical Report 1, ORA Project 04268, NASA Contract NAS-8-325, August, 1963.

21. Barakat, H. Z., Clark, J. A., "Transient Natural Convection Flows in Closed Containers, " Technical Report 2, ORA Project 04268, NASA Contract NAS-8-825, August, 1965.

22. Schwind, R. G. and Vliet, G. C., "Observations and Interpretations of Natural Convection and Stratification in Vessels." Proceedings of the *1964 Heat and Fluid Mechanics Institute,* Stanford University Press, 1964.

23. Vliet, C. C. and Brogan, J. J., "Experimental Investigation of the Effects of Baffles on Natural Convection Flow and on Stratification," *Proceedings of the Conference on Propellant Tank Pressurization and Stratification*, NASA, Huntsville, Alabama, January 20, 21, 1965.

24. Neff, B. D., "Study of Cryogenic Propellants Stratification Reduction, Final Report," The Martin Company, Report CR-65-33, under Contract NAS 8-5208, August, 1965.

25. Sparrow, E. M., "Laminar Free Convection on a Vertical Plate with Prescribed Nonuniform Wall Heat Flux or Prescribed Nonuniform Wall Temperature," NACA TN 3508, July, 1955.

26. Eckert, E. R. G. and Carlson, W. O., "Natural Convection in an Air Layer Enclosed Between Two Vertical Plates with Different Temperatures," International Journal of Heat Transfer, Vol. 2, pp. 106-120, Pergamon Press, 1961.

27. Brooks, Richard, V., "Free Convection Velocity Measurements by the Use of Neutral Density Particles," M. S. Thesis, Georgia Institute of Technology, June, 1965.

28. Jacobs, D., "Initial Development of Bénard Cells in Natural Thermal Convection of Water," Chemical Engineering Science, Vol. 18, No. 1, pp. 49-51, 1963.

29. Clark, J. A., "A Review of Pressurization, Stratification, and Interfacial Phenomena," *International Advances in Cryogenic Engineering*, Vol. 10, 1964, Plenum Press, New York.

30. Eckert, E. R. G. and Soehngen, E. E., "Studies on Heat Transfer in Laminar Free Convection with the Zehnder-Mach Interferometer," USAF, Air Material Command Technical Report 5747, 27 December, 1948.

31. Eckert, E. R. G. and Soehngen, E. E., "Interferometric Studies on the Stability and Transition to Turbulence of a Free Confection Boundary Layer," *Proceedings of the General Discussion on Heat Transfer*, American Society of Mechanical Engineers, New York, September, 1951.

32. Eckert, E. R. G., Diaguila, A. J. and Curren, A. N., "Experiments on Mixed-Free-and-Forced-Convective Heat Transfer Connected with Turbulent Flow Through a Short Tube," NACA TN 2974, July, 1953.

33. Mordchelles-Regnier, G. and Kaplan, Claude, "Visualization of Natural Convection on a Plane Wall and in a Vertical Gap by Differential Interferometry, Transitional and Turbulent Regimes," *Proceedings of the Heat Transfer Institute*, Stanford University Press, Pasadena, California, 1963.

34. Eckert, E. R. G., and Jackson, T. W., "Analysis of Turbulent Free-Convection Boundary Layer on Flat Plate," NACA TR 1015, pp. 6, 1951.

35. Griffiths, E. and Davis, A. H., "The Transmission of Heat by Radiation and Convection," Special Report No. 9, Food Investigation Board, British Department Science and Industrial Research, 1922, Revised Edition, 1931.

36. Hildebrand, F. B., *Introduction to Numerical Analysis*, pp. 264-268, McGraw-Hill Book Company, New York, 1956.

37. Fujii, T., "Experimental Studies of Free Convection Heat Transfer," Japan Society of Mechanical Engineers, Vol. 2, No. 8, pp. 555, 1959.

38. Coxe, E. F. and Tatom, J. W., "Analysis of the Pressurizing Gas Requirements for an Evaporated Propellant Pressurization System," *Advances in Cryogenic Engineering*, Vol. 7, Plenum Press, New York, 1962, pp. 234.

39. Arpaci, V. S., Clark, J. A., and Winer, W. O. *Advances in Cryogenic Engineering*, Vol. 6, Plenum Press, New York, 1961, pp. 310.

40. Gluck, D. F., and Kline, J. F. *Advances in Cryogenic Engineering*, Vol. 7, Plenum Press, New York, 1962, pp. 219.

41. Jakob, Max, *Heat Transfer*, Volume 1, John Wiley & Sons, New York, 1949, pp. 526.

VITA

John Wilbur Tatom was born in Montgomery, Alabama on August 21, 1933, the son of Elizabeth Buck Tatom and the late Thomas Athor Tatom. He was educated in the public schools of Montgomery and graduated from Sidney Lanier High School in May, 1951. He entered Georgia Institute of Technology the fall of that year and in June of 1955 graduated with a Bachelor of Mechanical Engineering degree and a commission as Second Lieutenant in the United States Army. After working briefly with Pratt and Whitney Aircraft in East Hartford, Connecticut, he entered the Army in January of 1956.

After serving 21 months in a guided missile battalion he was honorably discharged from the Army and entered the graduate program of Georgia Institute of Technology in the fall of 1957. In the fall of 1958, after a year of graduate studies, he was employed by Chance Vought Aircraft in Dallas, Texas as a propulsion engineer. In the spring of 1960, he returned to Atlanta to accept a position with the Lockheed-Georgia Company. In June of that year he received a Master of Science in Mechanical Engineering and was enrolled in the doctoral program.

Mr. Tatom was married in August, 1956 to the former Hilda Jean Hinton, daughter of Carmen Loveless Hinton and William Arthur Hinton.